COMPUTATIONAL AND EXPERIMENTAL PERFORMANCE ANALYSIS OF A RUNNER FOR GRAVITATIONAL WATER VORTEX POWER PLANT

Adam Faraji

Dissertation Submitted in Partial Fulfilment of the Requirements for the Degree of Doctor of Philosophy in Sustainable Energy Science and Engineering of the Nelson Mandela African Institution of Science and Technology

Arusha, Tanzania

August, 2024

ABSTRACT

Energy generation through water is one of the most economic sources of power. On the other hand, isolated and rural communities can both benefit from using micro-hydropower to power their homes. The gravitational water vortex power plant (GWVPP) has recently attracted interest due to its low initial investment, straightforward design, simple maintenance requirements, and low head requirements. However, the technology suffers a low performance caused by unoptimised parameters of its crucial components, such as the GWVPP runner. This study presents the results of numerical simulation and experimental approaches for the GWVPP runner. To understand how each factor affected the efficiency of GWVPP runner, four parameters (hub-blade angle, speed, runner profile, and number of blades) were examined. The (custom) design tool of Design-Optimal Expert was used to create twenty-four (24) experimental runs. Commercial Computational Fluid Dynamics (CFD) software, specifically Ansys CFX, was employed to simulate these runs and assess the system's efficiency. R^2 values of 0.9507 and 0.9603 for flat and curved profiles indicate a better model fitting to actual data. Additionally, the numerical analysis led to a 3.65% improvement in the efficiency of the curved blade profile runner, while the flat runner profile's efficiency increased by 1.69% compared to non-optimized scenarios. The validation process revealed that the comparison between the numerical investigation and experimental results demonstrated a promising agreement, further supporting the accuracy of the numerical analysis. The experimental finding depicts that the efficiency was 9.84 - 25.35%, torque was 0.08 – 0.23 Nm, and the output power was 2.96 – 7.33 W. Furthermore, the results portray the numerical efficiency to be slightly greater by 0.54% than the experimental efficiency, presumably because the frictional forces were not incorporated in the numerical analysis. Additionally, the exergy analysis of the system revealed a value of 43.58%. The power error range was between 0.1 and 0.5 W, with a low variation in the data points. The torque error range was relatively lower than the power error range, ranging from 0.01 to 0.03 Nm, and the torque measurements showed a low variation in the data points. The efficiency error range was generally low, with most errors falling within the 1.3-3.1% range. Therefore, the GWVPP runner efficiency can be improved significantly through numerical analysis and experimental studies. Also, based on the above results, the GWVPP runner and GWVPP system are recommended for energy generation in low-head and flowrate water sources.

DECLARATION

I, Adam Faraji Mfangavo hereby declare to the Senate of The Nelson Mandela African Institution of Science and Technology that, this dissertation is original work carried out by myself and that it has not been submitted for the attainment of any degree award in any other institution.

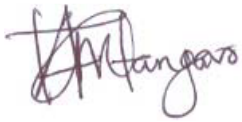

20.08.2024

Adam Faraji Mfangavo Date

The above declaration is confirmed by:

21.08.2024

Prof. Thomas Kivevele Date

21.08.2024

Prof. Yusufu Abeid Chande Jande Date

COPYRIGHT

CERTIFICATION

The undersigned certifies that he/she has read and hereby recommend for acceptance by the Nelson Mandela African Institution of Science and Technology a dissertation titled "Computational and Experimental Performance Analysis of a Runner for Gravitational Water Vortex Power Plant" in fulfillment of the requirements for the degree of Doctor of Philosophy in Sustainable Energy Science and Engineering of the Nelson Mandela African Institution of Science and Technology.

21.08.2024

Prof. Thomas Kivevele Date

21.08.2024

Prof. Yusufu Abeid Chande Jande Date

ACKNOWLEDGEMENT

I am humbly thankful for the gift of life and wisdom to God almighty; without him, this study would not have succeeded. I thank God countlessly for guiding me through all the challenges in this work.

Secondly, I sincerely thank my supervisors, Prof. Thomas Kivevele and Prof. Yusufu Abeid Chande Jande, for their tireless and generous efforts, insightful guidance, discussion and contribution to accomplishing this research.

Furthermore, I am grateful to the Centre of Water Infrastructure and Sustainable Energy Futures (WISE-Futures) for the financial support in my studies and to the Nelson Mandela African Institution and Technology, where this research was conducted.

To all my colleagues, academic staff, and laboratory technicians at (i): The Nelson Mandela African Institution and Technology and (ii) The Arusha Technical College, I appreciate your continuous support and assistance during my research.

May the Almighty God reward you abundantly.

DEDICATION

This work is dedicated to my family for their patience throughout my studies.

Specifically, this work is dedicated to my lovely wife, Prisca, for her moral support and looking after the family diligently for the whole period of my studies.

To my two children, Hans and Harris.

TABLE OF CONTENTS

LIST OF TABLES

LIST OF FIGURES

LIST OF APPENDICES

LIST OF ABBREVIATIONS AND SYMBOLS

2D	Two dimensional
3D	Three dimensional
ANOVA	Analysis of Variance
C.V	Coefficient of variation
CAD	Computer Aided Design
CFD	Computational Fluid Dynamics
EP	Experimental parameters
FSV	Free surface vortex
GWVHP	Gravitational Water Vortex Hydropower Plant
GWVPP	Gravitational Water Vortex Power Plant
hp	Horse power
kW	Kilowatt
MW	Megawatt
NA	Not applicable
NM-AIST	Nelson Mandela African Institution of Science and Technology
NP	Numerical parameters
OFAT	One Factor At a Time
RPM	Revolution per minute
RSM	Response Surface Methodology
SD	Standard Deviation
SHP	Small Hydropower
SST	Shear Stress Transport

CHAPTER ONE

INTRODUCTION

1.1 Background of the Problem

Energy demand is tremendously growing daily, along with the increase in economy and population. In order to support social-economic development activities, there is a rise in the demand for electricity in the industry, household, and service sectors in developing nations (Kaunda *et al.*, 2012). However, major sources of energy generation, especially renewable energy (solar, wind, waves, tidal, hydro), have not been exploited to their maximum. In the view of the global share of renewable energy, the status of hydropower shows that there is an increase of 3.9% from the year 2009 to 2020, as depicted in Fig. 1. In considering possible future renewable energy sources, hydropower (HP) provides the following advantages: - low annual maintenance cost, can be incorporated into multipurpose projects, highly efficient and long lifespan. In addition, the contribution of HP in the energy sector is recommendable. For example, Fig. 2 illustrates that in 2021, while renewable energy contributed about 28.3% to global electricity production, hydropower was reported to contribute 15% of the world's net electricity production (REN21, 2022). Either small or large hydropower systems can harness energy from hydropower.

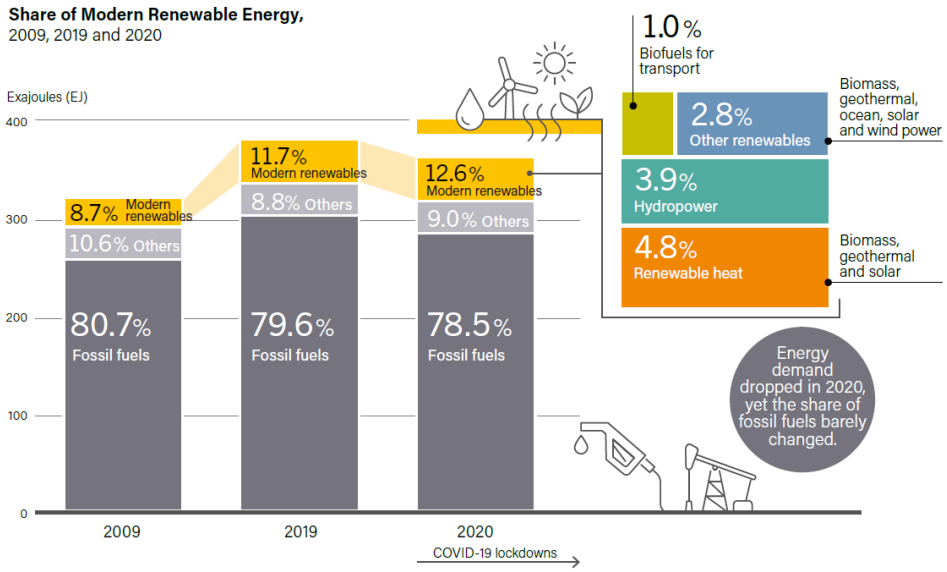

Figure 1: Renewable energy share: Global overview (REN21, 2022)

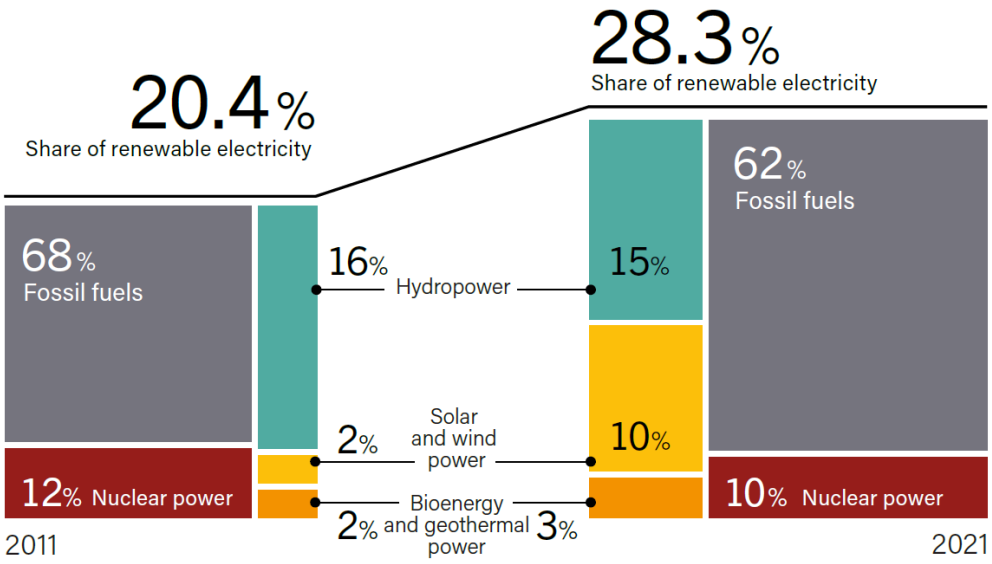

Figure 2: Share of renewable energy in electricity generation (REN21, 2022)

The HP projects are typically classified based on their size. The categorization of HP includes small hydropower (SHP) or large hydropower (LHP). However, since no generally agreed-upon definition exists, categorisation differs by country (Paish, 2002). For example, pico, micro, mini and small systems are subcategories of the SHP. Most nations and organisations define pico as an HP system that produces less than 10 kW, micro-HP as one that produces more than 10 kW but less than 100 kW, mini-HP as one that produces more than 100 kW but less than 1 MW, and small HP as one that produces more than 1 MW but less than 10 MW (Kaunda *et al.*, 2012; Timilsina *et al.*, 2018). The SHP can be a reservoir or a run-of-river type: run-of-river varieties have no water storage for power generation and divert water from the main river through a weir. Run-of-river small hydropower (SHP) systems are suitable for moderate capacities because the absence of a reservoir helps in reducing the investment cost per kW of installed energy. For SHP systems, the primary focus is on minimizing investment costs. The working principle of the HP system involves the energy from falling water being converted into rotating shaft power via a turbine. Turbines are classified according to their operating principle and can be either impulse Fig. 3a (Pelton, Turgo, and Cross-flow) or reaction Fig. 3b (Kaplan and Francis) (Paish, 2002).

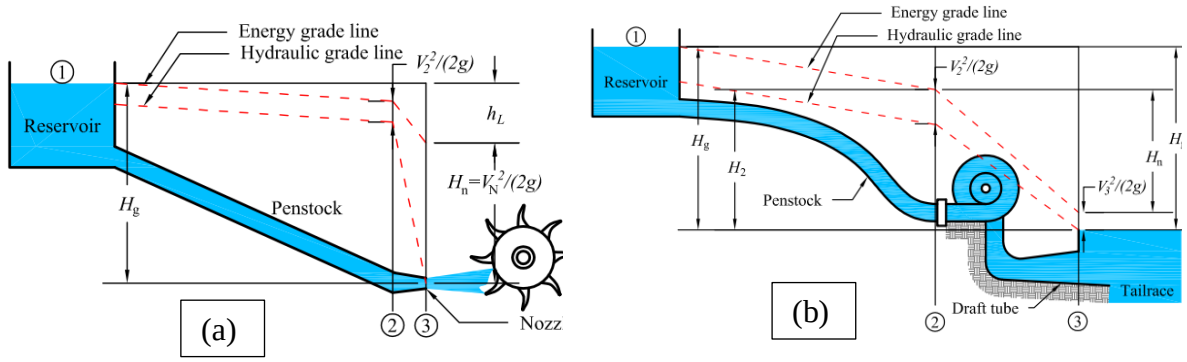

Figure 3: Sketch of a) impulse turbine b) reaction turbine (Leon & Zhu, 2014)

The notion of a micro-HP system as a potential renewable energy technology is gaining popularity. The energy supply in rural, distant, and mountainous places is insufficient, poor, and unreliable. Micro-HP, conversely, may deliver electricity to remote areas where grid extension is prohibitively expensive and users have low incomes (Williamson *et al.*, 2014). This scheme has lately gained global attention because of its critical role in meeting electricity demand in remote and rural locations. The site's characteristics decide the best turbine for any given HP site, the most essential of which is the available head and flow rate. The choice is also influenced by the required operating speed of the generator or other equipment powering the turbine. Other factors, such as the anticipated power generation of the turbine under low flow circumstances, are also crucial in the decision (Okot, 2013). For example, the Archimedes screw turbine, gravitational water vortex power plant, and waterwheel turbine are suitable micro-HP turbines at low head and flow rates.

The gravitational water vortex power plant (GWVPP) is a type of micro-HP scheme that works well in rivers and streams with low flowrates and heads, as shown in Fig. 4. In addition, GWVPP is a novel addition to the family of micro-HP systems that operate in the 0.7 m to 2 m head range (Zotlöterer, 2017). It is one of the micro hydropower systems and can be considered a useful application of the Free Surface Vortex (FSV) principle. An artificial water vortex flows tangentially through a rectangular canal and into a basin (cylindrical/spiral) with a bottom exit hole to power a water vortex turbine (Shabara *et al.*, 2015). This system doesn't require direct control mechanism and penstock. Hence, fabrication and construction costs are low and can be realized using locally available machines and equipment (Timilsina et al., 2018). Moreover, GWVPP is regarded as a promising renewable energy resource for remote communities, simultaneously contributing to endeavours aimed at reducing the greenhouse gas effect on the environment (Darmawi, 2019; Sipahutar *et al.*, 2013).

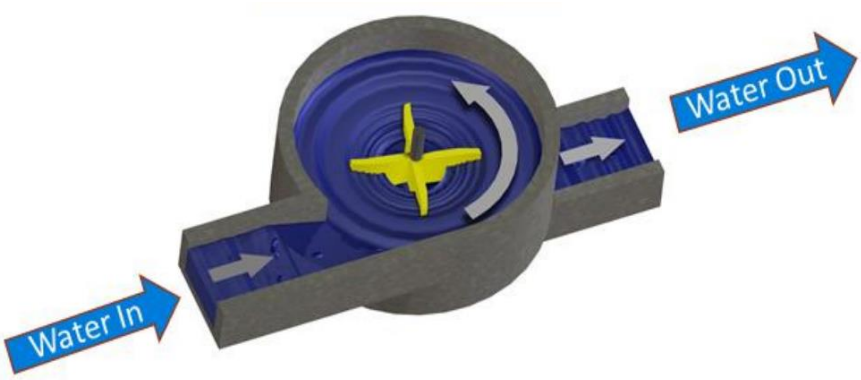

Figure 4: Schematic of GWVPP (Mohanan, 2016)

In recent times, there has been a growing interest in the advancement of GWVPP, leading to numerous research studies to assess its performance, with a particular focus on its energy efficiency. For example, researchers have been studying the impact of runner shapes (profiles) to determine the overall efficiency of the GWVPP. For example, a study by Dhakal *et al*. (2017) used numerical analysis to compare three runner profiles and determine which shape was best. The efficiency of the curved runner profile was reported to be 82% higher than that of the straight and twisted blades, which were 63% and 46% efficient, respectively. A study on the basin-to-blade ratio configurations utilizing different runner profiles revealed that cross-flow blades showed the best efficiency (Khan *et al*., 2018). Moreover, the flat and curved profiles of the runner were experimentally studied (Kueh *et al*., 2017). Despite the fact that the flat profile runner had an efficiency of 21.63% compared to the curved profile runner's 22.24%, the experimental constraints prevented this study from reaching its maximum efficiency. Curved profiles outperform other profiles due to increased surface area and flow control of the water.

The experimental study by Kueh *et al*. (2017) encountered several issues that could not be resolved, mainly due to testing constraints. For example, due to practical limits (failure to provide large frictional torque and low-capacity load-cells components), ideal operating speed was not achieved, resulting in failure to attain optimal efficiency. Furthermore, the optimization of the runner model via different design factors was not considered. Faraji *et al*. (2022) performed optimisation of the two runner profiles (flat and curved) through the alteration of four parameters (speed, blade-hub angle, number of blades and blade profile). The study reported curved profiles showing better efficiency of 9.80 – 25.89% over flat profile blades, which exhibited efficiency in the 8.08 - 23.32% range.

Runner as one of the essential components in GWVPP; its efficiency depends on the number of parameters such as number of blades, blade-hub angles, runner speed and blade profile. In recent times, there has been a growing interest in the advancement of GWVPP systems, leading to numerous research studies to assess its performance, with a particular focus on its efficiency (Dhakal *et al*., 2017; Khan *et al*., 2018; Kueh *et al*., 2017). Another study was on the effect of the materials on the efficiency of the runner, and the study concluded that lighter materials provide higher efficiency (Sritram *et al*., 2015). The effects of the baffles on the runner were also studied, and it was reported that baffles improved the efficiency of the system (Wichian & Suntivarakorn, 2016). However, it is worth noting that since this technology has been a few years since its existence, some of the parameters affecting the efficiency of the runner, such as the number of blades, blade-hub angles, runner speed and blade profile, are not comprehensively studied.

It is observed that most previous research on the performance of GWVPP was conducted based on traditional energy efficiency. Energy efficiency refers to the ratio of the useful energy output of a system to the energy input. While energy efficiency is essential for evaluating the performance of a hydropower system, exergy efficiency provides a complete picture of the quality of the energy being produced. Exergy is a measure of the valuable work that can be obtained from a system, taking into account the irreversibilities and inefficiencies of the process. Moreover, exergy efficiency is the ratio of the valuable exergy output to the exergy input of a system. In the case of hydropower, exergy efficiency would take into account factors such as the loss of energy due to friction, turbulence, and other inefficiencies in the conversion process.

Based on the observations mentioned earlier, an exergy-based method is suggested to assess the effectiveness of GWVPP, considering the system's irreversibilities. However, to the best of knowledge of this research, no single study on the GWVPP study using the exergy analysis exists. Therefore, the objective of this study is to perform numerical analysis, experimentally validate the numerical study and also to perform the exergy analysis of the GWVPP system. The study, in particular, involved a complete design, manufacturing and experimental testing of the GWVPP test rig. The test rig is tested at various rotational speeds, where power, torque, and efficiency performance parameters are evaluated. Moreover, the study applied the first law of thermodynamics to determine the system's exergy efficiency, where the fluid's steady flow energy equation through a control volume was employed.

This study is geared towards the performance improvement of the GWVPP runner efficiency by altering parameters responsible for the efficient performance of the GWVPP runner. Through numerical simulation and experimental approach for the GWVPP, four parameters (hub-blade angle, speed, runner profile, and number of blades) were explored.

1.2 Statement of the Problem

Despite the availability of various water bodies, such as run-of-river, their utilization as energy sources through small hydropower has been minimal due to technological limitations. The barriers to small hydropower development are low head and flow rates. Conventional technologies such as Kaplan or Francis at a very low head and flow rate face technical and economic limitations. Some limitations include the requirement of a special flow mechanism and the risk of environmental emissions (Senior *et al*., 2010). Additionally, little progress has been made in the study of power generation using low discharge and very low head (Dhakal *et al*., 2014). A good candidate to overcome the technical and economic limitations of conventional hydropower for the generation of electricity from an ultra-low head is the GWVPP. However, the runner, as one of the crucial components of GWVPP, has lower efficiency compared to other conventional hydropower due to less optimization of its crucial parameters. The GWVPP runner efficiency depends on the number of parameters such as number of blades, blade-hub angles, runner speed and blade profile. As such, parameters are not comprehensively studied and optimized (Rahman *et al*., 2017). For example, based on work of literature, some studies tried to improve the performance of GWVPP runners (Dhakal *et al*., 2017; Khan *et al*., 2018; Kueh *et al*., 2017). It is worth noting that most of these studies used a different methodology, mostly one-factor-at-a-time (OFAT), to improve the performance parameters. The significant challenge for OFAT is that it does not consider the potential interactions between different factors. The effect of one factor may depend on the level of another factor. This study has focused on the performance improvement of the runner by altering four parameters (number of blades, blades-hub angle, runner speed and runner profiles) responsible for the efficient performance of the runners by combining these parameters.

1.3 Rationale of the Study

This study has utilized the GWVPP system, which is classified as micro-hydropower, to solve unused waters, especially in the ultra-low head, such as run-of-rivers in flat areas. The justification of this study lies in thematic areas as follows:

(i) Sustainable Energy: The development of sustainable and renewable energy sources is crucial for reducing the dependence on fossil fuels and mitigating the adverse effects of climate change. Gravitational Water Vortex Power Plants (GWVPPs) are one such alternative energy source that has the potential to generate clean energy without producing harmful emissions. This research has helped to improve the efficiency of these power plants, making them more attractive to investors and contributing to the transition towards sustainable energy sources.

(ii) Economic Viability: Gravitational Water Vortex Power Plants (GWVPPs) are still a relatively new technology, and their economic viability is not yet fully established. Improving the performance of critical components like the runner could increase the plant's power output, making it more economically viable and competitive with other energy sources. This research can contribute to the commercialization of GWVPPs and help to establish them as reliable and profitable energy sources.

(iii) Computational Modeling: Computational modelling is essential in designing and optimising complex systems like GWVPPs. However, the accuracy and reliability of these models depend on their validation against experimental data. This research can help to improve the accuracy and reliability of computational models used to simulate the performance of water vortex power plants, contributing to the broader field of computational fluid dynamics.

1.4 Research Objectives

1.4.1 General Objective

The general objective of this study is to establish the optimal working parameters of a GWVPP runner through computational and experimental methods.

1.4.2 Specific Objectives

(i) To develop a GWVPP model comprising canal, basin and runner for numerical analysis.

(ii) To theoretically optimize GWVPP runner parameters responsible for the low performance of the GWVPP system (i.e., the number of blades, blade-hub angles, runner speed and blade profile).

(iii) To experimentally validate the numerical results of the optimized GWVPP runner.

1.5 Research Questions

(i) How can a comprehensive GWVPP model, incorporating canal, basin, and runner components, be developed to facilitate accurate numerical analysis and optimization?

(ii) What are the values of the GWVPP runner parameters to be improved through CFD for optimal performance of the GWVPP?

(iii) How do experimental performance values of the optimized GWVPP runner align with numerical values?

1.6 Significance of the Research

The rationale of the study was to contribute knowledge and further research on the area under study. The findings are useful to policy makers in decision-making with regard to GWVPP. The study has contributed to the following:

(i) Help to advance the knowledge and understanding of how GWVPP work, as well as improve the accuracy and reliability of computational models used to simulate the performance of such systems.

(ii) Development of environmentally friendly GWVPP through performance improvement of the GWVPP runner; and

(iii) Contribution to the development of sustainable and renewable energy sources, especially for low-head areas such as irrigation, open channel flow etc.

1.7 Delineation of the Study

This study is geared towards the performance improvement of the GWVPP runner efficiency by altering parameters responsible for the efficient performance of the GWVPP runner. Through numerical simulation and experimental approach for the GWVPP, four parameters (hub-blade angle, speed, runner profile, and number of blades) were explored. The centrel focus was to establish the optimal working parameters of a GWVPP runner through computational and experimental methods.

CHAPTER TWO

LITERATURE REVIEW

2.1 Research Framework

Figure 5 shows the research framework of the optimization of the runner for GWVPP. The framework has involved an iterative approach towards the identification and selection of a runner numerically. The optimal results have been validated through experimental testing.

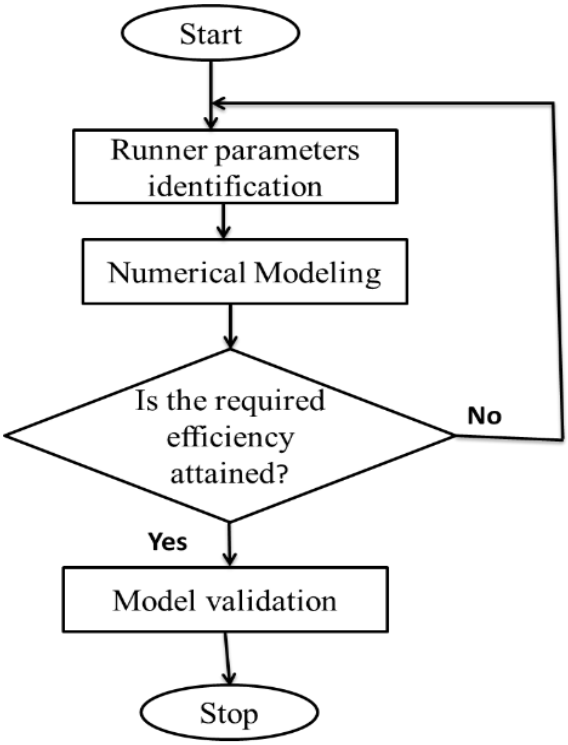

Figure 5: A research framework

2.2 Hydropower

Hydropower offers a wide range of project scales and types, allowing for customized designs to meet specific needs and site conditions. Large hydropower refers to the generation of electricity from the energy of falling or fast-flowing water in large-scale hydropower plants. One of the key advantages of hydropower is its minimal impact on water resources, as it neither consumes nor pollutes the water used for power generation, leaving it available for other vital purposes. Moreover, the revenues generated from electricity sales can be utilized to fund critical infrastructure projects that enhance human welfare. These consist of creating systems for the supply of clean drinking water, agricultural irrigation plans, navigation system upgrades, leisure facilities, and promoting ecotourism. Water is an essential resource that

sustains all life forms on our planet. However, its distribution is uneven across seasons and geographical regions, with some areas experiencing droughts and others facing the challenges of destructive floods. Throughout history, dams and reservoirs have played a crucial role in collecting, storing, and effectively managing water resources necessary for the survival and progress of civilizations. Hydropower generates electricity and supports essential water services such as flood control, irrigation, and drinking water supplies, facilitating the fair distribution and utilization of this invaluable resource (Yüksel, 2010). Figure 6 illustrates the typical schematic of the hydropower plant parts.

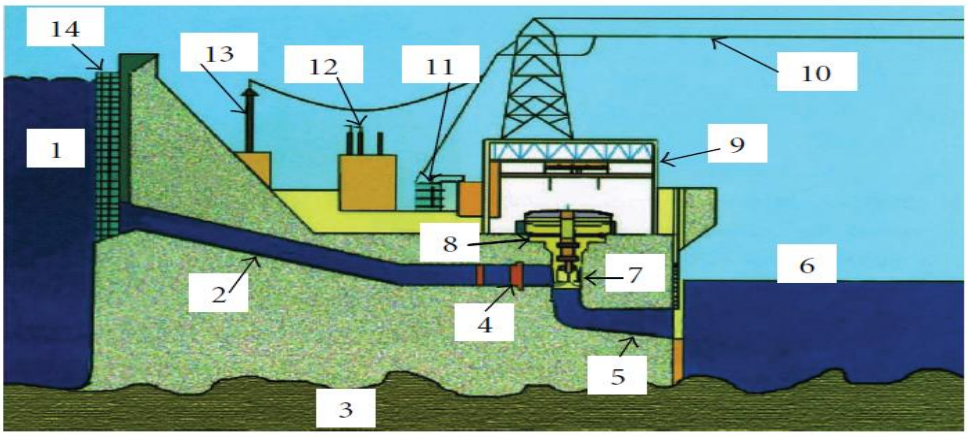

(1) Reservoir (6) Tailrace water (11) Transformer
(2) Penstock (7) Turbine (12) Insulators
(3) Bed rock (8) Generator (13) Transmission tower
(4) Valve (9) Power house (14) Trash rack
(5) Draft tube (10) Transmission lines

Figure 6: A schematic representation of a hydropower station and its main components (Kaunda *et al.*, 2012)

Hydropower stands as one of the most ancient and well-established forms of renewable energy. It boasts remarkable attributes, being nearly carbon neutral, technologically advanced, and cost-competitive. Its contributions toward attaining climate change goals, securing energy provision, and fostering a sustainable global energy system are substantial (Bilgen *et al*., 2008; Yuksel, 2010). Compared to newer technologies like wind power or solar energy, hydropower has already achieved significant development in capacity, particularly in Europe (Wagner *et al*., 2015). Hence, in addition to its advantages, it is crucial to consider the environmental impacts, such as disruptions to river ecosystems, as well as the social implications, including community resettlements. According to the latest available data, the global installed capacity of hydropower stands at 926 GW, resulting in an annual global generation of 3551 TWh/year (equivalent to 12 784 PJ). This accounts for approximately 16.3% of the world's electricity

generation. The estimated global technical potential for hydropower is around 14576 TWh (equivalent to 52 474 PJ). Europe has harnessed about 53% of its total potential, while other continents, such as Africa (8%), Asia (20%), and Australia (20%), possess significant untapped resources (Wagner *et al.*, 2015). Figure 7 illustrates the hydropower potential at various places.

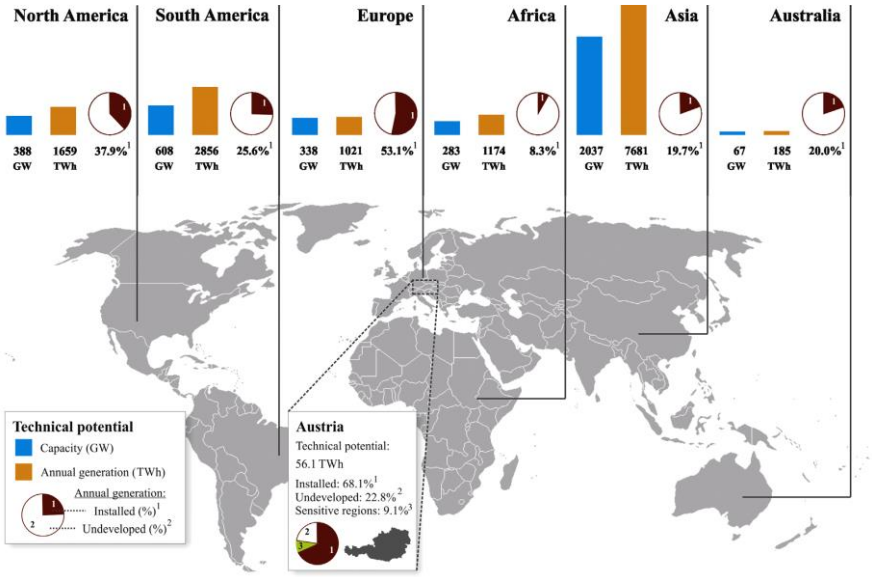

Figure 7: North America, South America, Europe, Africa, Asia, and Australia's technical hydropower potential in terms of installed capacity and annual generation, as well as the proportion of installed hydropower in 2009 (Wagner *et al.*, 2015)

2.2.1 Hydropower As a Renewable and Sustainable Energy Source

Consensus has been achieved by representatives from over 170 countries, affirming that all hydropower is renewable and deserving of international support. This agreement was initially established at the World Summit on Sustainable Development in Johannesburg in 2002 and reiterated at the 3rd World Water Forum in Kyoto in 2003. The following supporting evidence is provided (Wagner *et al.*, 2015).

(i) Hydropower stands as a renewable energy source, harnessing the power of flowing water to generate electricity. Since it does not deplete the resource, all types of hydropower projects, be they small or large, run-of-river or storage-based, fall under the renewable energy category.

(ii) Hydropower plays a vital role in promoting the advancement of other renewable energy sources. Hydropower facilities with reservoirs offer exceptional operational flexibility, allowing them to respond promptly to changes in electricity demand. This unique

feature, coupled with its storage capacity, positions hydropower as the most efficient and cost-effective method to facilitate the integration of intermittent renewables such as wind and solar power.

(iii) Hydropower plays a pivotal role in promoting energy security and ensuring price stability. Unlike fuel or natural gas, river water used for hydropower generation is a domestic resource that remains unaffected by market fluctuations. Additionally, as the only major renewable source of electricity, hydropower's cost-effectiveness, efficiency, flexibility, and reliability contribute to optimizing the utilization of thermal power plants.

(iv) Hydropower makes a significant contribution to fresh water storage by utilizing reservoirs to collect rainwater. These reservoirs serve a dual purpose as they not only generate electricity but also provide a valuable source of water for drinking and irrigation purposes. By effectively storing water, hydropower reservoirs help safeguard aquifers from depletion and mitigate the impacts of floods and droughts, enhancing our resilience to water-related challenges.

(v) Hydropower plays a crucial role in enhancing the stability and reliability of electric grids. The management of electricity grids relies on fast and flexible generation sources to meet peak power demands, stabilize system voltages, and restore service promptly after blackouts. Hydropower offers a unique advantage in this regard, as electricity generated from hydropower can be swiftly integrated into the grid, faster than any other energy source. Its exceptional capability to transition rapidly from zero power to maximum output enables hydropower to effectively meet fluctuating loads and provide essential ancillary electrical services. This capacity ensures the balance between electricity supply and demand, further strengthening grid resilience.

(vi) Hydropower plays a crucial role in combating climate change due to its minimal greenhouse gas (GHG) emissions throughout its life cycle. By offsetting emissions from gas, coal, and oil-fired power plants, hydropower contributes to the mitigation of global warming. It is worth noting that despite only 33% of potential hydro resources being developed, hydropower already makes a significant impact by averting the need to burn approximately 4.4 million barrels of oil equivalent per day worldwide. This substantial reduction in fossil fuel consumption further underscores the valuable role of hydropower in addressing climate change.

(vii) Hydropower significantly enhances air quality as hydropower plants do not produce any air pollutants. Frequently, they serve as a clean alternative to fossil-fueled power generation, leading to a reduction in acid rain and smog. Another notable advantage is that hydropower projects do not generate any toxic by-products, further contributing to a healthier environment. By promoting clean and pollutant-free electricity generation, hydropower plays a vital role in improving the air we breathe.

(viii) Hydropower profoundly impacts development by bringing essential infrastructure, such as electricity, roads, industry, and commerce, to communities. This, in turn, fuels economic growth, enhances access to healthcare and education, and enhances the overall quality of life. With a century-long track record, hydropower is a well-established and proven technology. Its impacts are comprehensively understood, and measures for mitigation and enhancement are readily available. Moreover, hydropower holds immense potential and can be deployed in areas where development is most needed, making it a valuable asset for sustainable progress.

(ix) Hydropower ensures the provision of clean and affordable power not just for the present but also for the future. Hydropower projects spanning 50 to 100 years serve as enduring investments that can benefit multiple generations. These projects can be readily upgraded to incorporate the latest technological advancements, ensuring their continued relevance and efficiency. Additionally, hydropower facilities boast remarkably low operation and maintenance costs, further enhancing their economic viability and long-term sustainability.

(x) Hydropower serves as a pivotal instrument for achieving sustainable development goals. Hydropower projects exemplify the essence of sustainable development when developed and operated in an economically viable, environmentally responsible, and socially conscious manner. Hydropower projects are vital in realising sustainable development aspirations by prioritizing economic viability, environmental stewardship, and social responsibility.

2.3 Classifications of Hydropower Schemes

Hydropower schemes are generally categorized according to their size. They can be small hydropower (SHP) or large hydropower. However, because no universally recognised definition exists, the classification varies between nations (Paish, 2002). The systems falling

within the SHP category are subcategorized into pico, micro, mini, and small. Most nations and organisations classify pico systems as producing less than 10 kW, microsystems as producing more than 100 kW but less than 1 MW, mini systems as producing more than 100 kW but less than 1 MW, and small systems as producing more than 1 MW but less than 10 MW (Kaunda *et al.*, 2012). Additionally, the small HP can be a run-of-river type or reservoir. Run-of-river types use water diverted from the main river by a weir rather than storing it for power generation. Run-of-river types are ideal for small SHP capacities because they have a lower investment cost per kW of installed electricity. After all, there is no need for a reservoir (the main goal of SHP systems is to lower investment cost).

A turbine transforms the force of falling water into rotating shaft power. Turbines can be classified as either impulse (Pelton, Turgo, and Cross-flow turbines) or reaction (Kaplan and Francis turbines) turbines based on how they work (Paish, 2002). The head-flow ranges of small hydro turbines are depicted in Fig. 8.

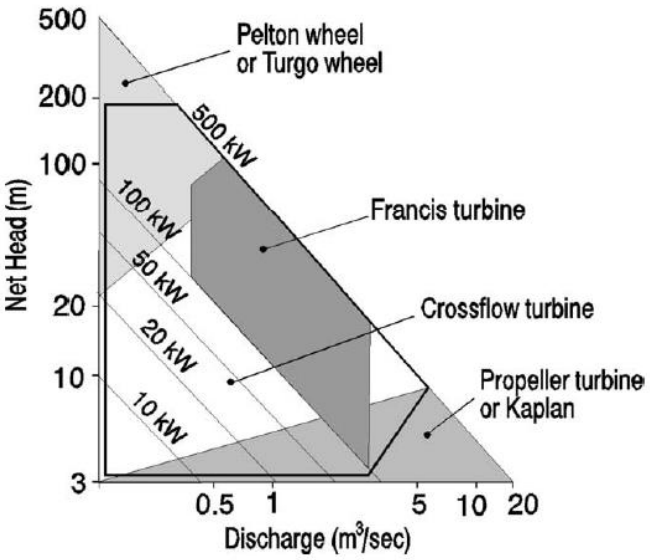

Figure 8: Small hydro turbine head-flow ranges (Paish, 2002)

2.4 Very Low-head Hydropower Technologies

A promising renewable energy technology is the idea of a micro hydropower system. Micro-hydropower systems can produce electricity close to a 100 kW capacity (Kaunda *et al.*, 2012). Rural, remote, and hilly areas have poor, inconsistent, and insufficient energy supplies. Alternatively, micro-hydropower can provide energy to rural areas where grid extension is expensive and the end users have low incomes (Williamson *et al.*, 2014). A hydro turbine transforms the force of falling water into rotating shaft power. The head and flow are the two

main site factors affecting which turbine is most appropriate for a specific hydro site. The decision is also influenced by the generator's or other loading device's desired operating speed. Other factors, like whether the turbine will be expected to produce power under reduced flow conditions, are also crucial in the selection process (Paish, 2002). Suitable micro-hydropower for low head includes Archimedes screw turbine, GWVPP and waterwheel turbine. This study`s focus is on the GWVPP.

2.5 Gravitational Water Vortex Power Plant

Micro hydropower plants are one class of green technology that includes Gravitational Water Vortex Power Plant (GWVPP). Due to the fact that the highest reported power generated did not exceed 100 kW, it is classified as micro hydropower (Rahman *et al*., 2017; Timilsina *et al*., 2018). The ultra-low hydraulic head requirement of this power plant is its main benefit (Wanchat *et al*., 2013) as well as the environmentally friendly (Zotlöterer, 2017). This plant's water supply is provided by a sizable, straight inlet that leads to a circular basin via tangential flow (Fig. 9). A strong vortex will then form in the water, and it will exit the outlet at the bottom of the shallow difference due to the vortex's dynamic force (Zotlöterer, 2017). As a result, when compared to other hydro power technologies, the GWVPP's development and power generation costs are extremely low. Due to the following characteristics of water vortex, gravitational vortex power plants are also found to be advantageous:

(i) The water surface area is increased.

(ii) Increases the water surface area's flow velocity to its maximum.

(iii) Spreads contaminants throughout the water uniformly.

(iv) Expands the contact surface of the dispersed contaminants for water plants and microorganisms.

(v) Naturally aerates the water due to the high flow velocity on the water's surface area.

(vi) Increase the heat of evaporation to allow water to cool the environment during the summer's rising temperatures.

(vii) To maximise the chance of microorganism survival concentrates, dense water (water at 40°C) in the centre of the ring-shaped structure (Zotlöterer, 2017).

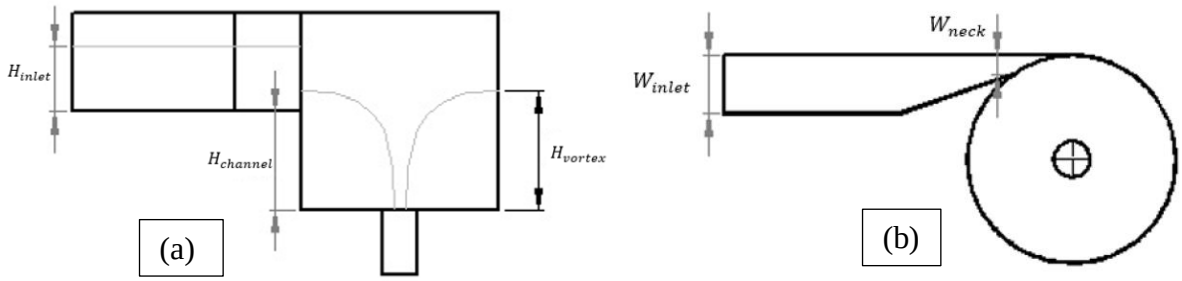

Figure 9: GWVPP (a) Side view (b) Top view (Rahman *et al.*, 2017)

Additionally, the advantages of using an artificial vortex above gravity-accelerated water are increased effectiveness, reduced costs, improved sustainability and health of the river, and reduced negative environmental effects (Power *et al.*, 2016). From Fig. 10, it can be observed that GWVPP gives promising application at the low head (below 1 m), and it can also be operated at a low flow rate compared to other turbines.

The GWVPP is a turbine technology wherein the kinetic energy of water is harnessed by a rotating tank (basin), converting its potential energy, and a turbine positioned at the centre of the vortex extracts this kinetic energy. The operating range of GWVPP in terms of head and flowrate is identified by Timilsina *et al.* (2018), as observed in Fig. 10. Moreover, this technology bridges the existing gap in the functioning of low-head hydropower systems. The GWVPP has been stated to have some advantages, including environmental safety, ease of manufacture, ease of installation, low operating and maintenance costs, no need for water storage, surface water area increase, maximized water flow velocity on the surface area, and is safe for aquatic life (Dhakal *et al.*, 2014; Khan *et al.*, 2018; Rahman *et al.*, 2017).

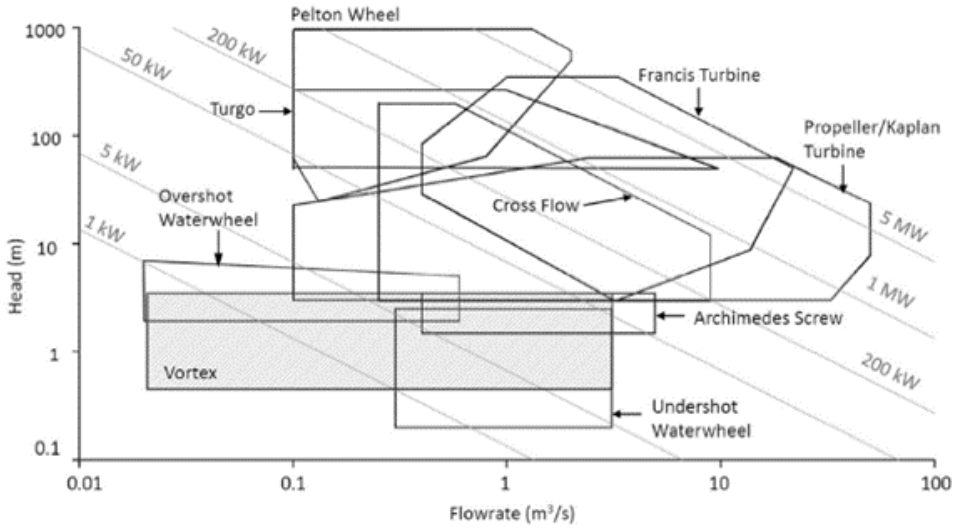

Figure 10: Chart of the vortex turbine's application range (Timilsina *et al.*, 2018)

2.5.1 Gravitational Water Vortex Power Plant System: History and Evolution

The GWVPP system is a micro hydropower system and can be considered a useful application of free surface vortex (FSV). In recent years, this innovative hydropower method has emerged as a competitive hydropower option against conventional systems. Franz Zotlöterer produced the GWVPP in 2006 (Zotlöterer, 2017). The device creates a whirlpool-like flow inside an open channel chamber or basin using an artificial free-surface vortex created by a tangential approach and a central intake (or orifice) situated on the bottom floor (Shapiro, 1962). However, some might argue that Viktor Schauberger was the one who first came up with the concept of using a vortex flow to collect water (Bartholomew, 2005). However, the 10 kW commercial installation made by Zotlöterer on a river in Obergrafendorf, Austria, in 2006 (as depicted in Fig. 11) is what really garnered attention for the technology worldwide (Dhakal *et al*., 2014; Mulligan & Casserly, 2010). Figure 11 (a) shows the overview of GWVPP, while Fig. 11 (b) shows the overview of GWVPP in 3D.

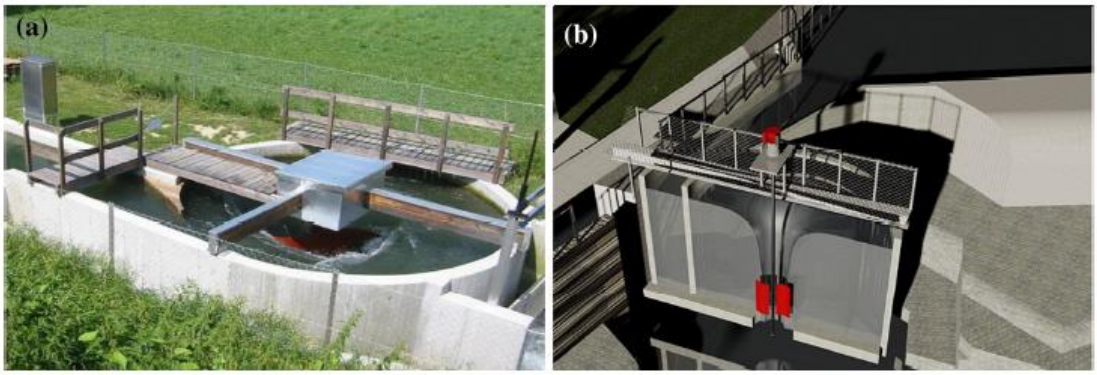

Figure 11: Overview of the GWVPP (Timilsina *et al*., 2018)

A runner is one of the essential components of GWVPP. Figure 12 (a) shows the first configuration of the runner, while Fig. 12 (b) shows the improved configuration of the runner.

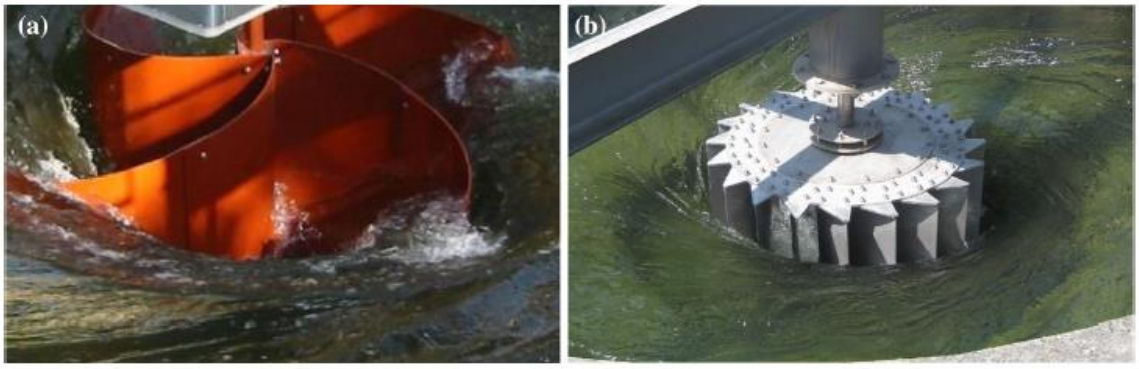

Figure 12: Early impeller (Zotlöterer, 2017)

2.5.1 Free Surface Vortex

In the discipline of hydraulic engineering, the FSV is a significant phenomenon. Depending on where it is, it might be a useful or dangerous source. Many researchers investigated the causes of this phenomenon's strength as well as its structure and location in an effort to either weaken or strengthen it (Yaakob *et al.*, 2014). "Hydropower-Naturally?" by the International Water Power and Dam Construction Journal editors was published in 1995 and mentioned the FSV once more as a technique for small, run-of-river hydropower generation (Reynolds, 1995). The article advocates for smaller low-head schemes with vortex technology as effective alternatives while arguing against river dams and also references the work of Schauberger (Reynolds, 1995). Kouris (2000) modified existing hydropower dams so that they could produce "additional energy" by generating a free-surface vortex. Later Brown (1968) patented a hydraulic turbine assembly, as displayed in Fig. 13. The creation of the vortex is achieved by extending the intake closer to the free surface. According to one theory, the Coriolis effects on flowing water have an impact on vortex formation.

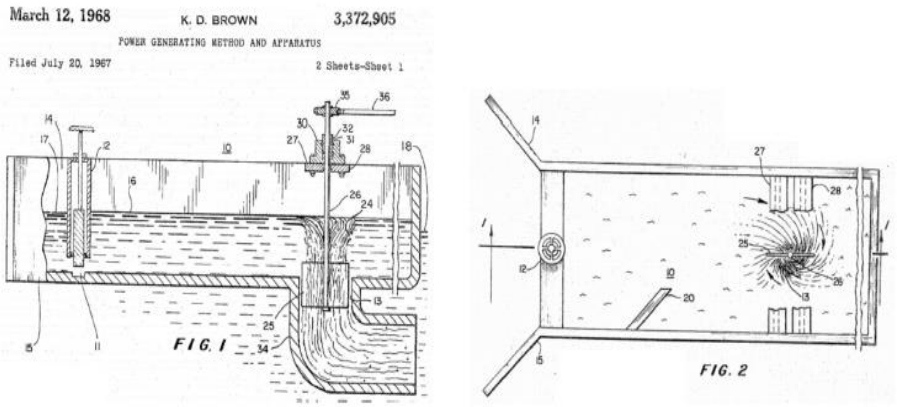

Figure 13: Free-surface vortex turbine concept (Brown, 1968)

2.6 Previous Research on Gravitational Water Vortex Power Plant

Since vortices can be both helpful, like for cyclone separators (Safikhani *et al*., 2011; Utikar *et al*., 2010) and harmful, like for hydraulic machinery and structures in hydropower plants (Hite & Mih, 1994; Rajendran *et al*., 1999), they have attracted research attention (Basu *et al*., 2013). However, the use of vortices for hydropower generation, or GWVPP, hasn't been thoroughly thought out yet. Moreover, since GWVPP research and practice are still relatively new, the operating conditions are largely unstudied or unknown. As a result, only a few studies like this one are solely focused on the analysis of GWVPP in detail.

2.6.1 Numerical Studies

The discipline of computational fluid dynamics (CFD) is a subset of numerical and computational sciences that focuses on solving discretized sets of the Navier-Stokes equations, which govern fluid flow, in order to produce three-dimensional and time-varying information on a particular flow field of interest. The main benefit of CFD is its capacity to produce results rapidly and inexpensively, making it ideally suited for optimization (Pulliam & Zingg, 2014). The drawback is that a particular simulation must strictly pass the model and requires quantitative validation through physical experimentation before being employed for development. The use of CFD models has led to a rise in research exploring novel designs for vortex basins and runners as a result of the development of less expensive CFD codes and high-speed computing. According to Mulligan *et al*. (2016), Fig. 14 shows the outcomes of a CFD simulation performed on a vortex chamber, showing the flow behaviour and velocity vectors for various depths.

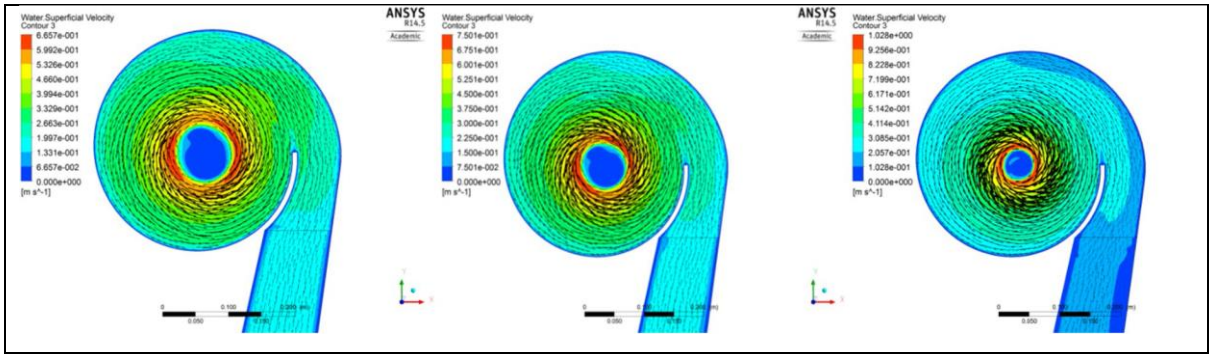

Figure 14: Computational Fluid Dynamics simulation of a vortex chamber to show flow behaviour and velocity vectors at different depths (Mulligan *et al.*, 2016)

Wanchat and Suntivarakorn (2012) investigated the variation in basin geometry to ensure a stable vortex for power generation. In this study, a cylindrical chamber with and without induced circulation was compared to a rectangular configuration of the basin. A guide plate similar to the one described in Brown (1968) patent was placed just before the entrance to the vortex chamber to induce circulation. According to the findings, a cylindrical basin with induced circulation is the most effective configuration for creating and maintaining a stable vortex. Subsequently, Wanchat *et al*. (2013) conducted an experimental and computational study on a cylindrical basin with induced circulation and an outlet tube positioned concentrically within the vortex basin. The outlet diameter of the vortex chamber was also varied in the study for varying flow rates and vortex heads; Nevertheless, the study did not provide any insights into the impact of geometry or hydraulic parameters that could be beneficial for GWVPP design.

In addition, Dhakal *et al*. (2015) used experimental and CFD data to compare cylindrical and conical vortex chambers. Except for the outlet tube geometry used by Dhakal *et al*. (2015), all geometric parameters were kept constant for the study. In Fig. 15, the altered outlet tube geometry is displayed. The basin's top diameter and height were reported to be 600 mm and 850 mm, respectively. Under similar head and flow conditions, geometrical parameters for both basins were developed. The power produced in these basins with the runner position adjusted along the vertical axis was compared using the runner having six blades, the one seen to be most efficient at various positions. The numerical and experimental study results indicated that the conical basin has the highest output power and efficiency. According to experimental results, the maximum efficiency for a conical and a cylinder basin was 36.84% and 27.74%, respectively (Dhakal *et al*., 2014).

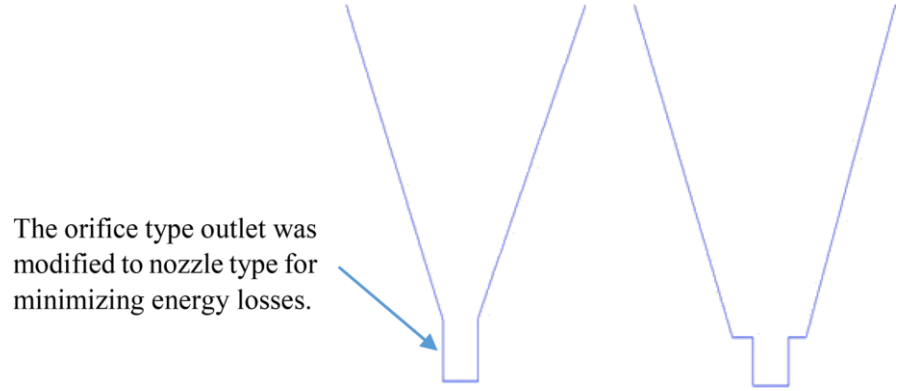

Figure 15: The basin geometry used by (Dhakal *et al*., 2015) and used by (Dhakal *et al*., 2014) on the left and right, respectively

Shabara *et al.* (2015) investigated the use of the commercial CFD code ANSYS Fluent to investigate the validity of the water vortex created by the model. The results demonstrate that ANSYS Fluent can model the water vortex system with acceptable error levels. The study does not, however, fully disclose all of the CFD model's specifics.

Gautam *et al.* (2016) examined how coupling multiple runners on the same shaft affects power production in the basin proposed by Dhakal *et al*. (2015). The investigation commenced with a 3D steady-state, single-phase numerical simulation of a conical basin equipped with a turbine runner within a vortex, utilizing ANSYS Fluent. Subsequently, an experimental study was conducted. The findings revealed that coupling these runners enhances their efficiency. During the experiments, the power generated was 6% higher compared to using a single runner to achieve maximum efficiency.

The ANSYS CFX was employed by Khan *et al*. (2018) to simulate a cylindrical basin with a stepped inlet. A parametric study was conducted by varying the geometric parameters like basin aspect ratio, basin diameter, and outlet diameter, along with the flow parameter of inlet velocity. The study examined the influence of these parameters on the water vortex's height, the increase in tangential velocity of water, the presence of an air core, and the velocity components in terms of cylindrical coordinates. The findings of this research were subsequently discussed and published in Chattha's work (Chattha *et al.*, 2017). Other researchers used ANSYS CFX to analyze various runner profiles before conducting actual experiments (Dhakal *et al.*, 2017; Khan *et al.*, 2018). Based on the results from both the computational and experimental studies, it was determined that curved blade profiles are more efficient compared to flat blade profiles. Dhakal's runner (Dhakal *et al.*, 2017) exhibited a curved top view, in contrast to the curved side view observed in the runner utilized by Khan *et*

al. (2018). Furthermore, according to Kueh's research, the runner features a curved exit part when viewed from the side (Kueh *et al*., 2017).

Additionally, Faraji *et al*. (2022) optimized two runner profiles (flat and curved) by changing four variables (speed, blade-hub angle, number of blades, and blade profile). According to the study, flat profile blades had an efficiency range of 8.08 to 23.32%, while curved profile blades had a range of 9.80 to 25.89%.

2.6.2 Experimental Studies

Mulligan and Casserly (2010) were the first to publish experimental studies on the vortex chamber for hydropower production. Due to the gravity-dominated free-surface conditions created in the vortex chamber, the Froude similitude was used in these studies. During this experimental campaign, the authors investigated the impact of the vortex chamber's shape and changed the exit hole diameter (d) by varying the ratio d/D, where D represented the vortex chamber's diameter. They came to the conclusion that when 14% d/D 18%, the vortex's strength was at its strongest. Additionally, they deduced that low and high head sites correspond to the lower and upper ranges of d/D. In their studies, the authors found that the cylindrical vortex chamber lacks verticality because of the asymmetrical tangential velocity conditions caused by the inlet. To address this issue, they proposed modifying the velocity field to achieve an asymmetric distribution from the inlet, incorporating a logarithmic spiral chamber wall. Additionally, the authors validated the analytical equations used to estimate the pressure distribution in a free-surface vortex when a turbine impeller is absent by employing a spiral vortex chamber. However, the authors conducted additional research on subcritical vortex chambers in vortex drop shafts. However, it is still possible to apply the findings of these studies to the water vortex hydropower plant.

Later studies were conducted on a vortex chamber in which the approach flow channel's invert level is higher than the vortex chamber base (Bajracharya & Chaulagai, 2012). The creation of straightforward slider mechanisms allowed researchers to observe that the vortex structure remained continuous from the inlet to the vortex chamber and extended to the exit hole. The system was found to be unable to maintain a stable vortex as the orifice of these geometries was increased; as a result, a high discharge was necessary. The design of Bajracharya and Chaulagai (2012) was later modified into a novel conical basin by Dhakal *et al*. (2014), who also created an impulse-type runner. The runner employed in the study was a cross-flow turbine

theory-based impulse type (Dhakal *et al.*, 2014). For the Bajracharya and Chaulagai (2012) type basin and the recently proposed conical basin, vortex strength (circulation) was experimentally measured in the study. According to the findings, a greater circulation could be attained in a conical basin. Under identical flow conditions examined in the Bajracharya and Chaulagai (2012) study, it was also discovered that the conical basin's power generation efficiency was higher. When a large number of blades were used, the impeller under study by Dhakal *et al.* (2014) showed a significant distortion of the vortex flow. Similar blade profiles were used in the study to create impellers with 3, 6, and 12 blades, all with the same outer radius. When there are more blades, less power is produced, as demonstrated by measurements of output power using torque and impeller speed.

Experimental research on the effects of various turbine materials, including steel and aluminium, was conducted by Sritram *et al*. (2015). This study discovered that lighter materials, like aluminium used in the impulse type runner, could withstand the flow conditions, leading to higher efficiencies because the turbine self-weight was reduced. The increased efficiency was achieved without changing the angular velocity by producing more torque. In those three basins, Rahman *et al*. (2016) experimental testing examined the hydraulic efficiency of four different turbine configurations and the vortex profiles for three different hydraulic head configurations. The outcome demonstrated that greater runner rotational speed does not always equate to greater hydraulic efficiency. The maximum efficiency was discovered when the turbine's rotational speed was half the vortex's tangential velocity, which is similar to how it was described in Mulligan and Casserly (2010). In addition, the study finds that the turbine with the fewest number of blades has the highest hydraulic efficiency. The authors do not fully disclose the basin diameter and method used for the theoretical vortex profile prediction.

The impact of turbine baffle plates on efficiency was investigated by Wichian and Suntivarakorn (Wichian & Suntivarakorn, 2016). Five blades were evenly spaced around the circumference of the impeller, and baffle plates were added at the top and bottom of each blade. Five distinct models with various baffle plate areas were examined. At three different flow rates, the developed runners were put to the test. According to the study, a turbine with baffle plates produced a higher efficiency than one without. It was discovered that an impeller with 50% baffle plates was the most effective, whereas increasing the number of plates causes the torque to decrease.

Power *et al.* (2016) carried out an experimental parametric study to better understand the various GWVPP operating conditions. The impeller's rotational speed, vortex height, and braking force were all measured while changing various design parameters. The blade size and blade number are related to the impeller among the five parameters that were taken into account for the investigation. As blade size increases, the height of the vortex decreases, but the braking force increases (due to an increase in impeller weight and inertia), increasing power output and efficiency. A similar outcome was observed with more blades, which added to the weight. Beyond a certain weight, the runner's speed and power output, however, decrease. The height of the inlet pipe and the flow rate both had an impact on the system's input power, with the highest flow and height values indicating the system's maximum efficiency. The additional test was run with varying braking force at the highest efficiency setting determined from earlier tests. The ideal setting was found to be between zero and the maximum applied force, which will simply bring the turbine to rest. This discovery is connected to the turbine and vortex speeds by Mulligan and Hull (2010) suggested. In the study, the maximum efficiency of 15.1% was observed when the braking force was applied at 60% of what was necessary to bring the turbine to a complete stop (Fig. 16).

Figure 16: (a) Impeller arrangement and (b) impeller configuration with baffle plates (Wichian & Suntivarakorn, 2016)

Both hydropower and GWVPP technologies offer significant advantages as renewable energy sources, contributing to a reduction in greenhouse gas emissions and providing reliable energy. However, they also face challenges, including environmental impact, high initial costs, geographical limitations, and regulatory hurdles. While hydropower is well-established and capable of large-scale energy production, it comes with more significant environmental and social challenges. The GWVPP technology, on the other hand, is more environmentally

friendly and suitable for small-scale applications but is limited in power output and is still in the early stages of widespread adoption. This study focuses on enhancing the efficiency of the GWVPP runner by modifying the parameters that influence its performance. Using both numerical simulations and experimental methods, the research investigates four specific parameters: hub-blade angle, speed, runner profile, and the number of blades.

CHAPTER THREE

MATERIALS AD METHODS

3.1 Numerical Approach

The applied numerical approach was divided into two steps. The first step was the selection of a basin and canal which can produce an air-core vortex and higher gain in tangential velocities, along with a reasonable height of the vortex. The second step was the comparison of two blade profiles (flat and curved) to achieve maximum power output through variation of the number of blades, blade-hub angle and runner speed. As a result, the comparison of the optimum blade profile for use in the GWVPP experimental test rig was established. Figure 17 depicts the general numerical optimization flow path for this study.

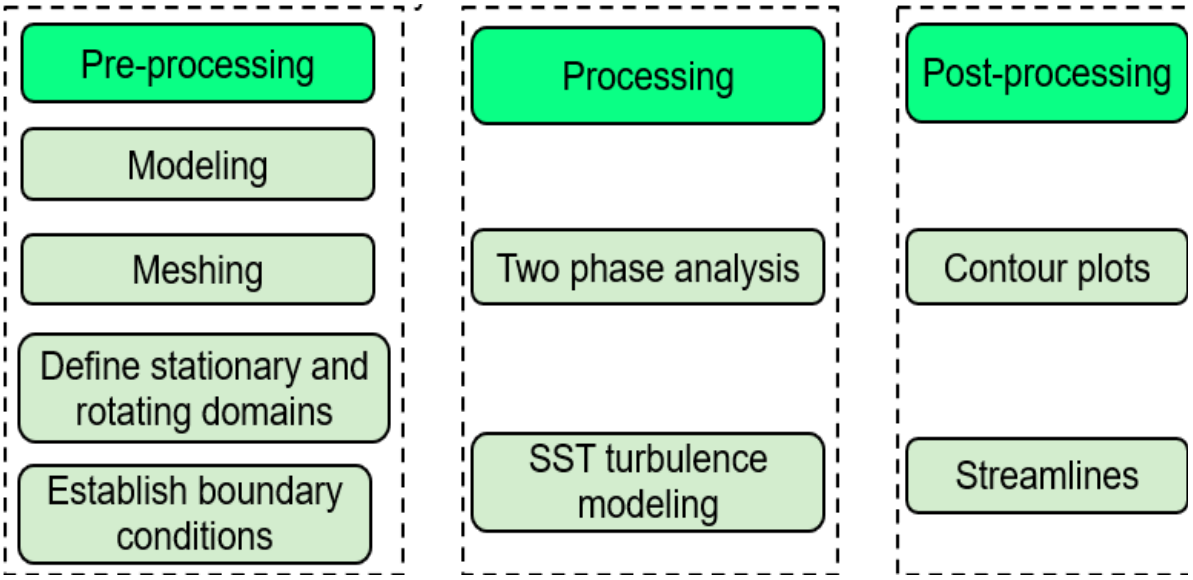

Figure 17: Numerical optimization flow process

3.1.1 Basin and Canal Selection

Literature suggests that the optimum basin diameter to outlet diameter ratio is 0.14 to 0.18 (Wanchat *et al.*, 2013). The literature information led to the selection of the basin. Moreover, the existing literature indicates that as the mean tangential velocity of water in a vortex basin rises, the water motion transitions from axial to tangential, resulting in an increase in the vortex's height and, consequently, an enhancement in vortex strength (Kueh *et al.*, 2014; Wanchat *et al.*, 2013). Hence, the emphasis was placed on choosing a basin that generates a free surface air core vortex with the highest attainable height and greater velocities at the core

of the vortex. For this purpose, a basin and canal were designed according to the dimension parameters shown in Table 1, where the basin parameters of basin diameter, basin height and basin outlet diameter are provided. The canal parameters include inlet width, depth, length, and notch angle. The 3D of the developed model containing the basin and canal is displayed in Fig. 18.

Table 1: Basin and canal parameters

Parameter	Basin Value	Canal Value
Basin diameter	1000 mm	NA*
Basin height	500 mm	NA
Outlet diameter	160 mm	NA
Inlet width	NA	100 mm
Inlet Depth	NA	150 mm
Canal length	NA	1750 mm
Notch angle	NA	165°

NA* Not applicable

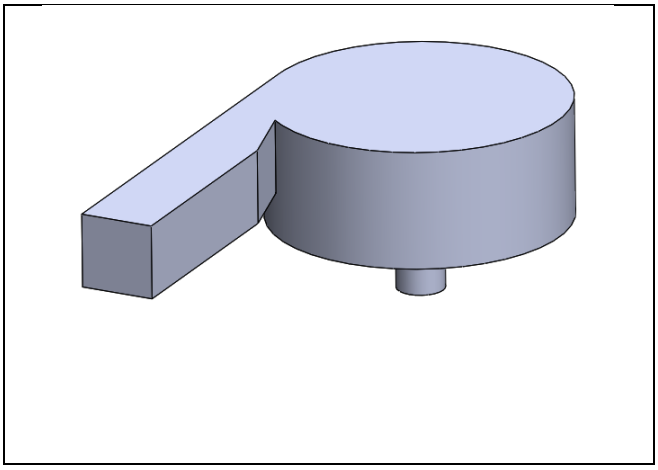

Figure 18: Model of the basin and canal

3.1.2 Models Development, Meshing and Analysis

Three-dimensional (3D) models of runner, canal and basin were developed by Computer-Aided Design (CAD) Solidworks software v.2017. The established models from the software were then transferred to Ansys ICEM for the meshing purpose. In addition, the meshed model from the Ansys ICEM was taken to the Ansys stand-alone CFX software to analyse and optimise the system by considering the selected parameters. Ansys ICEM and Ansys CFX were chosen for their complementary strengths in meshing and fluid dynamics simulation, ensuring that the

study's models are well-represented and the analysis is precise and comprehensive. The numerical analysis followed the following sequence. Firstly, the agreement of experimental results (for both flat and curved profiles) was checked using a numerical approach. The governing partial differential equations of fluid flow, commonly known as Navier-Stokes and continuity equations, have been discretized and solved over an area of interest with the known physically possible boundary conditions. The assumptions on computation were the steady, *viscous*, turbulent and incompressible flow. The continuity and Navier-Stokes equations are written in the Equations 1 - 4 as follows:

- Continuity equation:

$$\frac{\partial V_r}{\partial r} + \frac{\partial V_z}{\partial z} + \frac{V_r}{r} = 0 \tag{1}$$

- Navier-Stokes equations:

$$V_r \frac{\partial V_\theta}{\partial r} + V_z \frac{\partial V_\theta}{\partial z} - \frac{V_r V_\theta}{r} = v\left(\frac{\partial^2 V_\theta}{\partial r^2} + \frac{\partial V_\theta}{r\partial r} - \frac{V_\theta}{r^2} + \frac{\partial^2 V_\theta}{\partial z^2}\right) \tag{2}$$

$$V_r \frac{\partial V_r}{\partial r} + V_z \frac{\partial V_r}{\partial z} - \frac{V_\theta^2}{r} + \frac{\partial \rho}{\rho \partial r} = v\left(\frac{\partial^2 V_r}{\partial r^2} + \frac{\partial V_r}{r\partial r} - \frac{V_r}{r^2} + \frac{\partial^2 V_r}{\partial z^2}\right) \tag{3}$$

$$V_r \frac{\partial V_z}{\partial r} + V_z \frac{\partial V_z}{\partial z} + \frac{\partial \rho}{\rho \partial z} = g + v\left(\frac{\partial^2 V_z}{\partial r^2} + \frac{\partial V_z}{r\partial r} + \frac{\partial^2 V_r}{\partial z^2}\right) \tag{4}$$

In the given context, V_θ, V_r, and V_z represent the tangential, radial, and axial velocity components, respectively. The fluid density is denoted by ρ, gravitational acceleration by g, and kinematic viscosity by ν. The CFD model was used to study the hydrodynamics of the GWVPP runner model. The analysis of the model has been done by CFD package, CFX Ansys 17 tool to optimise the runner's output by changing parameters, namely, number of blades, hub-blade angle, rotation speed and blade profile. The complete simulation process is summarized in the form of a flow chart, as shown in Fig. 19.

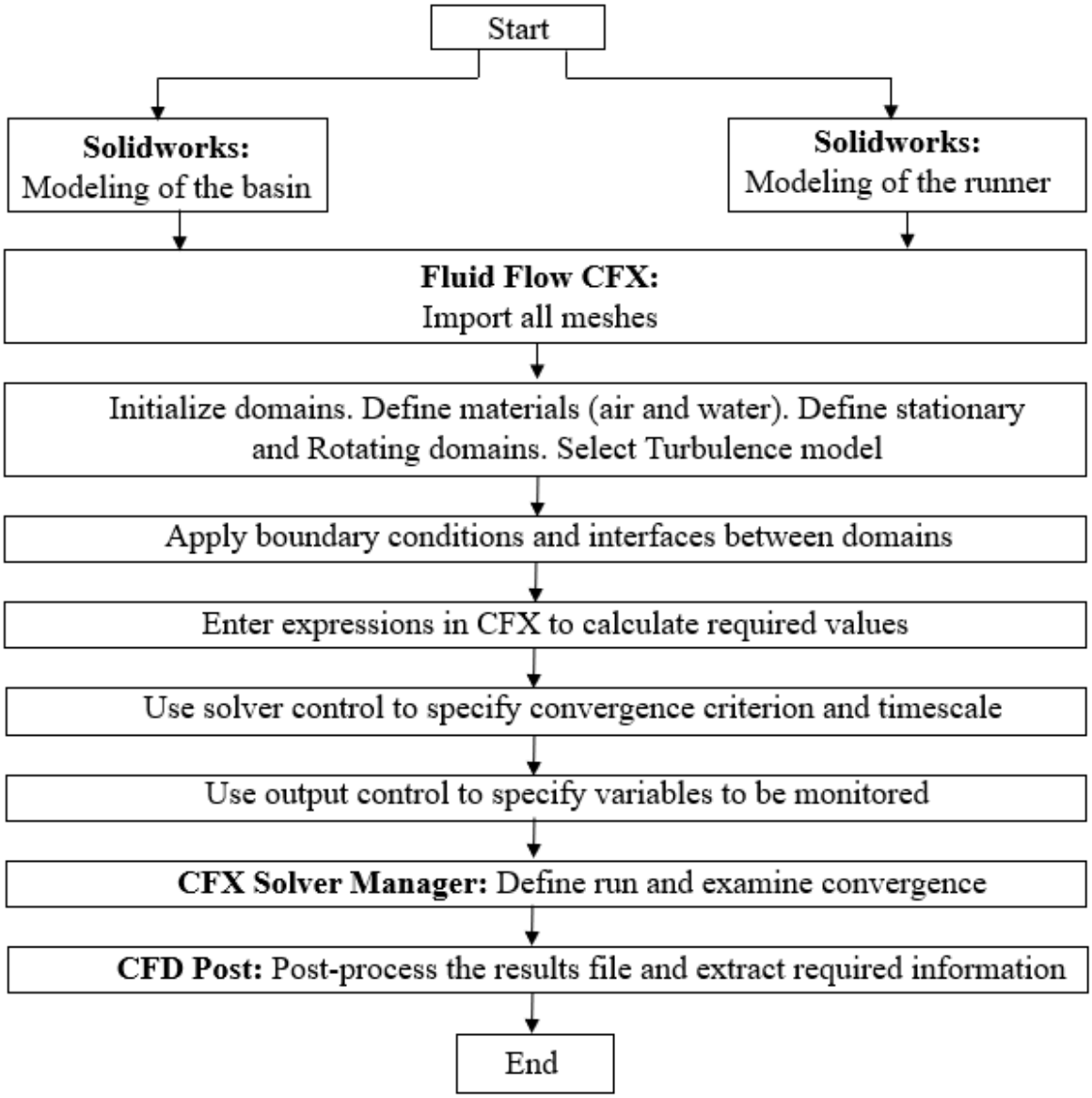

Figure 19: Simulation flow chart

A 1000 mm outer runner diameter contained four blades with a rotational speed of 4.08 to 2.5 rad/s. Figure 20 displays the base model of GWVPP. The entrance section, known as the canal, comprises the guide, which directs the water flow towards the basin. As the water enters the basin tangentially, it creates the runner's rotational velocity through blades; afterwards, the water is released into the outlet axially.

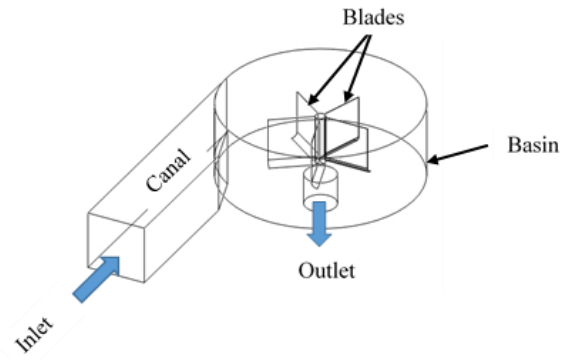

Figure 20: Three dimension (3-D) of the base case

The computational domains have primarily been divided into two parts. The first part encompasses a stationary domain, which includes the inlet, canal, runner-basin interface, opening, wall, and outlet. The second part comprises a rotating domain consisting of the runner and the runner-basin interface. Unstructured tetrahedral mesh computational grids were generated separately for both the stationary and rotating domains using Ansys ICEM CFD. After meshing each domain individually, all meshes were combined into a single computational domain within Ansys CFX. For a visual representation, please refer to Fig. 21 and Fig. 22, which illustrate the numerical mesh of the stationary domain (canal and basin) and the rotating domain (runner), respectively. To ensure the quality of the generated meshes, the Ansys ICEM tool was employed for verification and confirmation.

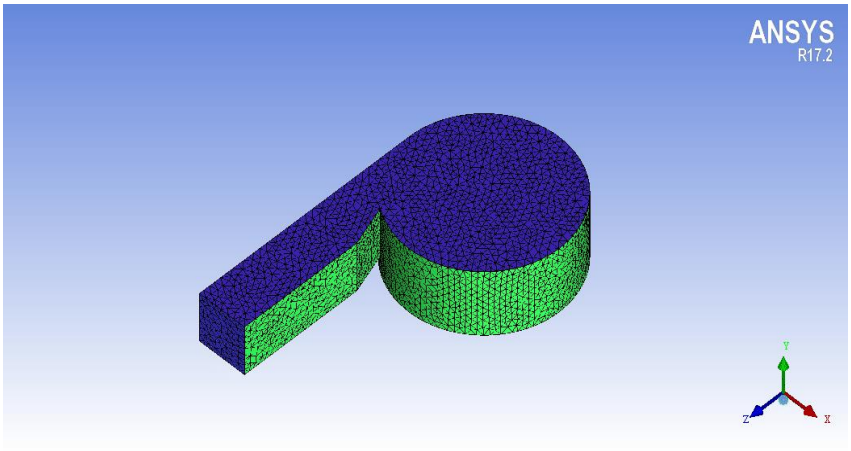

Figure 21: Numerical mesh in a stationary domain

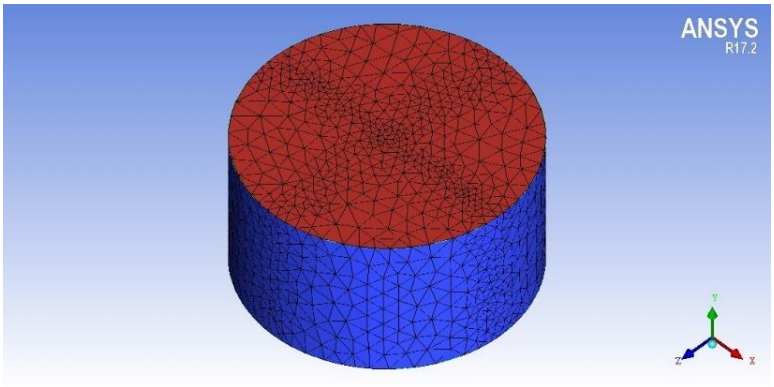

Figure 22: Numerical mesh in a rotating domain

The total number of nodes used for this analysis was 4 380 000. This number was achieved through testing of various meshes varying from 500 000 to 5 000 000 nodes. The node variation ensures the number of nodes does not compromise the final results (Inc., 2009). The outcome of the mesh dependency test is presented in Fig. 23. So, by observing Fig. 23, it was necessary to perform a mesh dependency sensitivity analysis. A general grid interface method was employed for the mesh connections between domains and interfaces. The SST turbulence model was considered to predict turbulence. Also, a two-phase flow, including air and water, was used and separated by a distinct interface during numerical analysis. The frozen rotor was set as a numerical treatment between the basin-runner interface. The set models' results gave a steady-state solution of the multiple frames of reference. The convergence criteria used was the root mean squared (RMS) with an average residual target of $1x10^{-4}$ considering mass, momentum and turbulence equations. The specific convergence criteria values were chosen to balance accuracy and computational efficiency, reflecting the accuracy requirements of the study and the available computational resources. They ensure that the simulation results are reliable and physically realistic while managing the computational effort required. These values are typically validated against convergence studies and established standards to ensure they are appropriate for the problem at hand. A physical time-step of 0.01 s, at the maximum iteration of 1000, was taken to achieve acceptable convergence. Moreover, Figure 24 displays the inlet section's mass flow rate and average static pressure at the stationary domain outlet. The design parameters and numerical boundary conditions are depicted in Tables 2 and 3, respectively.

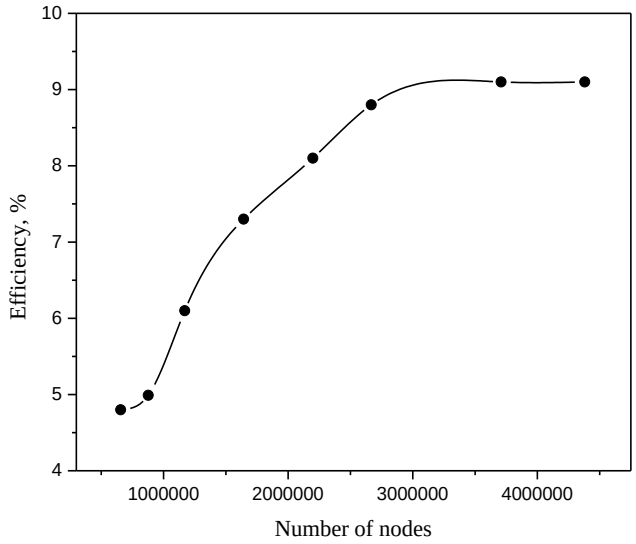

Figure 23: Mesh sensitivity analysis

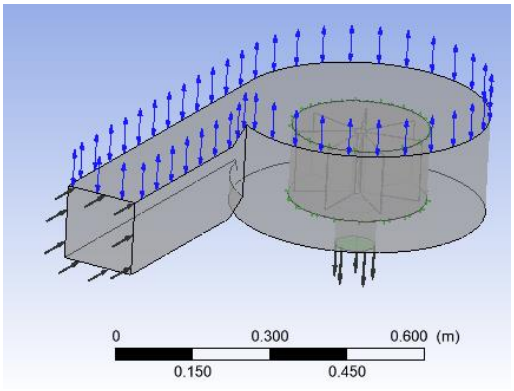

Figure 24: Base case setup

Table 2: Design Parameters

Head (H)	0.5 m
Number of blades	3 to 12
Hub-blade angle	15° to 22°
Rotational speed	Varying 2.5 to 4.08 rad/s

Source: Kueh *et al.* (2017)

Table 3: Numerical Boundary Conditions

Inlet	Mass flow
Outlet	Average static pressure
Turbulence model	Shear Stress Transport (SST)
Phase type	Phase (Air and Water at 25°C)

3.1.3 Base Model Validation

The base model, according to Kueh's experimental work (Kueh *et al.*, 2017), was developed for the numerical study. The numerical analysis parameters were extracted and listed, and their efficiencies were calculated based on the base model's parameters. The flow pattern and the velocity vectors were observed in each case. In the numerical analysis's first approach, Ansys CFX was used to check the base model's agreement with numerical analysis results.

3.1.4 Selection of Optimal Parameters (Experimental Design)

To eliminate the limitation of One Factor At-Time (OFAT), Response surface methodology (RSM) was employed to investigate the variables' effect on the GWVPP's performance. The RSM is a statistical, theoretical, and mathematical technique for model-building to optimise independent variables (Myers *et al.*, 2016). This tool is found in Design-Expert software. Factors used by RSM include runner speed (A), hub-blade angle (B), the number of blades (C) and blade profile (D). The RSM is designed along with coded and uncoded levels are presented in Table 4. Optimal (custom) design and quadratic model were used to design this experiment. Twenty-four runs (24), including five (05) interior points, eleven (11) vertex points, six (06) plane points and two (02) edge points, were randomly performed. In RSM using Design-Expert, "coded levels" are standardized values of factors (e.g., −1 to 1) used for simplified analysis, while "uncoded levels" are the actual real-world values applied in the experiment.

Table 4: Independent Variable (RSM Optimal Custom)

Independent variable	Symbol	Factor	Coded low	Coded high
Runner speed (rad/s)	A	Numeric	2.62	4.08
Hub-blade angle	B	Numeric	15°	22°
Number of blades	C	Numeric	3	12
Blade profile	D	Categoric	Flat	Curved

3.1.5 Theoretical Performance Optimisation of the System

The numerical analysis was used to perform an analysis that the braking system (in the experimental study) failed to provide due to significant friction torque requirement during experimental analysis, as reported by Kueh *et al*. (2017). The tested factors include the number of blades varying from 3 to 12, hub-blade angle ranging from 15° to 22° at an interval of 1° and runner rotational speed ranging from 2.62 to 4.08 rad/s. This approach aimed at determining these factors' effect on the final performance of the GWVPP. Optimal selection and combination of the parameters were achieved through design expert software v.13. As a

result, the efficiency of the base model and the final efficiency of the optimised model were related. Additionally, the observation was made on the water flow pattern through the simulation tools such as streamlines.

3.1.6 Theory

Both transient and steady-state equations can be solved using the Ansys CFX solver. Equations 5 and 6 show how to express the mass and momentum equations (Inc., 2009):

$$\frac{\partial \rho}{\partial t} + \nabla.(\rho U) = 0 \tag{5}$$

Where ρ stands for density, U shows the velocity vector $U_{x;y;z.}$

$$\frac{\partial(\rho U)}{\partial t} + \nabla.(\rho U \otimes U) = -\nabla p + \nabla.\tau + S_M \tag{6}$$

Where S_M stands for the external source term momentum, $\otimes$ displays a dyadic symbol and stress tensor τ, the is related to the strain rate (Inc., 2009).

$$\tau = \mu(\nabla U + (\nabla U)^T - \frac{2}{3}\delta \nabla. U) \tag{7}$$

Where μ represents molecular viscosity and T represents static temperature. The velocity fields are computed using the mass and momentum conservation equations in numbers 5 and 6. The final efficiency of the turbine is the criterion used to assess its performance. Efficiency is the ratio of the runner's input power to output power.

3.1.7 Theoretical Power

The following steps can be taken to obtain hydropower's maximum power output (Timilsina *et al.*, 2018):

$$P = \rho g Q H \tag{8}$$

Where Q is the flow rate, and H is the site's gross head.

The performance of GWVPP is obtained using its output efficiency, just like with conventional hydropower. The GWVPP runner is categorised as a hybrid turbine that combines an impulse and a reaction, and the power output is given in Equation 9 (Mulligan & Casserly, 2010):

$$P_{out} = T\omega = \frac{Q\rho(v_i - v_b)r\omega}{r\omega} \quad (9)$$

Where T is the torque at the shaft, ω is the angular velocity, and P_{out} is the shaft power of the runner.

The CFD-Post processing tool's function calculator was utilized to compute the interface velocity, runner blade velocity, and generated torque. A rotating domain was assigned to a runner. The runner's rotation axis is chosen to be in the y-direction. Equation 10 was used to calculate the angular velocity ω:

$$\omega = \frac{2.N.\pi}{60} \quad (10)$$

Thus, Equation 11 can be used to determine the turbine's efficiency:

$$\eta = \frac{(v_i - v_b)r\omega}{gH} \quad (11)$$

where v_b represents the blade velocity, and v_i represents the interface velocity.

3.2 Experimental Setup

The experimental test rig is shown in Fig. 25. The experimental system comprises the 1000-litre water storage tank, a 2-hp centrifugal pump, a 1000-litre overhead reservoir, a GWVPP basin, a canal, and a runner assembly. The water from the storage tank was pumped to the overhead reservoir. Additionally, to prevent water from the pump from directly flowing into the canal, the water is kept in an overhead reservoir and then guided to the canal only by gravity. A ball gate valve linked to the pipe from the overhead reservoir was adjusted to regulate the water flow rate and create the vortex height. A guide vane constructed of a small metallic sheet in the upstream channel was welded to produce a notch angle. As a result, the water was allowed to enter the basin tangentially via the canal. The basin and canal were positioned above the water storage tank. The outflow from the basin was collected by the water storage tank and recirculated using a centrifugal pump. The GWVPP runner has been designed to optimize the experimental design with specific parameters such as a 16° blade-hub angle, six blades, and a curved blade profile. These parameters were selected based on my previous study (Faraji *et al.*, 2022). In addition, replicates or controls were incorporated into the design to ensure that the data obtained was reliable and statistically significant. The performance of the GWVPP runner was evaluated by measuring the rotating speed (by using a digital tachometer RS 445-9557) and torque (using a prony brake dynamometer) at various operating speeds. The experimental

test rig was positioned at the main campus of the Nelson Mandela African Institution of Science and Technology (NM-AIST). Figure 26 illustrates the production drawings of the runner for: (a) Orthographic view and (b) Isometric view. The provided drawings were used during the fabrication of the runner.

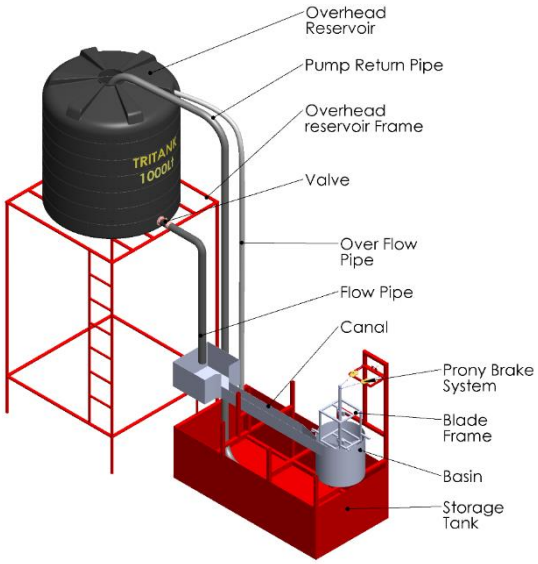

Figure 25: **Three-dimensional GWVPP** experimental setup

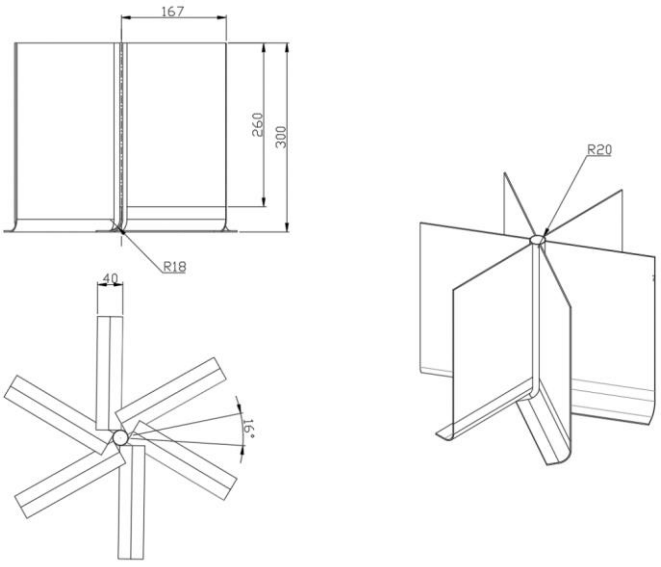

(a) (b)

Figure 26: **Curved runner (a) orthographic view (b) isometric view, all dimensions are in mm**

Other components that were essential for developing the experimental setup are presented in subsections (a) – (f).

(a) Blade frame/support: To keep the blades securely in place along the axis of the vortex core, a frame of mild steel sheet and angle iron were utilized. In addition, two bearings (CFK P206) were installed in the top frame to provide for frictionless contact.

(b) Overhead reservoir frame: The frame to support an overhead reservoir was fabricated from the black pipe steel of class B. Frame specifications is shown in Table 1.

(c) Pump: Water was supplied to an overhead reservoir by a pump. The pump was a two-hp centrifugal pump with 120 litres per minute discharge capacity. In addition, a pump was utilized to transfer water from the storage tank to the overhead reservoir.

(d) Piping: A flexible pipe of 50 mm diameter was utilised to supply water from the overhead reservoir to the inlet of the basin. A ball valve was used to control the flow rate.

(e) Storage tank: A storage tank was installed to create a closed loop of water flow to prevent wastage. The water from the basin outlet was collected in the storage tank and then pumped back to the overhead reservoir. The water storage tank with a capacity of 1 m^3 (1000 litres) was fabricated from a mild steel sheet.

(f) Overhead reservoir: An overhead reservoir was also considered to create an artificial flow to the canal. Direct flow of water from a pump to the canal was avoided because it is believed the pump would induce flowrate. The overhead reservoir eliminates the initial water velocity imposed by the water pump. Thus, the overhead reservoir stores the water that eventually flows to the canal inlet. The overhead reservoir was bought from stores with a capacity of 1 m^3 (1000 litres). The outlet of the overhead reservoir is coupled with a ball valve to regulate the water flow.

3.2.1 Materials Selection

Locally available materials, mainly steel, were utilized to fabricate the GWVPP experimental set-up (runner, canal, stand and basin). The reason for using steel to fabricate the experimental test rig was to facilitate the system's mobility and portability and reduce the cost of the system. A summary of the materials, specifications and the number of materials used to fabricate an experimental rig setup is given in Table 5.

Table 5: The Experimental Rig Setup Materials, Specifications and Quantity

Part	Materials	Specifications	Quantity
Basin	Mild steel sheet	1570x500x2 mm	1 pc*
Canal	Mild steel sheet	2100x400x2 mm	1 pc
Runner	Mild steel sheet	300x180x2 mm	6 pcs
	Black pipe	Φ50x300 mm	1 pc
Storage tank	Mild steel sheet	2000x600x2 mm	2 pcs
	Mild steel sheet	1000x600x2 mm	2 pcs
	Mild steel sheet	2000x1000x2 mm	1 pc
	Angle iron	40x40x3 mm	2 pcs
Runner support	Square hollow	20x20x1.5 mm	2 pcs
	section	40x40x3 mm	1 pc
	Angle Iron	Φ40x1200 mm	1 pc
	Mild steel shaft	CFK P206	2 pcs
	Bearing		
Prony brake	Square hollow	20x20x1.5 mm	1 pc
	section	Φ8x800 mm	1 pc
	Wire rope	M12x150 mm	1 pc
	Bolt and nut	12x12x300 mm	1 pc
	Iron block		
Overhead reservoir	Black pipe (class B)	Φ100x2500 mm	6 pcs
Frame	Square hollow	40x40x2 mm	4 pcs
	section		

* pc – piece

3.2.2 Basin and Canal Fabrication

The basin and canal structures were constructed with mild steel iron sheets. The specifications of the canal and basin are given in Table 1. The production drawings of the basin and canal are shown in Fig. 27. A metal sheet of the same material property was used at the inlet to alter the inlet width according to the optimized design of the basin. Based on the findings of Ansys CFX reported in previous work by Faraji *et al*. (2022), the dimensions of the optimized basin were used for the basin and canal fabrication.

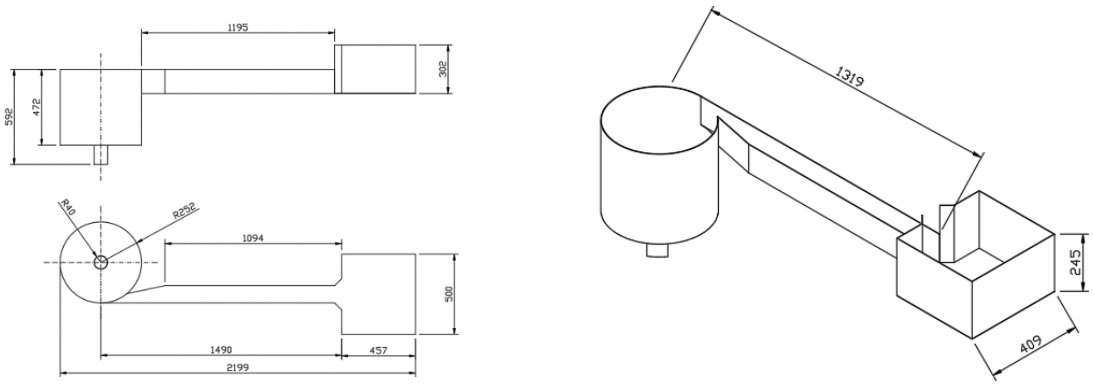

(a) (b)

Figure 27: Basin and canal (a) orthographic view (b) isometric view. all dimensions are in mm

3.2.3 Blade Fabrication

The runner for experimental work was a curved blade profile type with six (6) blades. The blades were all constructed from 1 mm mild steel sheets. The reason for using this material was to reduce the cost and acquire the runner's shape easily. The fabricated blades are shown in Fig. 28.

Figure 28: Fabricated blades for experimental setup (a) blades (b) blades with shaft support

3.2.1 Data Collection and Analysis

For experimental data collection, firstly, the flow rate was determined by closing the aperture at the basin's bottom and opening the overhead reservoir valve. A stopwatch was used to record the time it took to fill the basin. This flow rate measuring method is also known as bucket or volumetric. Some previous investigations employed the same approach to measuring open channel flow rate (Gheorghe-Marius & Tudor, 2013; Marian *et al.*, 2013; Nishi & Inagaki, 2017). Equation 12 was employed to determine the flow rate, Q, for the existing system.

$$Q = \frac{Volume\ of\ the\ basin}{Time\ spent\ to\ fill\ the\ basin} \quad (12)$$

The top frame is a black pipe class B that was fastened to the centre of the basin to support the shaft coupled with the bearings along the axis of the vortex air core. A Prony braking mechanism was utilised to measure the brake force (F) to determine the system's torque. A braking system was designed and installed at the runner shaft to measure the output power at various operating speeds. Furthermore, the braking system was tightened at various strengths to provide varying friction torques to the runner. The friction torque simulates the runner's operational load; hence, the required operating speed is determined. Moreover, scales were connected at both ends of the brake rope to quantify the tension force differential. The friction torque was calculated using this difference. Testing of the experimental test rig involved the determination of torque and rotational speed in revolution per minute (rpm) of the runner. A digital tachometer (RS 445-9557) measured the runner's rotational speed with a sensitivity of ±0.1rpm. The tachometer has a laser ray pointed to a reflector fixed on the runner blade whose speed is to be measured. The turbine was released to rotate freely. Then the runner's rotational speed was measured using a tachometer device (An average of three readings) was considered. Data collection began with the runner at rest, followed by flow initiation. Data collection started after the runner's rotational speed had been stable for about 20 seconds. As the brakes were applied, they caused the turbine to stop. In addition, during the experimental testing, the scale reading (scale 1 & scale 2) in gram (g) and the rotational speed in rpm of the blade were recorded. The system's output power, torque, and efficiency were determined by equations 13, 14 and 15, respectively.

The output power from the runner was determined using the following equation (Dhakal *et al*., 2017).

$$P_{output} = \frac{2\pi grN}{60} (M_{weight} - M_{counterweight}) \quad \text{(Dhakal } et\ al.\text{, 2017; Mulligan \& Hull, 2010)} \quad (13)$$

Where, r is the radius of pulley
M_{weight} is the mass of scale one
$M_{counterweight}$ is the mass of scale two

$$T = gr\Delta m \quad (14)$$

Where, g, is the acceleration due to gravity, r is pulley radius, Δm is the change in mass between scale 1 and scale 2.

$$\eta = \frac{T\omega}{\rho Q g H} \tag{15}$$

Where ω is rotational speed in revolutions per minute, H, is head.

3.2.2 Exergy Analysis of the System

The first law of thermodynamics is applied to determine the system's exergy. Exergy analysis is relevant to the study because it provides a detailed assessment of the system's efficiency by focusing on the quality of energy and identifying inefficiencies. It aids in optimizing system performance, comparing different technologies, and understanding sustainability impacts. By incorporating exergy analysis, the study can achieve a more comprehensive evaluation of the system and identify opportunities for improvement and innovation. The control volume of the GWVPP is considered an open system to conduct the system's exergy analysis (Fig. 29). The exergy analysis of a hydropower system for the control volume at a steady state is given by Equation 16 (Abuelnuor *et al.*, 2020).

$$0 = \sum \left(1 - \frac{T_o}{T_j}\right) \dot{Q} - W + \sum_i m_i e_{fi} - \sum_e m_e e_{fe} - E_d \tag{16}$$

where

T_j = temperature in the boundary (K).

T_o = temperature in the environment (K).

W = energy transfer via control volume (W).

m = mass flow rate (kg/s).

Q = heat transfer rate (W).

But,

$e_f = h - h_o - T_o(s - s_o) + 0.5\ (V^2) + gz$

h_o = enthalpy of the environment (kJ/kg).

h = enthalpy of the working fluid (kJ/kg).

V = velocity of the working fluid (m/s).

g = acceleration gravity (m^2/s).

s = entropy of the working fluid (kJ/kg K).

s_o = entropy of the environment (kJ/kg K).

E_d = exergy destruction due to irreversibility (W).

z = elevation (m).

The control volume operates at ambient conditions, which are assumed to be 25°C temperature, 1 atm of *static* atmospheric pressure, and 1,000 kg/m^3 density of water. These assumptions will reduce equation 16 to equation 17, which is utilized to calculate E_d :

$$E_d = \dot{m}\left[\left(\frac{c_1^2 - c_2^2}{2}\right) + g(z_1 - z_2)\right] - W \tag{17}$$

Where c_1 and c_2 are the water velocities in m/s at the inlet and outlet, respectively. Water velocities were determined through the division of flowrate by respective inlet and outlet areas and z_1 and z_2 are elevations in m at the inlet and outlet, respectively. Elevations were measured by taping measure, as shown in Fig. 29.

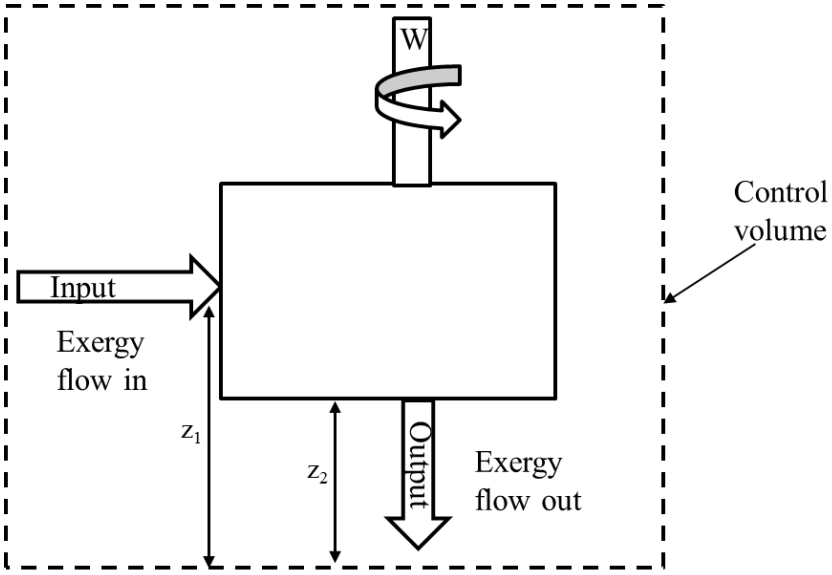

Figure 29: Schematic of exergy flow at the controlled volume of GWVPP system

Considering the conservation of energy of the controlled system, the steady flow energy equation (SFEE) is utilized to calculate the work done by the system. Equation 18 (Dixon & Hall, 2013) was utilized to determine the work-done in W of the system.

$$\dot{m}\left(h_1 + \frac{c_1^2}{2} + z_1 g\right) + Q = \dot{m}\left(h_2 + \frac{c_2^2}{2} + z_2 g\right) + W \tag{18}$$

Where h_1 and h_2 are the specific enthalpies at the inlet and outlet, respectively, $\frac{1}{2}c^2$ is the kinetic energy per unit mass, gz is the potential energy per unit mass, and W is the work (W).

For a hydraulic turbine, the assumption is that

(i) No heat transfer, Q = 0;

(ii) Work W = +W work produced

(iii) No change in internal energy; $u_1 = u_2$

Thus, $h_1 - h_2 = u_1 + p_1 v_1 - (u_2 + p_2 v_2)$

Since, $u_1 = u_2$

Then,

$$h_1 - h_2 = p_1 v_1 - p_2 v_2)$$

And equation 5 becomes

$$\dot{m}\left(p_1 v_1 + \frac{c_1^2}{2} + z_1 g\right) = \dot{m}\left(p_2 v_2 + \frac{c_2^2}{2} + z_2 g\right) + W \tag{19}$$

Thus, the exergy efficiency $\varphi = \frac{Exergy\ output}{Exergy\ input}$

$$\varphi = \frac{W}{W + E_d} \tag{20}$$

3.2.3 Experimental Error Analysis

In this study, an error analysis was conducted to identify and quantify sources of error in the experimental measurements. The tachometer used for speed recording, and the scales used for measuring masses were identified as potential sources of error. Since the experiment involved repeated tests, it was necessary to perform an error analysis to simultaneously capture the random uncertainty in measurement and the physical process (Bachynski *et al.*, 2019). To compute the random uncertainty of the experimental data, Equation 21 was used:

$$S_R = \frac{S_x}{\sqrt{N-1}} \tag{21}$$

Where S_x is the standard deviation of both speed and mass quantities.

The potential impact of errors on the tachometer and scale measurements on the power, torque, and efficiency parameters was taken into account by propagating the error. To assess the degree of error propagation, Equation 22 was utilized to determine the propagated error on power, while Equation 23 was utilized to determine the propagated error on torque. Furthermore, equation 24 was employed to compute the propagated error on efficiency (Figliola & Beasley, 2020).

$$\delta P = P\sqrt{\left(\frac{\delta\omega}{\omega}\right)^2 + \left(\frac{\delta\Delta m}{\Delta m}\right)^2} \tag{22}$$

$$\delta T = \delta\Delta m \tag{23}$$

$$\delta\eta = \eta\sqrt{\left(\frac{\delta T}{T}\right)^2 + \left(\frac{\delta\omega}{\omega}\right)^2} \tag{24}$$

CHAPTER FOUR

RESULTS AND DISCUSSION

4.1 Validation of the Results of Numerical against Experimental

The numerical validation process involved a meticulous analysis of the experimental test data conducted by Kueh *et al*. (2017), revealing a compelling level of concurrence between the numerical simulations and the actual experimental results. The outcomes of this validation effort are concisely presented in Fig. 30, which comprehensively showcases the combined numerical and experimental results obtained from conducting tests using both flat and curved blade profiles. The primary objective of these tests was to systematically evaluate the compatibility and agreement of the numerical approach with the established experimental method. By subjecting the numerical simulations to rigorous scrutiny against the experimental data, the researcher sought to assess the accuracy and reliability of the numerical approach in accurately capturing the complex phenomena under investigation. The comparison of the numerical and experimental results yielded encouraging outcomes, as they exhibited a commendable level of agreement. The small deviations observed between the numerical and experimental data serve as noteworthy points of discussion. Specifically, when examining the flat blade profile, a marginal deviation of merely 0.6% was observed at a rotational speed of 3.72 rad/s.

Similarly, a slightly higher but still negligible deviation of 1.11% for the curved blade profile was recorded at a rotational speed of 3.56 rad/s. These minimal discrepancies underscore the overall robustness and reliability of the numerical approach in accurately simulating the vortex system and reproducing the experimental findings. The successful validation of the numerical approach through its agreement with the experimental results holds profound implications for future investigations and optimization endeavours. The remarkable consistency between the numerical and experimental outcomes strongly indicates that the numerical approach can be effectively harnessed to investigate deeper into the dynamics of the vortex system. Leveraging the numerical simulations for the optimization process enables researchers to gain comprehensive insights into the underlying mechanisms governing the system's behaviour, thereby facilitating the refinement of design parameters and the enhancement of overall performance. The remarkable level of agreement between the numerical and experimental results also highlights the immense potential of the numerical approach in augmenting future

research endeavours. The numerical method offers a cost-effective and time-efficient alternative to extensive experimental testing. It proves to be an invaluable tool for studying complex phenomena and conducting parametric analyses in a virtual environment. Leveraging this capability can significantly expedite the design optimization process, enabling engineers and researchers to explore various design scenarios efficiently, ultimately leading to more efficient and effective design solutions. In conclusion, the numerical validation process, anchored in the experimental test data by Kueh *et al*. (2017), showcases a remarkable alignment between the numerical simulations and the experimental results.

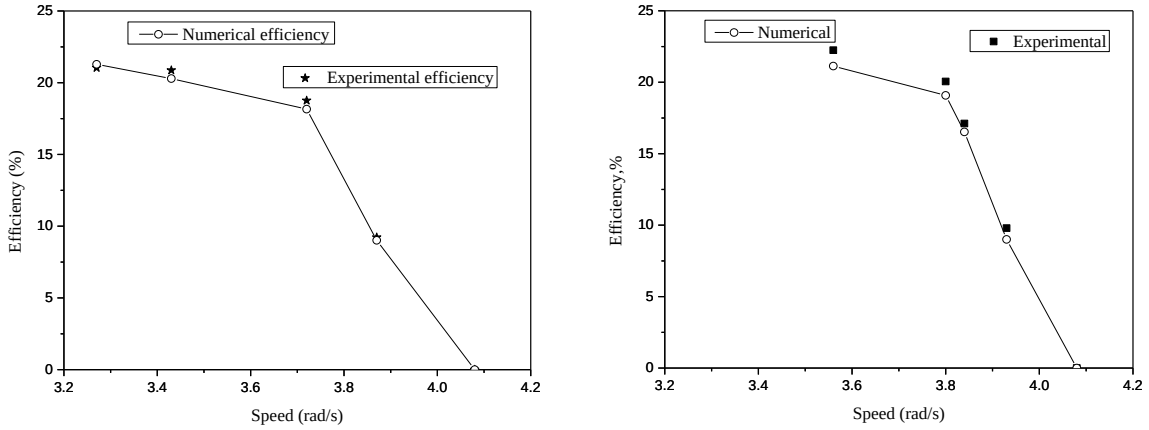

(a) (b)

Figure 30: Numerical versus experimental (a) flat blade profile (b) curved blade profile

4.2 Numerical Optimisation of Parameters by Response Surface Methodology

In the research study, the Design-Expert software played a crucial role in proposing the actual design parameters for the Gravitational Water Vortex Power Plant (GWVPP). These design parameters, along with their associated responses obtained through the utilization of Ansys CFX software, are meticulously presented in Table 6. This table serves as a comprehensive reference, showcasing the specific values of the design parameters and the corresponding responses, which could be numerical values representing the efficiency of the GWVPP. The output generated by the Design-Expert software proved to be highly valuable as it provided an unaliased quadratic model to analyze and predict the efficiency of the GWVPP. By employing this quadratic model, the researcher gained a deeper understanding of the intricate relationship between the design parameters and the overall efficiency of the GWVPP. The quadratic model offers a versatile framework for comprehending how to design parameter variations that impact the GWVPP's performance, providing valuable insights for subsequent analysis and optimization.

To capture the findings from the study, Equations 25-26 were derived, representing the final models of the quadratic equations for GWVPP efficiency. These equations were derived using the data and insights obtained from Design-Expert and Ansys CFX software. Equations 25-26 provide a concise mathematical representation of the complex relationship between the design parameters and the efficiency of the GWVPP. By plugging specific values for the design parameters into these equations, researchers and engineers can make accurate predictions about the efficiency of the GWVPP, enabling informed decision-making and optimization strategies. The integration of Design-Expert and Ansys CFX software in this research study showcases the power of utilizing multiple tools and approaches in the design and analysis process. Design-Expert facilitates the generation of a quadratic model, while Ansys CFX provides a robust platform for simulating and calculating the responses of the GWVPP efficiency. This integrated approach allows for a comprehensive exploration of the design space, enabling researchers to understand the underlying factors influencing the performance of the GWVPP.

In conclusion, the utilization of Design-Expert and Ansys CFX software, along with the subsequent derivation of quadratic models and equations, significantly contributes to the advancement of GWVPP design and optimization. The findings from this study, as presented in Table 6 and Equations 25-26, provide researchers and engineers with valuable insights to enhance the efficiency and sustainability of GWVPP systems, ultimately driving progress towards a cleaner and more renewable energy future.

Table 6: Simulated Factors and Their Responses

Run	Factor 1 A: speed rad/s	Factor 2 B: Angle °	Factor 3 C: blades	Response 1 Efficiency (flat) %	Response 2 Efficiency (curved) %
1	3.277	18	8	16.02	18.07
2	3.613	18	7	14.08	17.20
3	3.613	18	7	14.08	17.20
4	2.620	16	6	23.32	25.89
5	4.080	18	12	9.47	11.20
6	3.905	22	7	10.09	12.88
7	3.327	15	11	11.28	13.09
8	2.620	17	12	12.05	16.87
9	4.007	18	6	12.48	14.60
10	3.327	15	11	11.28	13.09
11	4.080	15	12	8.5	9.80
12	3.182	20	3	15.52	17.30
13	3.606	22	12	11.82	13.35
14	3.606	22	12	11.82	13.35
15	3.080	15	8	17.42	18.20
16	2.890	15	3	17.55	20.63
17	4.080	22	3	8.08	11.54
18	2.620	22	6	19.32	21.03
19	2.620	20	7	19.89	21.50
20	3.613	18	7	17.02	18.74
21	4.080	15	3	9.11	12.06
22	3.182	20	3	15.25	16.90
23	2.839	19	3	18.42	21.24
24	2.620	22	12	13.87	15.55

Efficiency (flat profile)

$$= 24.3584 - 7.60184A + 2.11494\,B - 1.40191C - 0.0393932AB + 0.588195AC + 0.0671479BC - 0.171252A^2 - 0.0674256B^2 - 0.142724C^2 \quad (25)$$

Efficiency (curved profile)

$$= 24.3584 - 7.60184A + 2.11494\,B - 1.40191C - 0.0393932AB + 0.588195AC + 0.0671479BC - 0.171252A^2 - 0.0674256B^2 - 0.142724C^2 \quad (26)$$

4.3 Statistical Analysis

4.3.1 Model Fitting

The effects of various independent variables on the performance of the GWVPP (Gravitational Water Vortex Power Plant) efficiency are presented in Table 6. These independent variables include runner speed (A), hub-blade angle (B), the number of blades (C), and blade profile (D). The results obtained from the experimentation show that the efficiency of the GWVPP was influenced differently by these variables. Specifically, the efficiency of the curved blade profile increased by 3.65%, indicating its superiority over other profiles. On the other hand, the flat blade profile showed a comparatively smaller improvement of 1.69%. To further analyze the relationship between the independent variables and the response variable, coefficients of the quadratic equation were derived from the experimental data. These coefficients enabled the prediction of the values of the response variable based on the given independent variables. In order to evaluate the adequacy of the model, the lack of fit F-value was computed for both blade profiles. In the case of the flat profile, Table 8 reveals a lack of fit F-value of 1.02, suggesting that the lack of fit is insignificant compared to the pure error. Similarly, for the curved profile, the F-value was found to be 4.26, indicating that the lack of fit is also insignificant in this case. Table 7 provides additional information on the response transformation and the fitting of the model, which aids in understanding the relationship between the independent variables and the efficiency of the GWVPP.

Table 7: Response Transformation and Model Fitting

Response (Efficiency)	Response range	Ratio*	Fitting	Transformation
Curved	9.80 – 25.89	2.64	Quadratic	None
Flat	8.08 – 23.32	2.89	Quadratic	None

* Ratio of maximum to minimum response

4.3.2 Analysis of Variance

Analysis of Variance (ANOVA) was conducted to ensure the validity and reliability of the derived model. The ANOVA aimed to assess the model's goodness of fit by testing the regression model's significance and the lack of fit coefficient. The evaluation was based on the determination of the F-value, which represents the confidence level, and the p-value, which indicates the probability value associated with the model's significance. Table 8 presents the results of the ANOVA, showcasing the outputs obtained from Equation (25) and (26). The F-

values of the GWVPP efficiency model for the flat profile and curved profile were found to be 30.02 and 37.62, respectively. Furthermore, the corresponding p-values for both profiles were determined to be less than 0.0001. These F-values and p-values provide crucial information regarding the significance and statistical accuracy of the models.

The high F-values and extremely low p-values indicate that the derived models are indeed significant and statistically accurate. The probability of obtaining such high F-values by chance or noise is only 0.01%. Therefore, it can be concluded with a high degree of confidence that the terms A, B, C, AB, AC, BC, A^2, B^2, and C^2 are all significant factors in the model. The ANOVA results provide strong evidence that the selected independent variables significantly impact the GWVPP efficiency. The models' confidence level and statistical accuracy confirm the reliability of the derived equations and their ability to explain and predict the efficiency of the GWVPP based on the given factors.

Table 8: ANOVA for the Quadratic Model

	Flat profile					**Curved profile**				
Source	**Sum of Squares**	**df**	**Mean Square**	**F-value**	**p-value**	**Sum of square**	**df**	**Mean square**	**F-value**	**p-value**
Model	316.54	9	35.17	30.02	< 0.0001	348.20	9	38.69	37.62	< 0.0001
A-speed	161.28	1	161.28	137.65	< 0.0001	178.28	1	178.28	173.37	< 0.0001
B-Angle	0.01	1	0.0103	0.0088	0.9265	1.82	1	1.82	1.77	0.2047
C-blades	27.94	1	27.94	23.85	0.0002	34.59	1	34.59	33.63	< 0.0001
AB	0.07	1	0.0658	0.0562	0.8161	5.38	1	5.38	5.23	0.0382
AC	25.84	1	25.84	22.05	0.0003	13.87	1	13.87	13.49	0.0025
BC	9.29	1	9.29	7.93	0.0137	11.83	1	11.83	11.51	0.0044
A^2	0.03	1	0.0305	0.0260	0.8741	3.55	1	3.55	3.45	0.0843
B^2	2.84	1	2.84	2.42	0.1421	8.98	1	8.98	8.74	0.0104
C^2	37.18	1	37.18	31.73	< 0.0001	31.73	1	31.73	30.86	< 0.0001
Residual	16.40	14	1.17			14.40	14	1.03		
Lack of Fit	10.60	9	1.18	1.02	0.5228	12.74	9	1.42	4.26	0.0625
Pure Error	5.80	5	1.16			1.66	5	0.3322		
Cor Total	332.94	23				362.59	23			

Table 9 provides a comprehensive summary of the statistical parameters derived from the study. The R^2 or the coefficient of determination, is a statistical metric that indicates the percentage of variation in the dependent variable (the outcome or target being predicted) that is accounted for by the independent variable(s) (the predictors) in a regression model. The closer the R^2 value is to 1, the better the model fits the data. The R^2 values obtained for the flat and curved blade profiles were found to be 0.9507 and 0.9603, respectively. These R^2 values demonstrate that the quadratic model employed in this study adequately captures and describes the influence of the independent variables, including speed (A), hub-blade angle (B), blade number (C), and blade profile (D), on the GWVPP efficiency. The higher the R^2 value, the closer it is to one, indicating a better fit of the model to the actual data (Myers & Cook, 2016). In addition to the R^2 values, the predicted R^2 values for both the flat and curved profiles were compared to the adjusted R^2 values. This comparison revealed a strong correlation between the predicted and adjusted R^2 values, suggesting that the data obtained from Ansys CFX are accurate and that any deviations observed are insignificant. These findings further validate the predicted models, indicating that they can be effectively utilized to explore the design space.

Moreover, the study found that the predicted R^2 values of 0.8165 and 0.8555 for the flat and curved profiles, respectively, reasonably agree with the adjusted R^2 values of 0.9191 and 0.9348. The difference between the predicted and adjusted R^2 values is less than 0.2, further reinforcing the reliability and robustness of the models. Overall, the statistical parameters presented in Table 9, including the R^2 values, the correlation between predicted and adjusted R^2 values, and the agreement between predicted and adjusted R^2 values, provide strong evidence that the quadratic models employed in this study accurately represent the relationship between the independent variables and the GWVPP efficiency for both flat and curved blade profiles.

Table 9: Statistical Parameters

Parameter	Flat profile	Curved profile
Standard deviation	1.08	1.01
Mean	13.99	16.30
C.V. %	7.74	6.22
R^2	0.9507	0.9603
Adjusted R^2	0.9191	0.9348
Predicted R^2	0.8165	0.8555
Ade. precision	19.0980	23.0059

A graph comparing the actual data with the simulated data was plotted to assess the model's validity. This graph aimed to visualize and analyze the relationship between the experimented data and the predicted values. The residuals, which represent the difference between the experimented data and the predicted values, were also examined to evaluate the accuracy of the model.

Figure 31a–b depicts the correlation between the predicted and simulated data. The data points were observed to be clustered around the line of best fit, indicating a strong agreement between the simulated data and the predicted values. The absence of any noticeable abnormalities or deviations from the line of best fit further supports the validity of the models. The graph provides compelling evidence that the simulated data aligns well with the predicted values. The close alignment between the predicted and simulated data indicates that the model accurately captures the relationships between the independent variables and the GWVPP efficiency. This alignment also suggests that the model is capable of generating reliable and consistent predictions, as the simulated data closely matches the actual data without any significant discrepancies. Overall, the graph of actual versus simulated data, along with the observed correlation and absence of abnormalities, supports the conclusion that the model is valid and capable of accurately predicting the GWVPP efficiency based on the given independent variables.

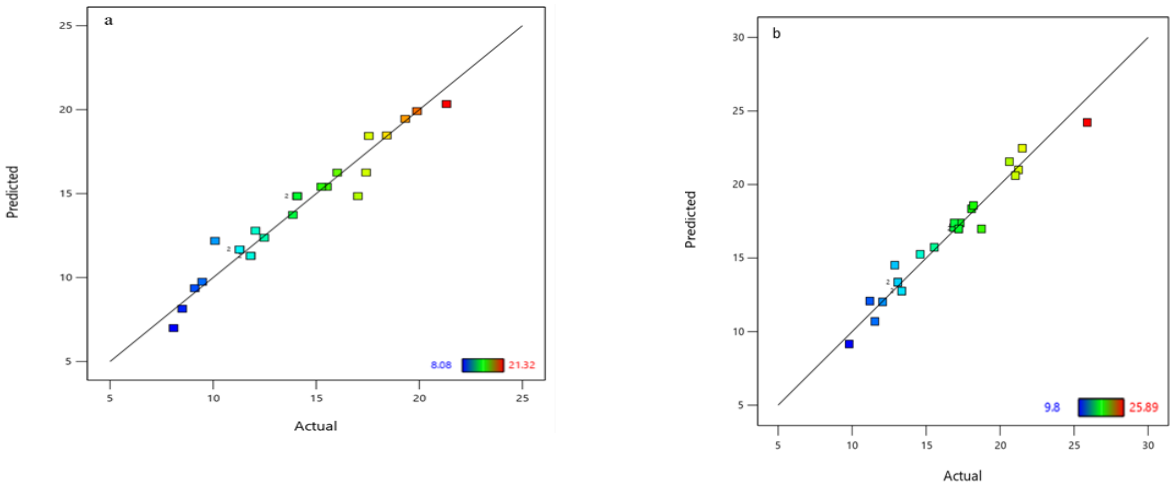

Figure 31: Predicted vs simulated values for the efficiency of (a) flat profile, (b) curved profile

4.4 Derived Models Interpretation

The Design-Expert software was utilized to generate response graphs, which offered a comprehensive and visually appealing representation of the interactions among the factors examined in this study. These response graphs played a crucial role in understanding the relationships between each parameter and their collective impact on the overall performance of the GWVPP (Wanchat *et al*., 2013). To capture the intricate interactions and visualize the effects of the independent variables, both three-dimensional (3D) plots and contour plots were employed. These plots provided a comprehensive view of the relationships between the factors and their contributions to the final performance of the GWVPP. In Fig. 32 – 34, the surface plots for both the flat and curved runner profiles were presented. These plots offer a multi-dimensional representation of the relationships among the independent variables and the GWVPP performance. Examining the surface plots makes it easier to comprehend the complex interactions and observe the effects of the individual parameters on the response variable. The 3D plots allow for a visual exploration of the response variable in relation to the changes in the independent variables. The contour plots, on the other hand, provide a two-dimensional visualization of the response variable by illustrating the lines of constant response along the planes defined by the independent variables. This enables a clearer understanding of the effects of each parameter and their combined influence on the GWVPP performance.

Overall, the response graphs obtained from the Design-Expert software, including the 3D and contour plots presented in Fig. 32 – 34, provide valuable insights into the interactions among the factors under investigation. These plots offer a powerful visualization tool to interpret the relationships between the independent variables and the performance of the GWVPP, enhancing our understanding of the system and aiding in the design and optimization processes. Figure 30 showcases the blending characteristic between two crucial factors: speed (A) and hub-blade angle (B). The surface plots presented provide valuable insights into the influence of these two factors on the final efficiency of the system, considering both the flat and curved blade profiles. Upon analyzing the surface plots, it becomes evident that both speed and hub-blade angle significantly impact the efficiency of the system being studied. The surface plots illustrate the complex interactions between these factors and their combined effect on the performance of the system.

It is worth highlighting that the optimal values leading to maximum efficiency differ based on the blade profile. For the flat blade profile, the surface plots indicate that the highest efficiency

is achieved at lower speeds, specifically in the 2.62 to 2.90 rad/s range. Within this speed range, the optimal hub-blade angle falls between 15 to 19 degrees. This finding suggests that a lower speed and a specific hub-blade angle contribute to achieving optimal efficiency for the system with a flat blade profile. On the other hand, for the curved blade profile, the surface plots indicate that the optimal efficiency is obtained at a lower speed range of 2.62 to 2.70 rad/s. Similar to the flat blade profile, the optimal hub-blade angle for the curved profile is observed to be between 15 to 19 degrees. The insights gained from these findings can guide the design and operation of the system, as they identify the specific combinations of speed and hub-blade angle that yield the highest efficiency for each blade profile. By focusing on the optimal speed and angle ranges, engineers and designers can make informed decisions to enhance the overall performance and efficiency of the system.

Figure 32 depicts the interactions between two important factors, speed (A) and hub-blade angle (B). These plots provide valuable insights into the contribution of speed and hub-blade angle to the performance of the GWVPP across all the profiles studied. It is evident from the plots that both parameters play a significant role in determining the performance of the GWVPP within specific ranges. Analyzing Fig. 32 (a) for the flat profile, a shallow bell-shaped structure can be observed. This indicates that the performance of the GWVPP is influenced by both speed and hub-blade angle, with an optimal range of values that leads to the best performance. The plot's shape suggests an interplay between these two factors, and their combined effect contributes to the system's overall efficiency. This finding aligns with existing literature on the subject, including the works of Dhakal *et al.* (2014), Khan *et al.* (2018), Rahman *et al.* (2017), and Timilsina *et al.* (2018) which also highlight the significance of speed and hub-blade angle in GWVPP performance.

On the other hand, Fig. 32 (b) reveals a strong bell-shaped structure in the interactions for the curved profiles. This indicates that speed and hub-blade angle have a pronounced impact on the performance of the GWVPP for the curved profiles. The distinctive bell-shaped structure emphasizes the importance of finding the optimal values for these factors to achieve the highest efficiency. The agreement of these findings with previous research further strengthens their significance and highlights the consistency of the relationship between speed, hub-blade angle, and GWVPP performance.

Overall, Fig. 32 provides clear visual evidence of the interactions between speed and hub-blade angle and their impact on the performance of the GWVPP across different profiles. The

presence of bell-shaped structures in both the flat and curved profiles underscores the critical role of these factors and their interplay in determining the system's overall efficiency. These findings align with existing literature, confirming the significance of speed and hub-blade angle in optimizing GWVPP performance.

Figure 33 examines the effects of interactions between factor A (speed) and factor C (number of blades). The plots provide insights into how these two factors influence the performance of the GWVPP. Notably, a clear bell-shaped structure is observed for the flat profile in Fig. 33 (a), while the plots for the curved profile in Fig. 33 (b) exhibit a twisting pattern. The bell-shaped structure seen in Fig. 33 (a) indicates that both speed and the number of blades have a significant impact on the performance of the GWVPP with a flat blade profile. The plot suggests that there is an optimal range of values for both speed and the number of blades that leads to maximum efficiency. Within this range, the system achieves its highest performance. The presence of the bell-shaped structure confirms the importance of appropriately selecting the values for speed and the number of blades to optimize the GWVPP's efficiency for the flat blade profile.

Contrasting this, Fig. 33(b) displays a twisting pattern for the curved profile. The twisting nature of the plot suggests a more complex interaction between speed and the number of blades for the curved profile. While there is still an optimal range of values for both factors, the twisting pattern implies that the interaction between speed and the number of blades is not optimally blended. This twist may indicate that achieving maximum efficiency requires balancing these two factors for the curved profile. This observation is consistent with past research (Khan *et al.*, 2018), which emphasizes the importance of finding the optimal combination of factors for GWVPP performance.

Additionally, it is noteworthy that the optimal values for maximum efficiency in both the flat and curved profiles correspond to lower speeds, ranging from 2.62 to 2.90 rad/s for the flat profile and 2.62 to 2.70 rad/s for the curved profile. Furthermore, the optimal number of blades falls within the range of 3 to 7 for both profiles. These findings highlight the importance of carefully selecting speed and the number of blades to achieve the best performance for the GWVPP system. Furthermore, the influence of factor B (hub-blade angle) and factor C (number of blades) on the performance of the GWVPP is examined to gain a deeper understanding of their impact. The flat and curved profiles are considered, and the corresponding plots are shown in Fig. 34 (a) and 34 (b), respectively. In both plots, a bell-

shaped structure is evident, indicating a significant relationship between the hub-blade angle and the number of blades with the performance of the GWVPP. This behaviour suggests that these two factors play crucial roles in determining the efficiency and overall performance of the system. The presence of the bell-shaped structure reinforces the findings of several studies in the literature (Dhakal *et al.*, 2017; Dhakal *et al.*, 2014; Khan *et al.*, 2018; Power *et al.*, 2016; Timilsina *et al.*, 2018).

These studies have consistently shown that the runner's speed follows a bell-shaped curve, implying that the performance of the GWVPP initially increases as the speed rises. However, after reaching an optimal speed, the performance starts to decline. The bell-shaped structure observed in Fig. 34 (a) and Fig. 34 (b) suggests a similar trend for the hub-blade angle and the number of blades. It implies that there is an optimal range for both factors that yields the highest efficiency of the GWVPP. Deviating from this range, whether by increasing or decreasing the values, leads to a decrease in performance. The agreement between these findings and the existing literature underscores the importance of carefully selecting the hub-blade angle and the number of blades to optimize the GWVPP performance. Designers and engineers can use this knowledge to identify the optimal range for these factors, ensuring the system operates at its peak efficiency.

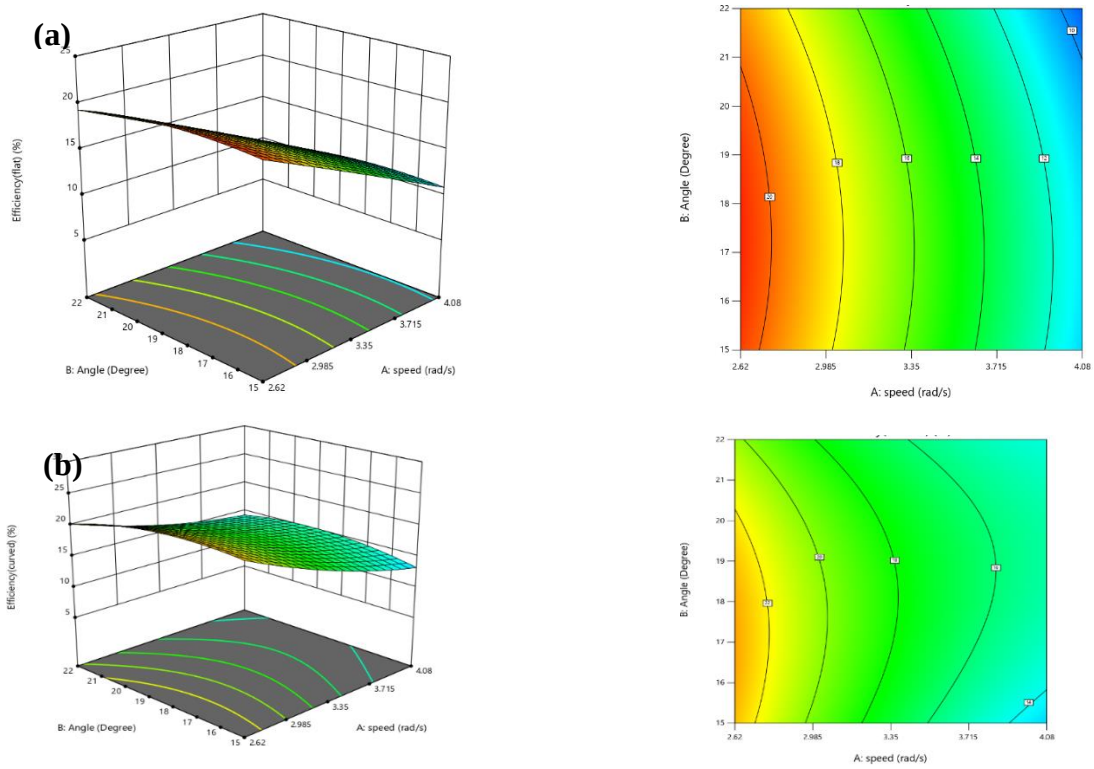

Figure 32: Three Dimensional Plot and contour for (a) flat profile, (b) curved profile (factors A and B)

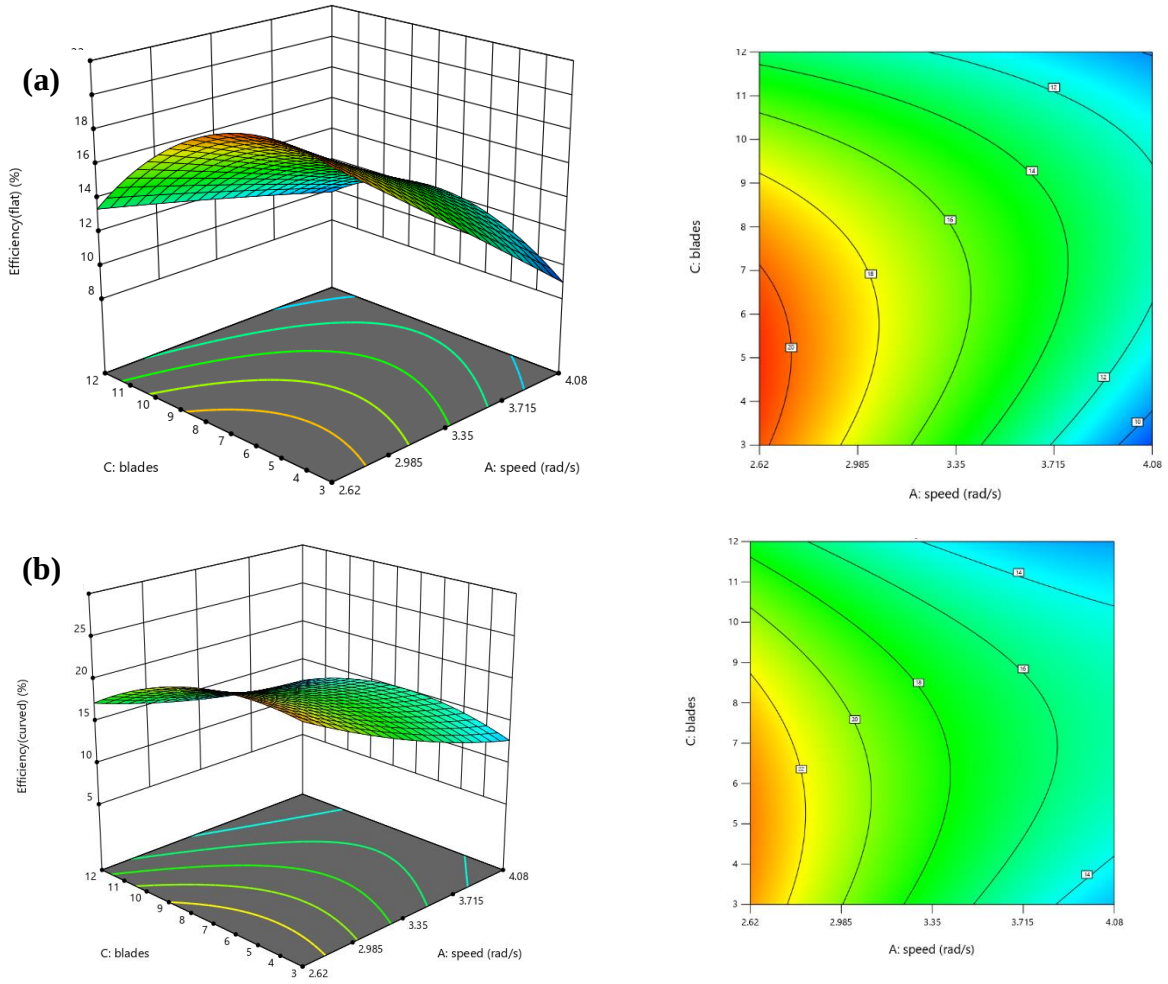

Figure 33: Three Dimensional Plot and contour for (a) flat profile and (b) curved profile (factors A and C)

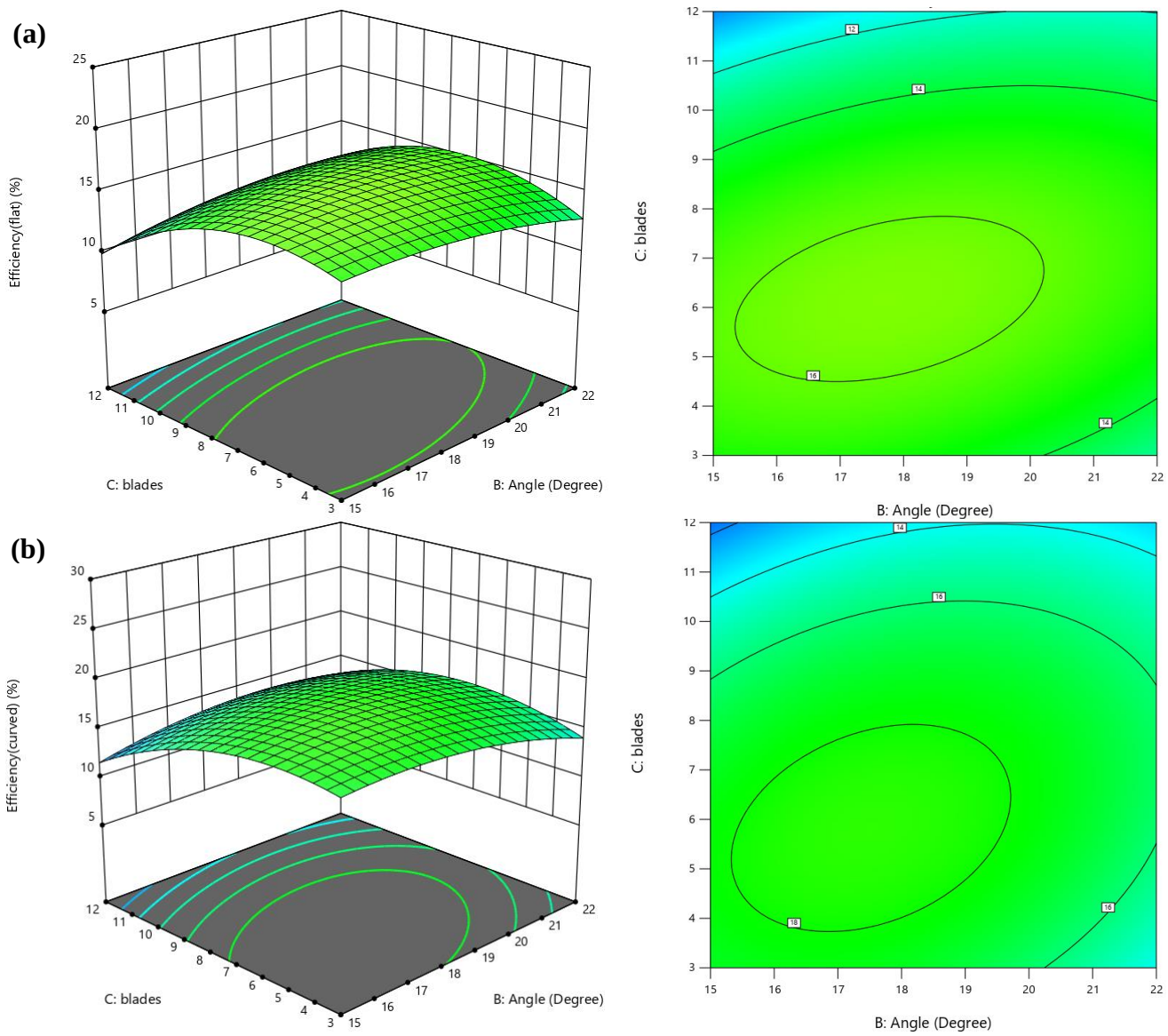

Figure 34: Three Dimensional Plot and contour for (a) flat profile and (b) curved profile (factors B and C)

4.5 Experimental Results

Figure 35 provides a comparison between the efficiency results obtained from numerical and experimental studies. The numerical results were obtained by considering various performance parameters such as rotational speed, number of blades, hub-blade angle, and blade profile, as documented in a previous study by Faraji and others (Faraji *et al.*, 2022). On the other hand, the experimental results were based on optimized numerical parameters and aimed to determine the performance efficiency of the GWVPP systems.

For the experimental performance (EP), the maximum efficiency achieved was 23.75% at a rotational speed of 33.08 rpm. In contrast, the numerical performance (NP) yielded a higher maximum efficiency of 25.89%. Although the numerical efficiency surpassed the experimental

results, the findings closely resemble the numerical analysis presented in my previous work (Faraji *et al.*, 2022). The higher values obtained in the numerical results can be attributed to the ideal conditions assumed in the numerical approach, where frictional forces were not considered.

Notably, a notable convergence between the numerical and experimental results was observed at a rotational speed of 33 rpm, with both approaches yielding an efficiency of 25%. Additionally, at higher rotational speeds, the centrifugal forces significantly impacted the vortex height, leading to increased torques on the runner blades (Khan *et al.*, 2018). Consequently, it can be concluded that, considering certain experimental limitations such as mechanical losses, the experimental design effectively predicts the results quantitatively and accurately.

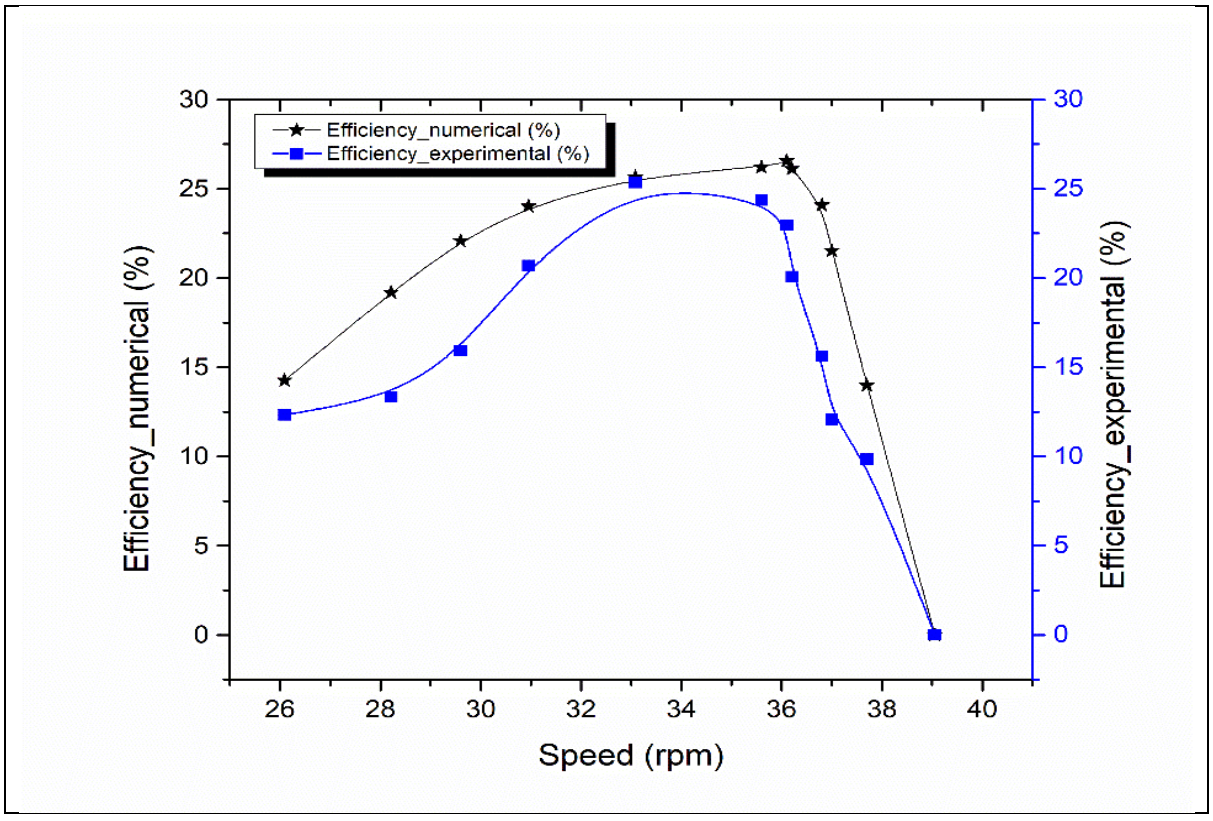

Figure 35: Efficiency versus rotation speed

4.5.1 Determination of Volume Flow Rate

Several calculations were performed based on the given parameters to determine the volume flow rate. Firstly, the volume of the basin was determined using the formula:

The volume of the basin = $\pi r^2 h$

The radius of a basin, r = 0.25 m

Height of the basin, h = 0.5 m

Then volume of the basin = 3.14 x (0.25 m)^2 × 0.5 m= 0.098125 m^3

Time t spent to fill the basin = 32 seconds

Then the volume rate, $\dot{Q} = \frac{Volume}{Time} = \frac{0.098125}{32}$ = 0.003066 m^3/s

Therefore, the volume flow rate is determined to be 0.003066 cubic meters per second (m^3/s). This value represents the rate at which the basin is filled with fluid over a given period.

4.5.2 Performance Analysis of GWVPP Runner

The performance results of the GWVPP runner showed that the output power varied between 2.96 and 7.33 W (Fig. 36), torque ranged from 0.08 to 0.23 Nm (Fig. 37), and efficiency ranged from 9.84 to 25.35% (Fig. 38). The efficiency presented in this study (25.35%) was slightly higher as compared the experimental studies (Kueh *et al*., 2017). The higher efficiency of a GWVPP runner exhibited in this study was due to optimised working parameters (speed, blade-hub angle, number of blades and blade profile) reported by Faraji *et al.* (2022) was 25.89%. The efficiency of experimental work is slightly lower, signifying that the numerical analysis assumed ideal conditions. Furthermore, performance curves were developed to understand each parameter better, as depicted in Fig. 36-38. The developed performance curves visually represent the relationship between the input and performance parameters, allowing for a more in-depth data analysis. The findings revealed that at a speed of 2.64 rad/s, the maximum power of 7.63 W and maximum torque of 0.231 Nm were observed, as shown in Fig. 34 and 35.

Additionally, the highest efficiency of 25.35% was achieved at the same speed, as depicted in Fig. 36. As reported in the literature, it is believed that at this speed, the vortex flow is stable and lacks distortion (Dhakal *et al*., 2017; Khan *et al*., 2018). Moreover, the stability and distortion-free vortex flow contribute to the excellent performance observed in the experiment. It provides a constant and uniform water flow to the turbine, resulting in maximum power, torque, and efficiency output. When the rotational speed is reduced through the braking system application, the performance parameters decrease due to the existence of a distorted vortex caused by flow disturbance of the vortex and change in water level in the basin. Therefore, optimal speed is crucial in ensuring the maximum output of the runner's power, torque, and

efficiency. The maximum power and torque observed at a rotational speed of 2.64 rad/s are noteworthy, as they indicate that this speed is optimal for the runner to perform at its highest level.

Furthermore, the findings show that the output power, torque, and efficiency are highly dependent on the rotational speed of the runner. Through the experimentation, the following findings were observed. A zero-output power, torque, and efficiency value correspond to the maximum rotational speed (3.26 rad/s) without braking force (load) on the shaft. Upon applying the load (through the braking system), the rotational speed decreased as the power, torque, and efficiency performance parameters increased. An increase in the performance parameter values while the rotational speed decrease suggests an increase in braking force and undistorted flow of the vortex, where this trend is supported by various literature such as Khan *et al*. (2018) in Fig. 7.

Further reduction of the rotational speed of 2.64 rad/s through the braking system application also decreases the performance parameters. This trend of reduction in performance parameter values is attributed to the existence of a distorted vortex due to flow disturbance of the vortex and change in the water level in the basin (Khan *et al*., 2018; Kueh *et al*., 2017). The performance parameters and rotational speed showed an inverse relationship until a maximum value was reached before the performance parameters started to decline, which aligns with the results of other similar studies such as Khan *et al*. (2018) in Fig. 9, Ullah *et al*. (2019) in Fig. 7-12 and (Saleem *et al*., 2020) in Fig. 16. Similarly, the literature reports that the highest efficiency is achieved when the runner's rotational speed is half the vortex's speed (Mulligan & Casserly, 2010; Rahman *et al*., 2016). The reason being the vortex flow creates a pressure gradient along the turbine blades, which causes them to generate lift and rotate. If the runner rotates too slowly, the lift generated by the blades will be insufficient to turn the turbine efficiently. On the other hand, if the runner rotates too quickly, the lift generated by the blades will be too high and cause unnecessary drag, reducing the turbine's efficiency.

These findings have practical implications for designing and optimising similar GWVPP micro hydropower systems. By understanding the relationship between input and performance parameters, engineers can optimize the system's efficiency and performance by adjusting the input parameters accordingly. Overall, the results of this study provide valuable insights into the design and operation of micro hydropower systems and can inform future research in the field.

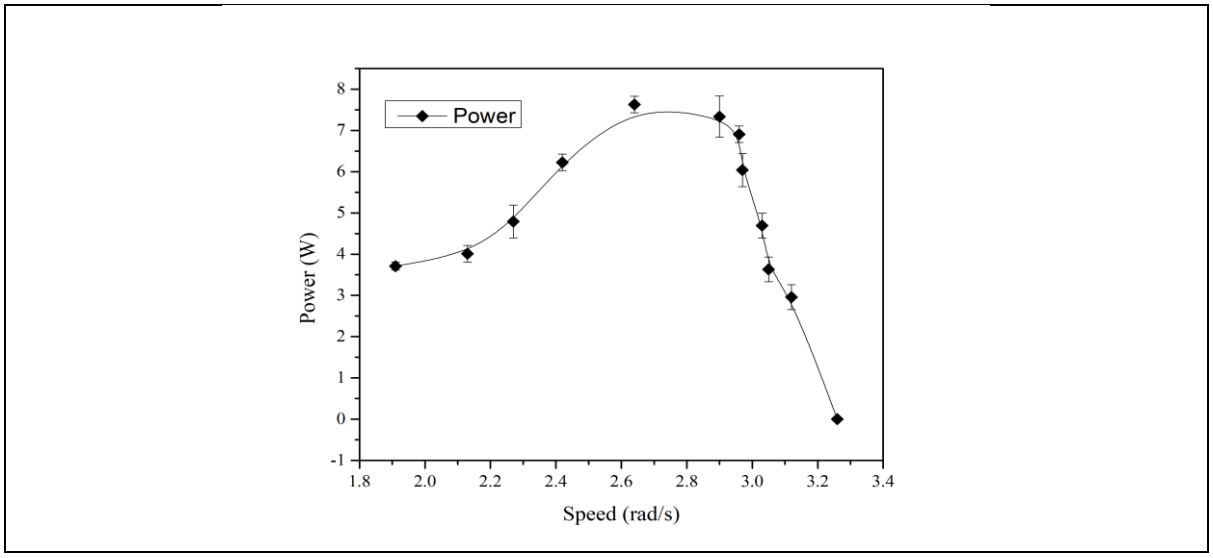

Figure 36: Effect of rotation speed on runner power

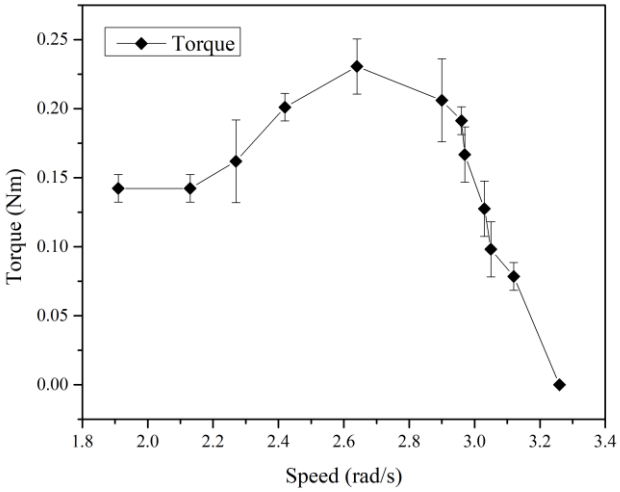

Figure 37: Effect of rotation speed on runner torque

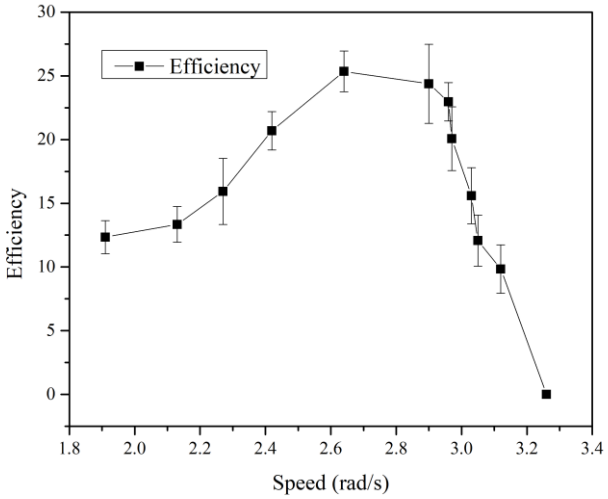

Figure 38: Effect of rotation speed on runner efficiency

4.5.3 Exergy Analysis

The exergy efficiency of the GWVPP runner was determined to be 43.58% using Equation 9. This exergy efficiency surpasses the values reported in other studies conducted by Hossain *et al*. (2020) (35.0% to 39.2%) and Maruf *et al*. (2021) (35.07% to 36.59%). The high exergy efficiency of the GWVPP runner can be attributed to the optimized working parameters of the experimental rig, including speed, blade-hub angle, number of blades, and blade profile. The obtained exergy efficiency of the GWVPP runner signifies the proportion of input energy that is effectively converted into useful work. It provides a measure of the valuable work that can be obtained from the available energy sources within the system. It indicates the extent to which energy is degraded into less useful forms, such as heat or waste (Rosen & Dincer, 2001). The exergy efficiency represents the quality of energy utilization in a system and quantifies the fraction of the maximum possible useful energy output over the input energy.

By achieving a higher exergy efficiency, the GWVPP runner demonstrates its capability to convert a significant portion of the input energy into useful work while minimizing energy degradation. This highlights the effectiveness of the optimized operational parameters in maximizing the utilization of available energy sources and minimizing energy losses in the system. The higher exergy efficiency obtained in this study indicates a more efficient utilization of energy resources, leading to improved overall performance and sustainability of the GWVPP runner.

4.5.4 Error Analysis Results

The error ranges reported for power, torque, and efficiency measurements play a crucial role in assessing the reliability and accuracy of the experimental results. In this study, the power error range varied from 0.1 to 0.5 W. Examining Fig. 34, it is evident that the power measurements exhibit a high level of consistency, with the data points showing a relatively low variation. This consistency indicates that the power measurement process was reliable and produced reliable results. On the other hand, the torque error range was relatively lower than the power error range, ranging from 0.01 to 0.03 Nm. Referring to Fig. 35, it is observed that the torque measurements also demonstrate a high degree of consistency, with minimal variation among the data points. This suggests that the torque measurement process was more reliable and less susceptible to errors compared to the power measurement process.

One possible explanation for the difference in error ranges between power and torque measurements is the propagation of errors in these parameters. The power error is influenced by two parameters, namely speed and mass, which can introduce additional sources of error. On the other hand, the torque error is contributed by only one parameter: speed. With fewer parameters involved in the torque measurement process, the potential for error propagation is reduced, leading to more reliable and consistent results. Overall, the reported error ranges provide valuable insights into the accuracy and precision of the experimental measurements. The consistency observed in the power and torque measurements indicates the reliability of the measurement techniques employed in this study, while the differences in error ranges highlight the importance of considering error propagation when assessing measurement uncertainties.

Upon examining the efficiency error range, it is evident that the errors are generally low, with the majority falling within the 1.3-3.1% range. Figure 36 illustrates the efficiency measurements, showing a trend of decreasing efficiency with increasing power output, which aligns with the expected behaviour of a GWVPP system. However, some variations in the data points are also observed, particularly at higher power outputs. The presence of variations in the efficiency measurements can be attributed to a combination of random and systematic errors inherent in the measurement process. Random errors may arise from factors such as fluctuations in environmental conditions or slight inconsistencies in the experimental setup. On the other hand, systematic errors may stem from calibration issues or limitations in the measurement instruments. The presence of these errors, particularly at higher power outputs, can lead to deviations from the expected trend and contribute to the observed variations in the data points.

It is important to note that the efficiency error depends on both power and torque errors, which explains the broader range of errors observed in this parameter compared to power and torque measurements. Any uncertainties or errors in power and torque measurements can propagate and influence the calculated efficiency, potentially leading to larger deviations. Furthermore, the results indicate that the error in the efficiency parameter tends to be relatively lower at lower rotational speeds and higher at higher rotational speeds. This behaviour can be attributed to the interplay between various factors affecting the efficiency of the system, such as fluid flow dynamics and mechanical losses. At lower rotational speeds, the system may operate in a more stable and controlled manner, resulting in reduced error contributions. In contrast, the system may experience more complex fluid flow patterns and increased mechanical losses at

higher rotational speeds, leading to higher error magnitudes in efficiency measurements. Overall, the error analysis results suggest that this study's experimental setup and instrumentation were reasonably accurate, with relatively small errors observed in power, torque, and efficiency measurements. While variations and errors exist, they do not significantly compromise the overall reliability of the experimental data and conclusions drawn from the study.

CHAPTER FIVE

CONCLUSION AND RECOMMENDATIONS

5.1 Conclusion

The performance of the GWVPP is evaluated in this study using numerical and experimental methods. The results indicate that the GWVPP is a highly efficient power generation system, particularly for low head and flow rates. Furthermore, its ability to generate power easily makes it a promising option for power generation.

This study employed a numerical approach to validate experimental tests through the use of Computational Fluid Dynamics (CFD). Key components of the GWVPP were modelled in 3D using Solidworks software, including the water canal and basin as stationary domains and the runner as a rotating domain. To optimize the interactions of four parameters - runner speed (factor A), hub-blade angle (factor B), number of blades (factor C), and blade profile (factor D) - Design-Expert software was utilized with the response surface methodology (RSM). The parameters were designed with both coded and uncoded levels, and RSM was utilized to determine the optimum combination of each parameter for the most efficient blend. This approach was chosen to overcome the limitations of one-factor-at-a-time (OFAT) selection and improve the system's performance. The findings demonstrate that a numerical approach, when combined with appropriate parameter selection, can be utilized to analyze the GWVPP effectively. Furthermore, the results revealed that the selected parameters exhibit interactions that affect the GWVPP, as observed in the RSM

The performance of the GWVPP was experimentally examined to validate the numerical study. The GWVPP components, including the canal, basin, runner (curved profile), overhead reservoir frame, prony brake system, runner support, and overhead reservoir, were designed and modelled in 3D using Computer-Aided Design software, Solidworks. The experimental test rig was developed based on the optimized parameters from the previous numerical work. The experimental efficiency results were compared with the numerical analysis outcomes, and the system's exergy analysis and error analysis were performed.

The numerical results exhibited excellent agreement with the experimental data, albeit with the assumption of perfect conditions and no mechanical losses. As a result, the numerical results outperformed the experimental results. The numerical study reported curved profiles showing

better efficiency of 9.80 – 25.89% over flat profile blades, which exhibited efficiency in the 8.08 - 23.32% range.

The experimental results revealed that the efficiency ranged from 9.84% to 25.35%, torque ranged from 0.08 to 0.23 Nm, and output power ranged from 2.96 to 7.33 W. The efficiency findings from the experimental and numerical studies agreed with an uncertainty of 0.54%. The outcome discrepancy was due to the ideal conditions assumed for the numerical study. Furthermore, the exergy analysis of the system indicated a value of 43.58%, which was higher than the experimental value, indicating some mechanical losses in the experimental efficiency. The exergy efficiency of a GWVPP system, which represents the proportion of input energy that is converted into valuable work, is a critical performance metric. It gauges the amount of valuable work that can be extracted from available energy sources in a system and the degree to which energy is lost as heat or waste (Rosen & Dincer, 2001). The exergy efficiency of 43.58% and the energy efficiency of 25.35% are two different measures of system performance. Exergy efficiency quantifies the quality of energy utilized in a system. It denotes the fraction of the maximum possible useful energy output over input energy, whereas energy efficiency evaluates the system's proficiency in converting input energy into valuable output energy. Exergy efficiency is generally expected to exceed energy efficiency since it considers energy quality. In this case, the GWVPP system's exergy efficiency of 43.58% is more significant than its energy efficiency of 25.35%, indicating that the system utilizes energy relatively efficiently.

The study's error analysis provides valuable information on the accuracy and reliability of the experimental measurements for power, torque, and efficiency. The power error range was found to be between 0.1 and 0.5 W, with a low variation in the data points. The torque error range was relatively lower than the power error range, ranging from 0.01 to 0.03 Nm, and the torque measurements showed a low variation in the data points. The efficiency error range was generally low, with most errors falling within the 1.3-3.1% range. However, some variation in the data points was observed, particularly at higher power outputs. This variation could be due to a combination of random and systematic errors in the measurement process. It is important to note that the efficiency error depends on both power and torque errors, which explains the broader range of errors observed in this parameter. The error analysis results suggest that the experimental setup and instrumentation were reasonably accurate, with relatively small errors observed in power, torque, and efficiency measurements.

Additionally, the results indicate that the error in the efficiency parameter is relatively lower at lower rotational speeds and higher at higher rotational speeds. The study underscores the potential of GWVPPs as a viable alternative to traditional hydropower plants, given their low initial investment, simple design, ease of maintenance, and low head utilisation. Overall, the study has shown that the GWVPP system has significant potential as an effective and low-cost solution for generating electricity, and further research could help to optimize its performance and make it a viable alternative to traditional energy sources.

5.2 Recommendations

The aim of this research was to explore the potential of using gravitational water vortex power plants (GWVPPs) for energy generation. Both numerical and experimental approaches were utilized in this study. To make GWVPPs a viable option for generating energy from low head and low flow rate water bodies, further research should focus on the:

(i) Evaluate the effect of guide vane in GWVPP systems since this component is crucial to conventional hydropower systems.

(ii) Perform testing of the proposed blade profiles in different basin geometries.

(iii) Explore the use of alternative mesh structures, such as structured tetrahedrons, in numerical analysis to compare their performance and establish a baseline.

(iv) Develop advanced control systems for GWVPPs to optimize power generation and protect the system from adverse hydraulic conditions, such as flooding or debris accumulation.

(v) Conduct economic and environmental assessments of GWVPPs to evaluate their viability as a renewable energy source and compare them with other energy generation options.

(vi) Collaborate with stakeholders, including water resource managers, regulators, and local communities, to identify potential sites for GWVPP installation and assess the social and environmental impacts of the technology.

(vii) The study mainly focuses on short-term efficiency and performance metrics. To make GWVPPs a more attractive option, further research should consider long-term performance and durability under various conditions.

(viii) To make GWVPPs a viable renewable energy source, conducting economic and environmental assessments is crucial. This should include a comparison with other energy generation options to determine its competitiveness and sustainability.

REFERENCES

Abuelnuor, A. A., Ahmed, K., Saqr, K. M., Nogoud, Y. A., & Babiker, M. E. (2020). Exergy analysis of large and impounded hydropower plants: Case study El Roseires Dam (280 MW). *Environmental Progress & Sustainable Energy*, *39*(3), e13362. https://doi.org/10.1002/ep.13362

Bachynski, E., Thys, M., & Delhaye, V. (2019). Dynamic response of a monopile wind turbine in waves: Experimental uncertainty analysis for validation of numerical tools. *Applied Ocean Research, 89*, 96-114. https://doi.org/https://doi.org/10.1016/j.apor.2019.05.002

Bajracharya, T. R., & Chaulagai, R. (2012). Developing innovative low head water turbine for free-flowing streams suitable for micro-hydropower in flat (Terai) regions in Nepal. *Kathmandu: Center for Applied Research and Development (CARD), Institute of Engineering, Tribhuvan University, Nepal*. https://scholar.google.com/scholar?q=related:22GNNj49vIoJ

Bartholomew, A. (2005). *Hidden Nature: the startling insights of Viktor Schauberger*. Adventures Unlimited Press.

Basu, P., Agarwal, D., Tharakan, T. J., &

Salih, A. (2013). Numerical studies on air-core vortex formation during draining of liquids from tanks. *International Journal of Fluid Mechanics Research*, *40*(1) 743 - 761. https://doi.org/10.1615/InterJFluidMechRes. v40.i1.30

Bilgen, S., Keleş, S., Kaygusuz, A., Sarı, A., & Kaygusuz, K. (2008). Global warming and renewable energy sources for sustainable development: A case study in Turkey. *Renewable and Sustainable Energy Reviews, 12*(2), 372-396. https://doi.org/10.1016/j.rser.2006.07.016

Brown, K. D. (1968). Power generating method and apparatus. In: Google Patents.

Chattha, J. A., Cheema, T. A., & Khan, N. H. (2017). *Numerical investigation of basin geometries for vortex generation in a gravitational water vortex power plant*. 2017 8th International Renewable Energy Congress (IREC), Amman, Jordan. doi:10.1109/irec.2017.7926028.

Darmawi, D. (2019). Renewable Energy and Hydropower Utilization Tendency Worldwide (Peer Review). *17*, 213-215.

Dhakal, R., Bajracharya, T., Shakya, S., Kumal, B., Khanal, K., Williamson, S., Gautam, S., & Ghale, D. (2017). *Computational and experimental investigation of runner for gravitational water vortex power plant*. 2017 IEEE 6th International Conference on Renewable Energy Research and Applications (ICRERA), San, Diego, USA. https://ieeexplore.ieee.org/document/8191

Dhakal, S., Nakarmi, S., Pun, P., Thapa, A. B., & Bajracharya, T. R. (2014). Development and testing of runner and conical basin for gravitational water vortex power plant. *Journal of the Institute of Engineering*, *10*(1), 140-148. https://doi.org/10.3126/jie.v10i1.10895

Dhakal, S., Timilsina, A. B., Dhakal, R., Fuyal, D., Bajracharya, T. R., & Pandit, H. P. (2014). *Effect of dominant parameters for conical basin: Gravitational water vortex power plant. Proceedings of IOE graduate conference, Nepal.*

Dhakal, S., Timilsina, A. B., Dhakal, R., Fuyal, D., Bajracharya, T. R., Pandit, H. P., & Amatya, N. (2015). *Mathematical modeling, design optimization and experimental verification of conical basin: Gravitational water vortex power plant. dalam World Largest Hydro Conference,* https://doi.org/10.1061/(254)

Dixon, S. L., & Hall, C. (2013). *Fluid mechanics and thermodynamics of turbomachinery*. Butterworth-Heinemann. https://books.google.co.tz/books?hl=en

Faraji, A., Jande, Y. A. C., & Kivevele, T. (2022). Performance analysis of a runner for gravitational water vortex power plant. *Energy Science and Engineering*. *10*, 1055-1066 https://doi.org/10.1002/ese3.1085

Figliola, R. S., & Beasley, D. E. (2020). *Theory and design for mechanical measurements*. John Wiley & Sons. https://www.wiley.com/ p-9781119475651

Gautam, A., Sapkota, A., Neupane, S., Dhakal, J., Timilsina, A. B., & Shakya, S. (2016). *Study on effect of adding booster runner in conical basin: Gravitational water vortex power plant: A numerical and experimental approach. Proceedings of IOE Graduate Conference, Nepal.* http://conference.ioe.edu.np/publications/ioegc2016/IOEGC-2016-14.

Gheorghe-Marius, M., & Tudor, S. (2013). Energy capture in the gravitational vortex water flow *Journal of Marine Technology & Environment*, *1*, 89 - 106.

Hite Jr, J. E., & Mih, W. C. (1994). Velocity of air-core vortices at hydraulic intakes. *Journal of Hydraulic Engineering*, *120*(3), 284-297. https://doi.org/10.1061/(ASCE)0733-9429(1994)120:3(284)

Hossain, S., Chowdhury, H., Chowdhury, T., Ahamed, J. U., Saidur, R., Sait, S. M., & Rosen, M. A. (2020). Energy, exergy and sustainability analyses of Bangladesh's power generation sector. *Energy Reports*, *6*, 868-878. https://doi.org/10.1016/j.egyr.2020.04.010

Inc., A. (2009). Governing equations, CFX-Solver Theory Guide.

Kaunda, C. S., Kimambo, C. Z., & Nielsen, T. K. (2012). Potential of small-scale hydropower for electricity generation in Sub-Saharan Africa. *ISRN Renewable Energy*.1 - 15 https://doi.org/10.5402/2012/132606 .

Khan, N. H., Cheema, T. A., Chattha, J. A., & Park, C. W. (2018). Effective basin–blade configurations of a gravitational water vortex turbine for microhydropower generation. *Journal of Energy Engineering*, *144*(4), 04018042. https://doi.org/doi.org/10.1061/(ASCE)EY.1943-7897.00005.

Kouris, P. S. (2000). Hydraulic turbine assembly. In: Google Patents.

Kueh, T., Beh, S., Ooi, Y., & Rilling, D. (2017). *Experimental study to the influences of rotational speed and blade shape on water vortex turbine performance*. *Fifteenth Asian congress of fluid mechanics (15ACFM)*, Sarawak, Malaysia. doi 10.1088/1742-6596/822/1/012066.

Kueh, T. C., Beh, S. L., Rilling, D., & Ooi, Y. (2014). Numerical analysis of water vortex formation for the water vortex power plant. *International Journal of Innovation, Management and Technology*, *5*(2), 111-129.

Leon, A. S., & Zhu, L. (2014). A dimensional analysis for determining optimal discharge and penstock diameter in impulse and reaction water turbines. *Renewable energy*, *71*, 609-615. https://doi.org/10.1016/j.renene.2014.06.024.

Marian, M. G., Sajin, T., & Azzouz, A. (2013). Study of micro hydropower plant operating in gravitational vortex flow mode. Applied Mechanics and Materials, 7, 119-132.

Maruf, M. H., Rabbani, M., Ashique, R. H., Islam, M. T., Nipun, M. K., Haq, M. A. U., Al Mansur, A., & Shihavuddin, A. (2021). Exergy based evaluation of power plants for sustainability and economic performance identification. *Case Studies in Thermal Engineering*, *28*, 101393. https://doi.org/10.1016/j.csite.2021.101393.

Mohanan, A. (2016). Power generation with simultaneous aeration using a gravity vortex turbine. *International Journal of Scientific & Engeenering Research*, *7*(2), 5, 233 - 250.

Mulligan, S., & Casserly, J. (2010). The hydraulic design and optimisation of a free water. vortex for the purpose of power extraction. *Sligo: Institute of Technology Sligo*. *3*, 577-589.

Mulligan, S., Casserly, J., & Sherlock, R. (2016). Experimental and numerical modelling of free-surface turbulent flows in full air-core water vortices. *Advances in Hydroinformatics: SIMHYDRO 2014*, 549-569. https://doi.org/10.1007/978-981-287-615-7_37.

Mulligan, S., & Hull, P. (2010). Design and optimisation of a water vortex hydropower plant. *Sligeach: Department of Civil Engineering and Construction, IT Silgo*. 2, 375-386.

Myers, R., & Cook, C. (2016). *Response surface methodology _ process and product optimization using designed experiments*.doi:10.2307/1270613.

Nishi, Y., & Inagaki, T. (2017). Performance and flow field of a gravitation vortex type water turbine. *International Journal of Rotating Machinery, 2, 230-250*. https://doi.org/ 10.1155/2017/2610508.

Okot, D. K. (2013). Review of small hydropower technology. *Renewable and sustainable energy reviews*, *26*, 515-520. https://doi.org/10.1016/j.rser.2013.05.006.

Paish, O. (2002). Small hydro power: Technology and current status. *Renewable and Sustainable Energy Reviews*, *6*, 537-556. https://doi.org/10.1016/S1364-0321(02) 00006-0.

Power, C., McNabola, A., & Coughlan, P. (2016). A parametric experimental investigation of the operating conditions of gravitational vortex hydropower (GVHP). *Journal of Clean Energy Technologies*, *4*(2), 112-119. https://doi.org/10.7763/JOCET.2016.V4.263

Pulliam, T. H., & Zingg, D. W. (2014). *Fundamental algorithms in computational fluid dynamics*. Springer Science & Business Media. doi:10.1007/978-3-319-05053-9.

Rahman, M., Hong, T. J., Tang, R., Sung, L. L., & Tamiri, F. B. M. (2016). Experimental study the effects of water pressure and turbine blade lengths & numbers on the model free vortex power generation system. *International Journal of Current Trends in Engineering & Research (IJCTER)*, *2*(9), 13-17.

Rahman, M., Tan, J., Fadzlita, M., & Muzammil, A. (2017). *A Review on the development of Gravitational Water Vortex Power Plant as alternative renewable energy resources*. International Conference on Materials Technology and Energy, doi:10.1088/1757-899X/217/1/012007.

Rajendran, V., Constantinescu, S., & Patel, V. (1999). Experimental validation of numerical model of flow in pump-intake bays. *Journal of Hydraulic Engineering*, *125*(11), 1119-1125. https://doi.org/10.1061/(ASCE)0733-9429(1999)125:11(111.

REN21, R. (2022). Global Status Report, REN21 Secretariat, Paris, France. In *Tech. Rep.* (pp. 91-93).

Reynolds, P. (1995). *Hydropower naturally? International water power and dam construction handbook*. https://www.infona.pl/resource/bwmeta1.element.elsevier-455be495-c785-3592-8f15-faf9e6df1c2e.

Rosen, M. A., & Dincer, I. (2001). Exergy as the confluence of energy, environment and sustainable development. *Exergy, an International Journal*, *1*(1), 3-13. https://doi.org/10.1016/S1164-0235(01)00004-8.

Safikhani, H., Hajiloo, A., & Ranjbar, M. (2011). Modeling and multi-objective optimization of cyclone separators using CFD and genetic algorithms. *Computers & Chemical Engineering*, *35*(6), 1064-1071. https://doi.org/10.1016/j.compchemeng.2010.07.017.

Saleem, A. S., Cheema, T. A., Ullah, R., Ahmad, S. M., Chattha, J. A., Akbar, B., & Park, C. W. (2020). Parametric study of single-stage gravitational water vortex turbine with cylindrical basin. *Energy*, *200*, 117464. https://doi.org/10.1016/j.energy.2020.117464.

Senior, J., Saenger, N., & Müller, G. (2010). New hydropower converters for very low-head differences.*Journal of Hydraulic Research*, *48*(6),703-714. https://doi.org/10.1080/00221686.2010.529301.

Shabara, H., Yaakob, O., Ahmed, Y. M., Elbatran, A., & Faddir, M. S. (2015). CFD validation for efficient gravitational vortex pool system. *Jurnal Teknologi*, *74*(5), 97 - 100.

Shapiro, A. H. (1962). Bath-tub vortex. *Nature*, *196*(4859), 1080-1081.

Sipahutar, R., Bernas, S. M., & Imanuddin, M. S. (2013). Renewable energy and hydropower utilization tendency worldwide. *Renewable and Sustainable Energy Reviews*, *17*, 213-215. https://doi.org/10.1016/j.rser.2012.09.010.

Sritram, P., Treedet, W., & Suntivarakorn, R. (2015). *Effect of turbine materials on power generation efficiency from free water vortex hydro power plant*. IOP Conference Series: Materials Science and Engineering, doi:10.1088/1757-899X/103/1/012018.

Timilsina, A. B., Mulligan, S., & Bajracharya, T. R. (2018). Water vortex hydropower technology: A state-of-the-art review of developmental trends. *Clean Technologies and Environmental Policy*, *20*(8), 1737-1760. https://doi.org/10.1007/s10098-018-1589-0.

Ullah, R., Cheema, T. A., Saleem, A. S., Ahmad, S. M., Chattha, J. A., & Park, C. W. (2019). Performance analysis of multi-stage gravitational water vortex turbine. *Energy Conversion and Management*, *198*, 111788. https://doi.org/10.1016/j.enconman. 2019.111788.

Utikar, R., Darmawan, N., Tade, M., Li, Q., Evans, G., Glenny, M., & Pareek, V. (2010). Hydrodynamic simulation of cyclone separators. In *Computational fluid dynamics* (pp. 241-266). In Tech.

Wagner, B., Hauer, C., Schoder, A., & Habersack, H. (2015). A review of hydropower in Austria: Past, present and future development. *Renewable and sustainable energy reviews*, *50*, 304-314. https://doi.org/10.1016/j.rser.2015.04.169.

Wanchat, S., & Suntivarakorn, R. (2012). Preliminary design of a vortex pool for electrical generation. *Advanced Science Letters*, *13*(1), 173-177.

Wanchat, S., Suntivarakorn, R., Wanchat, S., Tonmit, K., & Kayanyiem, P. (2013). A parametric study of a gravitation vortex power plant. *Advanced Materials Research*, *805 - 806*(2013), 811-817. https://doi.org/10.4028/www.scientific.net/AMR.805-806.811.

Wichian, P., & Suntivarakorn, R. (2016). The effects of turbine baffle plates on the efficiency of water free vortex turbines. *Energy Procedia*, *100*(100), 198-202. https://doi.org/10. 1016/j.egypro.2016.10.165.

Williamson, S., Stark, B., & Booker, J. (2014). Low head pico hydro turbine selection using a multi-criteria analysis. *Renewable energy*, *61*, 43-50. https://doi.org/10.1016/j.renene.2012.06.020.

Williamson, S. J., Stark, B. H., & Booker, J. D. (2014). Low head pico hydro turbine selection using a multi-criteria analysis. *Renewable energy*, *61*, 43-50. https://doi.org/10.1016/j.renene.2012.06.020.

Yaakob, O., Ahmed, Y. M., Elbatran, A., & Shabara, H. (2014). A review on micro hydro gravitational vortex power and turbine systems. *Jurnal Teknologi*, *69*(7), 1 - 7.

Yuksel, I. (2010). As a renewable energy hydropower for sustainable development in Turkey. *Renewable and sustainable energy reviews*, *14*(9), 3213-3219. https://doi.org/10.1016/j.rser.2010.07.056.

Yüksel, I. (2010). Hydropower for sustainable water and energy development. *Renewable and sustainable energy reviews*, *14*(1), 462-469. https://doi.org/10.1016/j.rser.2009.07.025.

Zotlöterer. (2017). *Gravitation water vortex power plants*. http://www.zotloeterer.com/welcome/gravitation-water-vortex-power-plants/. Accessed on 2 May 2022.

APPENDICES

Appendix 1: The GWVPP experimental setup storage tank

Appendix 2: The GWVPP experimental setup reservoi

Appendix 3: The Runner unit with its support

Appendix 4: The GWVPP experimental setup frame support

Appendix 5: Comparison of numerical and experimental efficiencies (flat runner profile)

Speed, rad/s	Numerical efficiency	Experimental efficiency
4.08	0	0
3.87	9.22	9.01
3.72	18.76	18.16
3.43	20.87	20.29
3.27	21.04	21.28

Appendix 6: Comparison of numerical and experimental efficiencies (curved runner profile)

Speed, rad/s	Numerical efficiency	Experimental efficiency
4.08	0	0
3.93	9.79	9.00
3.84	17.11	16.52
3.80	20.05	19.08
3.56	22.24	21.13

Appendix 7: The GWVPP experimental data (Efficiency)

Speed	Efficiency	Efficiency error
3.26	0	0
3.12	9.84	1.9
3.05	12.07	2
3.03	15.6	2.2
2.97	20.07	2.5
2.96	22.96	1.5
2.9	24.38	3.1
2.64	25.35	1.6
2.42	20.69	1.5
2.27	15.93	2.6
2.13	13.34	1.4
1.91	12.34	1.3

Appendix 8: The GWVPP experimental data (Power)

Speed	Power	Power error
3.26	0	0
3.12	2.9587	0.3
3.05	3.6297	0.3
3.03	4.6931	0.3
2.97	6.03707	0.4
2.96	6.90575	0.2
2.9	7.33396	0.5
2.64	7.6261	0.2
2.42	6.2242	0.2
2.27	4.7912	0.4
2.13	4.01273	0.2
1.91	3.71117	0.1

Appendix 9: The GWVPP experimental data (Torque)

Speed	Torque	Torque error
3.26	0	0
3.12	0.07848	0.01
3.05	0.0981	0.02
3.03	0.12753	0.02
2.97	0.16677	0.02
2.96	0.19129	0.01
2.9	0.20601	0.03
2.64	0.23053	0.02
2.42	0.20111	0.01
2.27	0.16187	0.03
2.13	0.14225	0.01
1.91	0.14225	0.01

Appendix 10: Scale 1 reading and error calculation

Trial	Values	Average	Deviation	Deviation square	SD	Standard error, SR
1	0	0.000	0	0	0.0000	0.0000
	0		0	0		
	0		0	0		
2	0.11	0.127	-0.017	0.000289	0.0153	0.0108
	0.13		0.003	0.000009		
	0.14		0.013	0.000169		
3	0.19	0.197	-0.007	0.000049	0.0115	0.0081
	0.21		0.013	0.000169		
	0.19		-0.007	0.000049		
4	0.22	0.220	0.000	0.000000	0.0100	0.0071
	0.21		-0.010	0.000100		
	0.23		0.010	0.000100		
5	0.28	0.293	-0.013	0.000169	0.0231	0.0163
	0.32		-0.013	0.000169		
	0.28		0.027	0.000729		
6	0.34	0.333	0.007	0.000049	0.0115	0.0081
	0.32		-0.013	0.000169		
	0.34		0.007	0.000049		
7	0.43	0.440	-0.010	0.000100	0.0265	0.0187
	0.47		0.030	0.000900		
	0.42		-0.020	0.000400		
8	0.48	0.467	0.013	0.000169	0.0153	0.0108
	0.45		-0.017	0.000289		
	0.47		0.003	0.000009		
9	0.58	0.583	-0.003	0.000009	0.0058	0.0041
	0.58		-0.003	0.000009		
	0.59		0.007	0.000049		
10	0.67	0.657	0.013	0.000169	0.0321	0.0227
	0.62		-0.037	0.001369		
	0.68		0.023	0.000529		

Trial	Values	Average	Deviation	Deviation square	SD	Standard error, SR
11	0.76	0.763	-0.003	0.000009	0.0058	0.0041
	0.76		-0.003	0.000009		
	0.77		0.007	0.000049		
12	0.86	0.843	0.017	0.000289	0.0153	0.0108
	0.84		-0.003	0.000009		
	0.83		-0.013	0.000169		

Appendix 11: Scale 2 reading and error calculation

Trial	Values	Average	Deviation	Deviation square	SD	Standard error, SR
1	0	0.000	0.000	0.000000	0.0000	0.0000
	0		0.000	0.000000		
	0		0.000	0.000000		
2	0.28	0.283	-0.003	0.000009	0.0058	0.0041
	0.28		-0.003	0.000009		
	0.29		0.007	0.000049		
3	0.38	0.387	-0.007	0.000049	0.0115	0.0081
	0.4		0.013	0.000169		
	0.38		-0.007	0.000049		
4	0.46	0.477	-0.017	0.000289	0.0153	0.0108
	0.49		0.013	0.000169		
	0.48		0.003	0.000009		
5	0.63	0.623	0.007	0.000049	0.0058	0.0041
	0.62		-0.003	0.000009		
	0.62		-0.003	0.000009		
6	0.72	0.717	0.003	0.000009	0.0058	0.0041
	0.72		0.003	0.000009		
	0.71		-0.007	0.000049		
7	0.84	0.850	-0.010	0.000100	0.0100	0.0071
	0.86		0.010	0.000100		
	0.85		0.000	0.000000		
8	0.95	0.953	-0.003	0.000009	0.0058	0.0041
	0.96		0.007	0.000049		
	0.95		-0.003	0.000009		
9	1	0.987	0.013	0.000169	0.0153	0.0108
	0.97		-0.017	0.000289		
	0.99		0.003	0.000009		
10	0.99	0.997	-0.007	0.000049	0.0058	0.0041
	1		0.003	0.000009		
	1		0.003	0.000009		

Trial	Values	Average	Deviation	Deviation square	SD	Standard error, SR
11	1.03	1.047	-0.017	0.000289	0.0153	0.0108
	1.06		0.013	0.000169		
	1.05		0.003	0.000009		
12	1.12	1.123	-0.003	0.000009	0.0058	0.0041
	1.13		0.007	0.000049		
	1.12		-0.003	0.000009		

Appendix 12: Tachometer reading and error calculation

Trial	Values	Average	Deviation	Deviation square	SD	Standard error, SR
1	3.25	3.260	-0.010	0.00010	0.0265	0.0187
	3.29		3.290	10.82410		
	3.24		3.240	10.49760		
2	3.10	3.120	-0.020	0.00040	0.0200	0.0141
	3.12		3.120	9.73440		
	3.14		3.140	9.85960		
3	3.04	3.047	-0.007	0.00005	0.0115	0.0081
	3.04		3.040	9.24160		
	3.06		3.060	9.36360		
4	3.01	3.027	-0.017	0.00029	0.0208	0.0147
	3.05		3.050	9.30250		
	3.02		3.020	9.12040		
5	2.96	2.970	-0.010	0.00010	0.0100	0.0071
	2.98		2.980	8.88040		
	2.97		2.970	8.82090		
6	2.95	2.957	-0.007	0.00005	0.0208	0.0147
	2.94		2.940	8.64360		
	2.98		2.980	8.88040		
7	2.92	2.903	0.017	0.00029	0.0153	0.0108
	2.89		2.890	8.35210		
	2.90		2.900	8.41000		
8	2.63	2.643	-0.013	0.00017	0.0115	0.0081
	2.65		2.650	7.02250		
	2.65		2.650	7.02250		
9	2.41	2.420	-0.010	0.00010	0.0100	0.0071
	2.43		2.430	5.90490		
	2.42		2.420	5.85640		
10	2.28	2.273	0.007	0.00005	0.0115	0.0081
	2.28		2.280	5.19840		
	2.26		2.260	5.10760		

Trial	Values	Average	Deviation	Deviation square	SD	Standard error, SR
11	2.13	2.130	0.000	0.00000	0.0100	0.0071
	2.14		2.140	4.57960		
	2.12		2.120	4.49440		
12	1.90	1.913	-0.013	0.00017	0.0115	0.0081
	1.92		1.920	3.68640		
	1.92		1.920	3.68640		

Appendix 13: Experimental data summary

Exp no	Volume flow rate m^3/s (Q)	Scale 1 (kg)	Scale 2 (kg)	Mass change (Δm), kg	Torque, Nm ($gr_p\Delta m$)	Input power, W (ρgQH)	Operating speed ω, rad/s	Output power, W ($\omega gr_p\Delta m$)	Efficiency, %
1	0.003066	0.00	0.00	0.00	0.00	30.0775	3.26	0.00	0.00
2	0.003066	0.12	0.28	0.16	0.07848	30.0775	3.12	2.958696	9.84
3	0.003066	0.19	0.39	0.20	0.0981	30.0775	3.05	3.6297	12.07
4	0.003066	0.22	0.48	0.26	0.12753	30.0775	3.03	4.693104	15.60
5	0.003066	0.28	0.62	0.34	0.16677	30.0775	2.97	6.037074	20.07
6	0.003066	0.33	0.72	0.39	0.191295	30.0775	2.96	6.9057495	22.96
7	0.003066	0.43	0.85	0.42	0.20601	30.0775	2.90	7.333956	24.38
8	0.003066	0.48	0.95	0.47	0.230535	30.0775	2.64	7.6260978	25.35
9	0.003066	0.58	0.99	0.41	0.201105	30.0775	2.42	6.22419975	20.69
10	0.003066	0.67	1.0	0.33	0.161865	30.0775	2.27	4.791204	15.93
11	0.003066	0.76	1.05	0.29	0.142245	30.0775	2.13	4.01273145	13.34
12	0.003066	0.83	1.12	0.29	0.142245	30.0775	1.91	3.71117205	12.34

Appendix 14: Technical drawings of the experimental rig

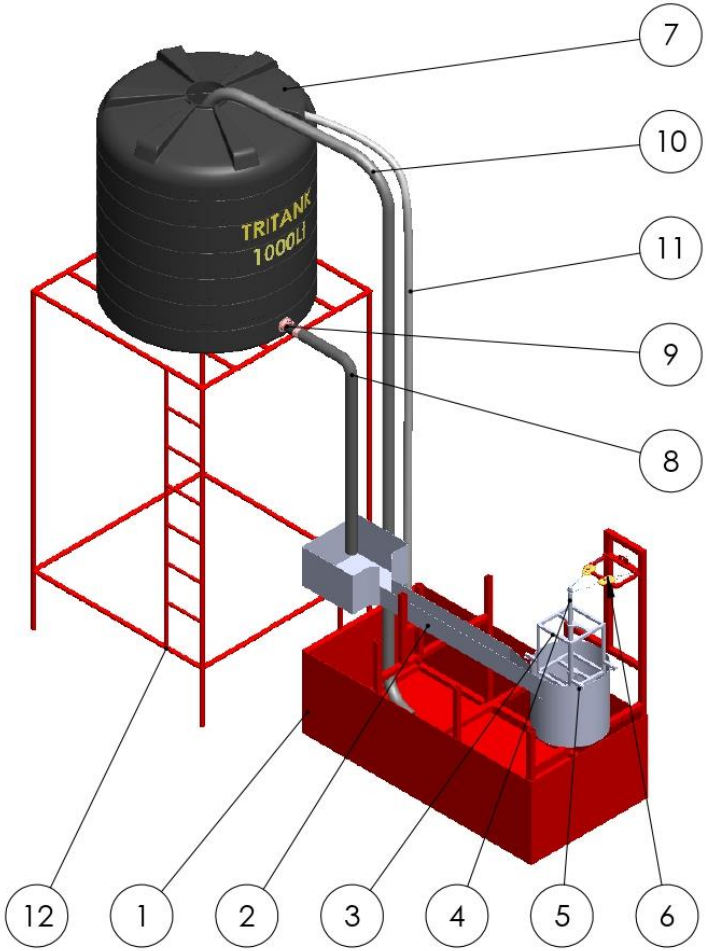

ITEM NO.	PART NUMBER	DESCRIPTION	QTY.
1	V-001	Storage Tank	1
2	V-025	Basin and Canal Assy	1
3	V-032	Blade Support	1
4	V-038	Runner SubAssy	1
5	V-031	Blade Frame Support	4
6	V-042	Prony Brake System	1
7	V-045	Plastic Tank (1000Litres)	1
8	V-046	Flow Pipe (76.2mm Diameter x 2000mm Length)	1
9	v-047	Valve (76.2mm Diameter Pipe)	1
10	V-048	Pump Return Pipe(76.2mm Diameter x 5500mm Length)	1
11	V-049	Overflow Pipe (50.8mm Diameter x 3000mm Length)	1
12	V-050	Reservoir Tank Support	1
13	ISO 4015 - M8 x 35 x 22-S	Bolt	5
14	ISO - 4035 - M8 - S	Nut	5

V-000	Main Assy		2 x 1043 x 1050	1	
PART No	PART NAME	MATERIAL	SPECIFICATION	QUANTITY	REMARKS
	SCALE:1:30	DRAWN: ADAM MFANGAVO		SHEET 1 OF 2	
	DIMENSION: mm	CHECKED:		DEBUR AND BREAK SHARP EDGES	
	DATE: JUNE 2023	APPROVED:			
NM-AIST P.O Box 447 ARUSHA		GRAVITATIONAL WATER VORTEX POWER PLANT		DRG No. V-000	FORMAT A4

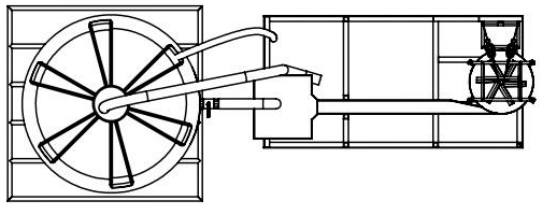

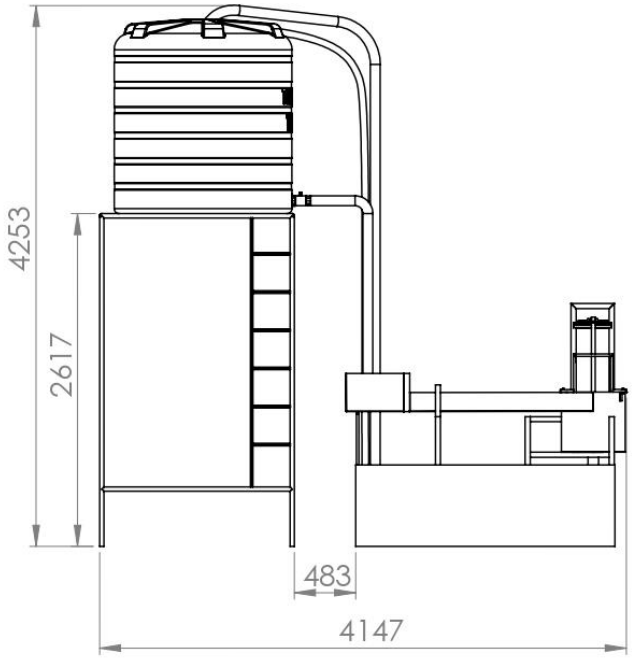

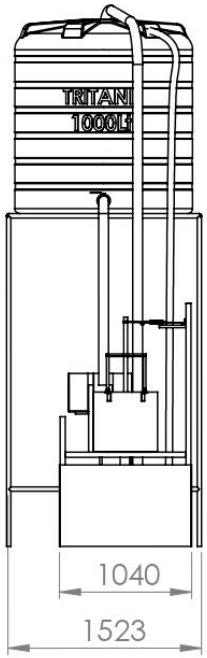

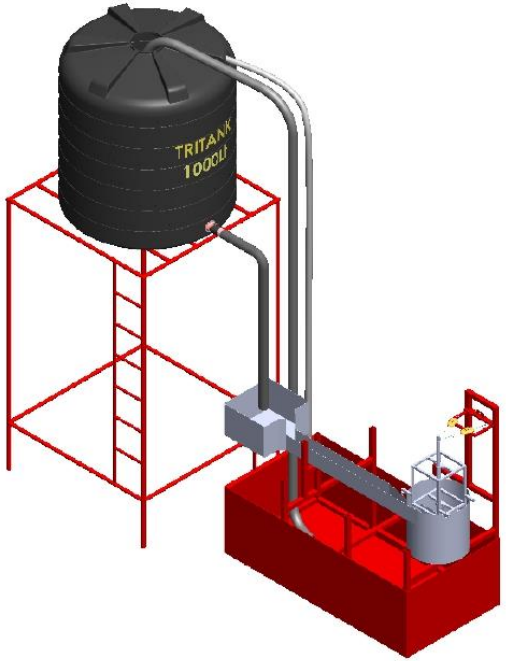

V-000	Main Assy		2 x 1043 x 1050	1	
PART No	PART NAME	MATERIAL	SPECIFICATION	QUANTITY	REMARKS
	SCALE:1:50	DRAWN: ADAM MFANGAVO		SHEET 2 OF 2	
	DIMENSION: mm	CHECKED:		DEBUR AND BREAK SHARP EDGES	
	DATE: JUNE 2023	APPROVED:			
NM-AIST P.O Box 447 ARUSHA		GRAVITATIONAL WATER VORTEX POWER PLANT		DRG No. V-000	FORMAT A4

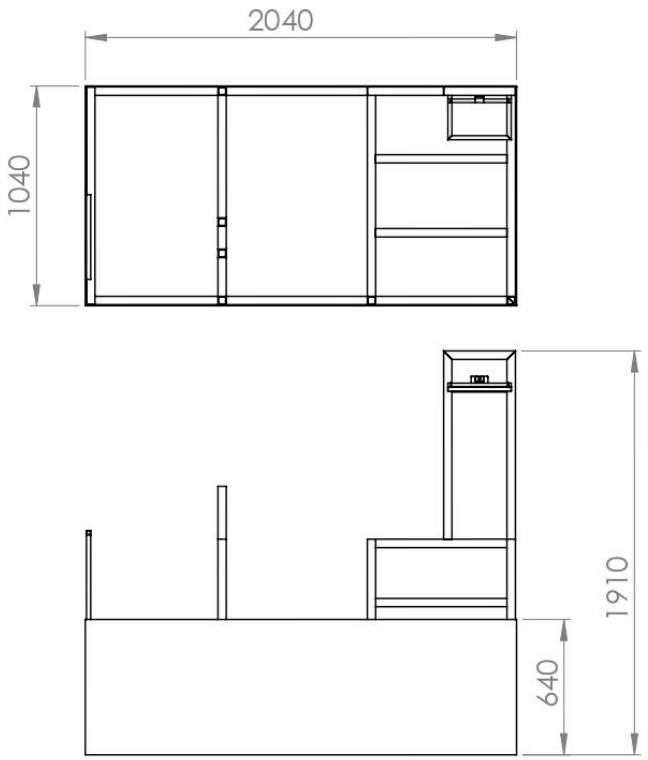

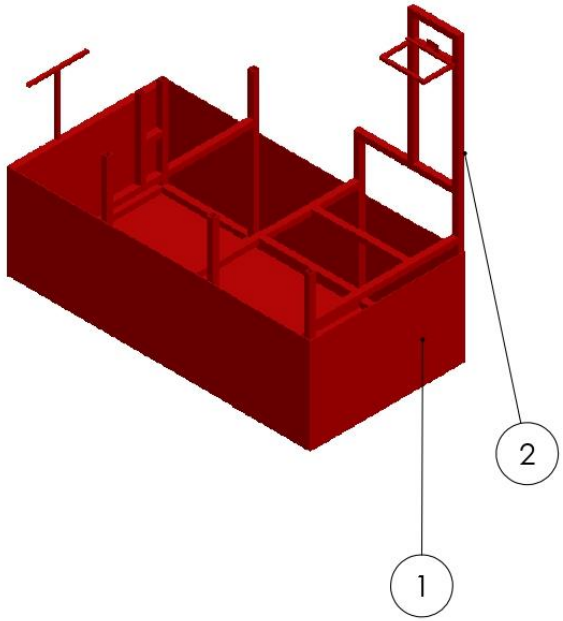

ITEM NO.	PART NUMBER	DESCRIPTION			QTY.
1	V-002	Storage Tank Cover			1
2	V-006	Storage Tank Frame			1
V-001	Storage Tank		2 x 1043 x 1050	1	
PART No	PART NAME	MATERIAL	SPECIFICATION	QUANTITY	REMARKS

SCALE:1:30	DRAWN: ADAM MFANGAVO	SHEET 1 OF 1	
DIMENSION: mm	CHECKED:	DEBUR AND BREAK SHARP EDGES	
DATE: JUNE 2023	APPROVED:		

NM-AIST P.O Box 447 ARUSHA	GRAVITATIONAL WATER VORTEX POWER PLANT	DRG No. V-001	FORMAT A4

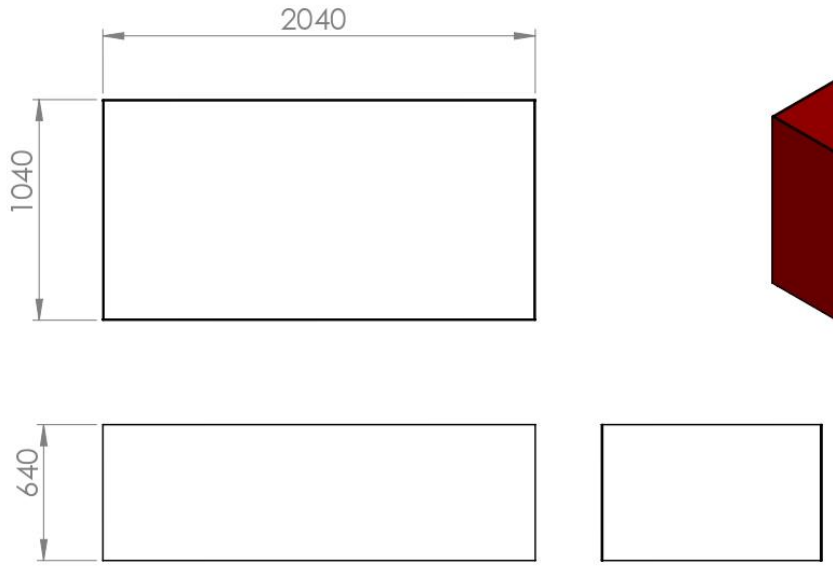

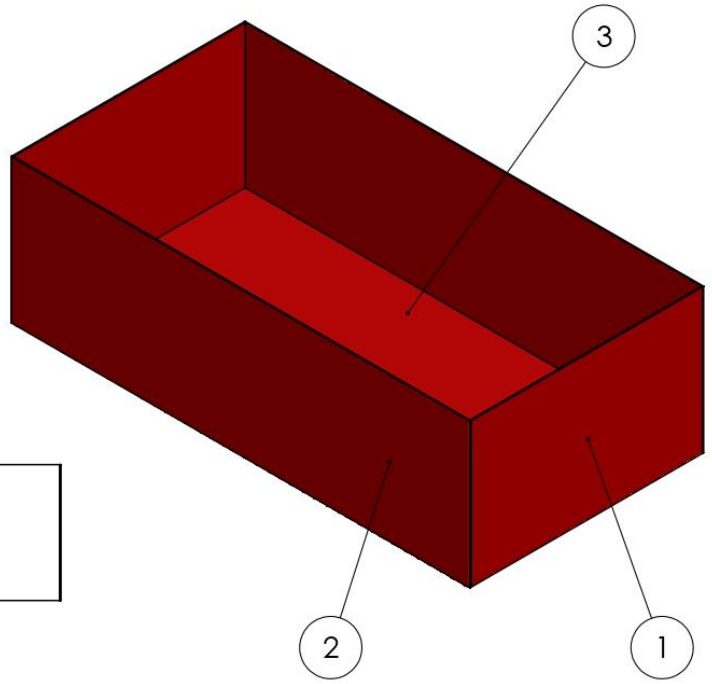

ITEM NO.	PART NUMBER	DESCRIPTION	QTY.
1	V-003	SM 5 x 640 x 1030	2
2	V-004	SM 5 x 640 x 2040	2
3	V-005	SM 5 x 1030 x 2030	1

V-002	Storage Tank Cover	Mild Steel	2 x 1043 x 1050	1	
PART No	PART NAME	MATERIAL	SPECIFICATION	QUANTITY	REMARKS

SCALE:1:30	DRAWN: ADAM MFANGAVO	SHEET 1 OF 1	
DIMENSION: mm	CHECKED:	DEBUR AND BREAK SHARP EDGES	
DATE: JUNE 2023	APPROVED:		

NM-AIST P.O Box 447 ARUSHA	GRAVITATIONAL WATER VORTEX POWER PLANT	DRG No. V-002	FORMAT A4

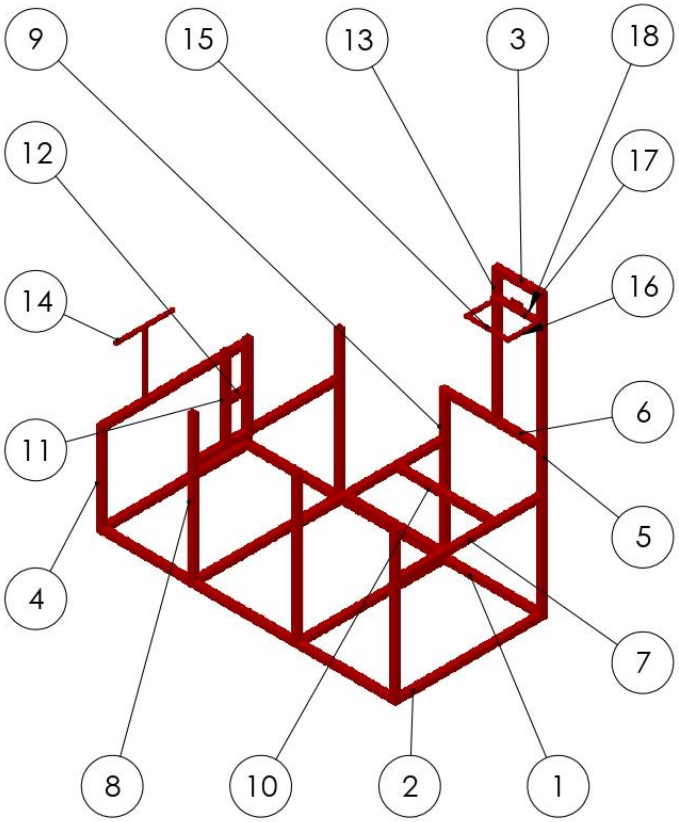

ITEM NO.	PART NUMBER	DESCRIPTION	QTY.
1	V-007	40x40x4x2030 (45deg Chopped Both Ends)	2
2	V-008	40x40x4x1030 (45deg Chopped Both Ends)	3
3	V-009	40x40x4x340 (45deg Chopped Both Ends)	1
4	V-010	40x40x4x595 (45deg Chopped one End)	2
5	V-011	40x40x4x1865 (45deg Chopped One End)	1
6	V-012	40x40x4x661 (45deg Chopped One End)	1
7	V-013	40x40x4x950	5
8	V-014	40x40x4x975	4
9	V-015	40x40x4x975 (45deg Chopped One End)	1
10	V-016	40x40x4x621	2
11	V-017	40x40x4x530	2
12	V-018	40x40x4x108	1
13	V-019	40x40x4x890 (45deg Chopped One End)	1
14	V-020	20x20x2x400	2
15	V-021	20x20x2x300 (45deg Chopped Both Ends)	1
16	V-022	20x20x2x210 (45deg Chopped One End)	2
17	V-023	1/2inches x 300mm Length Square Bar	1
18	V-024	40x40x4x260	1

PART No	PART NAME	MATERIAL	SPECIFICATION	QUANTITY	REMARKS
V-006	Storage Tank Frame	Mild Steel	2 x 1043 x 1050	1	

SCALE:1:30	DRAWN: ADAM MFANGAVO	SHEET 1 OF 2
DIMENSION: mm	CHECKED:	DEBUR AND BREAK SHARP EDGES
DATE: JUNE 2023	APPROVED:	

NM-AIST
P.O Box 447
ARUSHA

GRAVITATIONAL WATER VORTEX POWER PLANT

DRG No. V-006

FORMAT A4

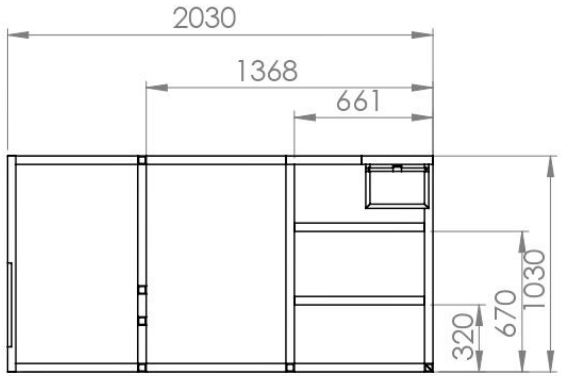

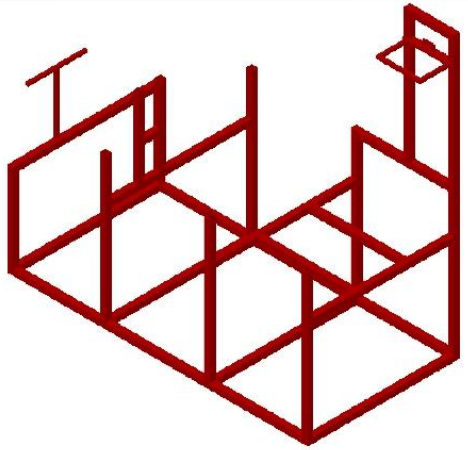

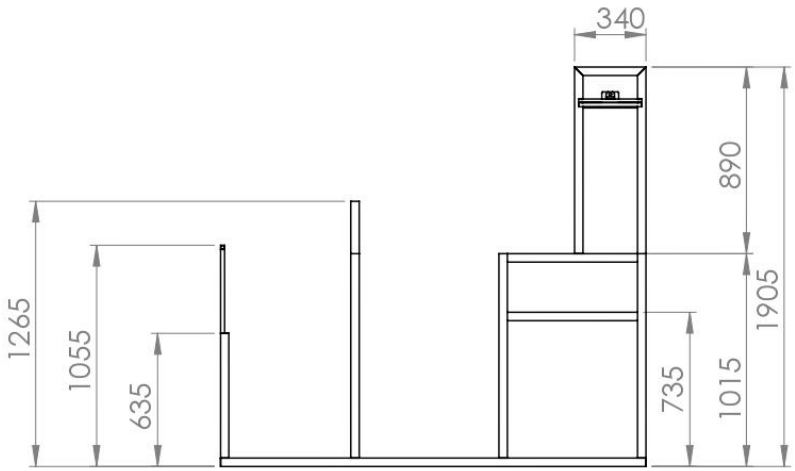

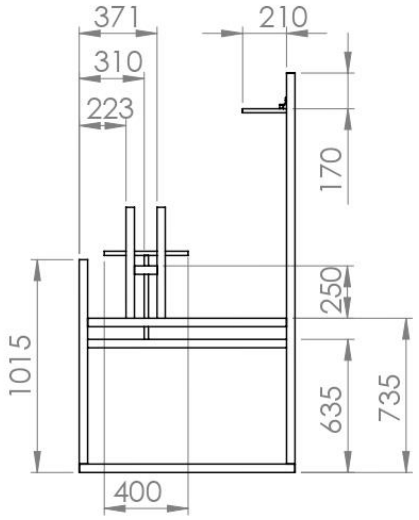

V-006	Storage Tank Frame	Mild Steel	2 x 1043 x 1050	1	
PART No	PART NAME	MATERIAL	SPECIFICATION	QUANTITY	REMARKS
	SCALE:1:30	DRAWN: ADAM MFANGAVO		SHEET 2 OF 2	
	DIMENSION: mm	CHECKED:		DEBUR AND BREAK SHARP EDGES	
	DATE: JUNE 2023	APPROVED:			

NM-AIST
P.O Box 447
ARUSHA

GRAVITATIONAL WATER VORTEX POWER PLANT

DRG No. V-006

FORMAT A4

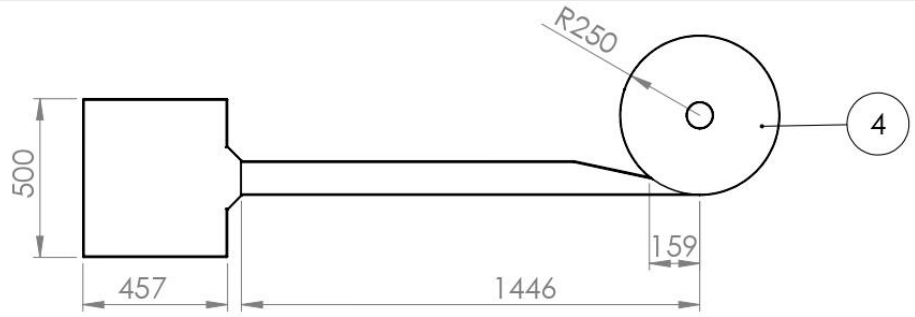

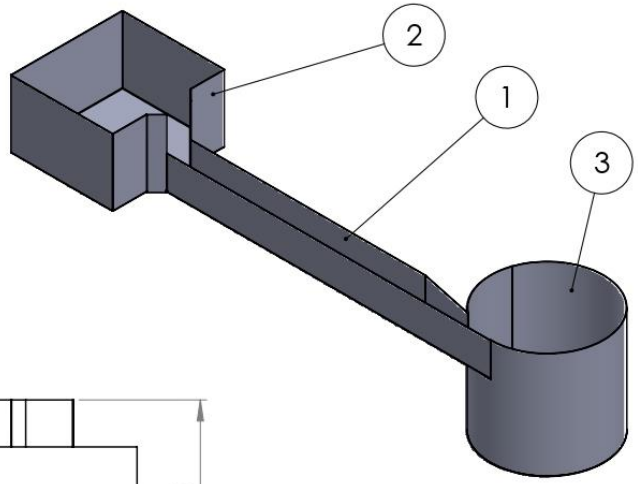

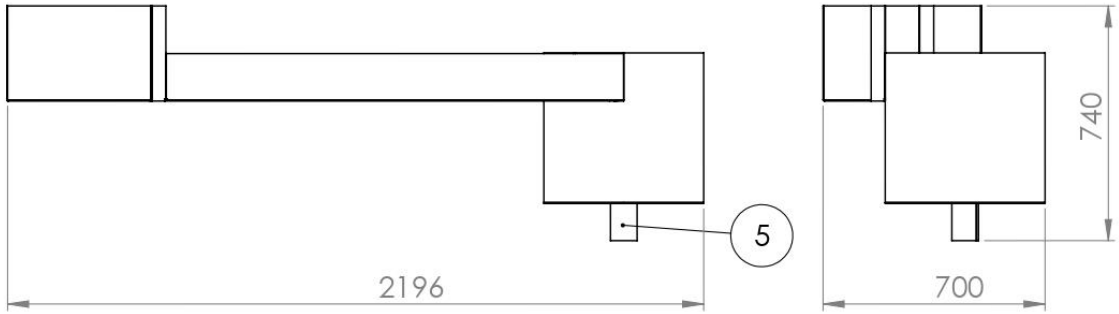

ITEM NO.	PART NUMBER	DESCRIPTION	QTY.
1	V-026	Canal	1
2	V-027	Water Receiver	1
3	V-028	Basin Side Sheet	1
4	V-029	Basin Bottom Sheet	1
5	V-030	Basin Water Exit	1

V-025	Basin and Canal Assy	Mild Steel	2 x 1043 x 1050	1	
PART No	PART NAME	MATERIAL	SPECIFICATION	QUANTITY	REMARKS

SCALE:1:20	DRAWN: ADAM MFANGAVO	SHEET 1 OF 1	
DIMENSION: mm	CHECKED:	DEBUR AND BREAK SHARP EDGES	
DATE: JUNE 2023	APPROVED:		

NM-AIST P.O Box 447 ARUSHA	GRAVITATIONAL WATER VORTEX POWER PLANT	DRG No. V-025	FORMAT A4

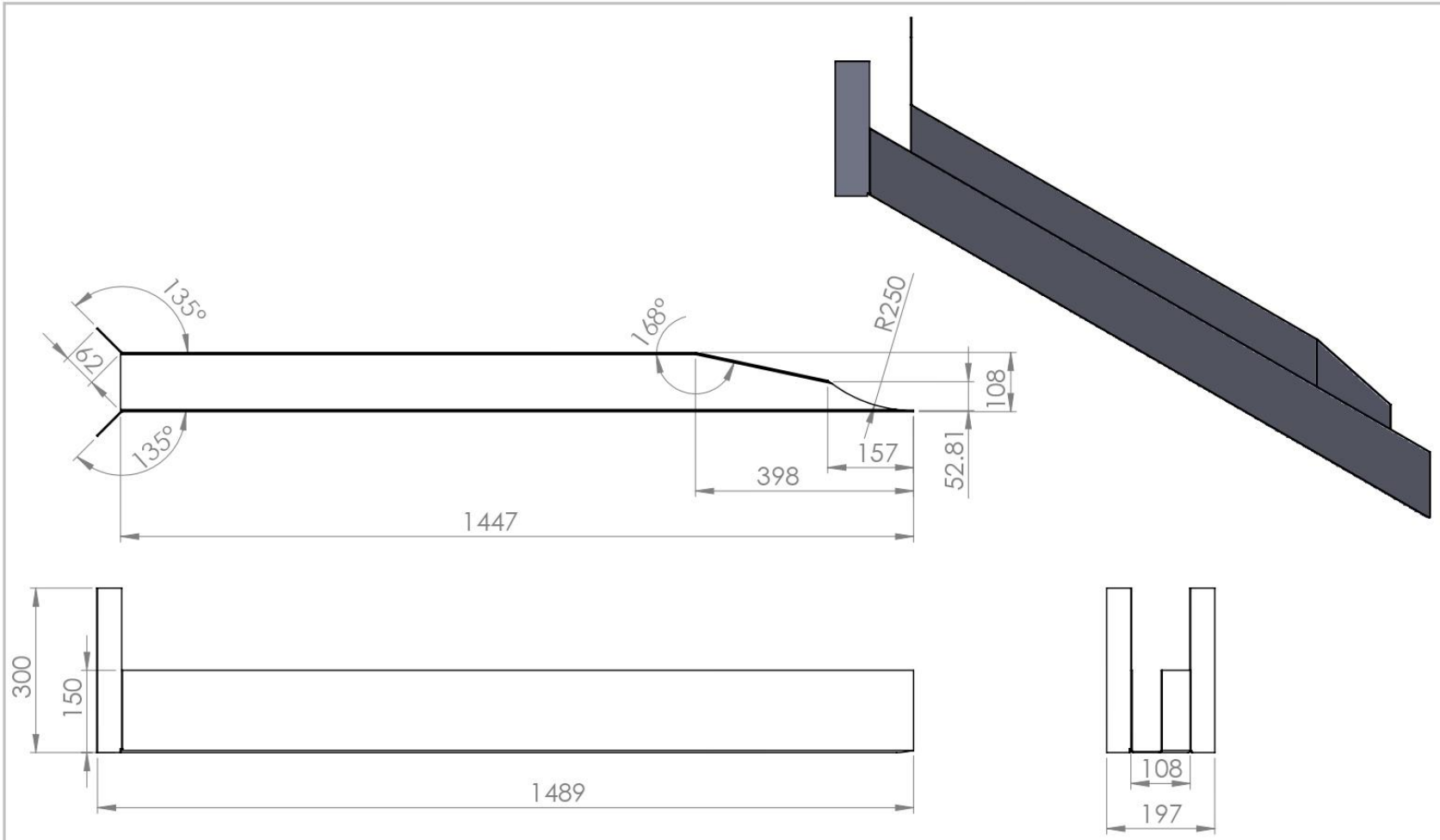

V-026	Canal	Mild Steel	2 x 1043 x 1050	1	
PART No	PART NAME	MATERIAL	SPECIFICATION	QUANTITY	REMARKS
	SCALE:1:10	DRAWN: ADAM MFANGAVO		SHEET 1 OF 2	
	DIMENSION: mm	CHECKED:		DEBUR AND BREAK SHARP EDGES	
	DATE: JUNE 2023	APPROVED:			

NM-AIST P.O Box 447 ARUSHA	GRAVITATIONAL WATER VORTEX POWER PLANT	DRG No. V-026	FORMAT A4

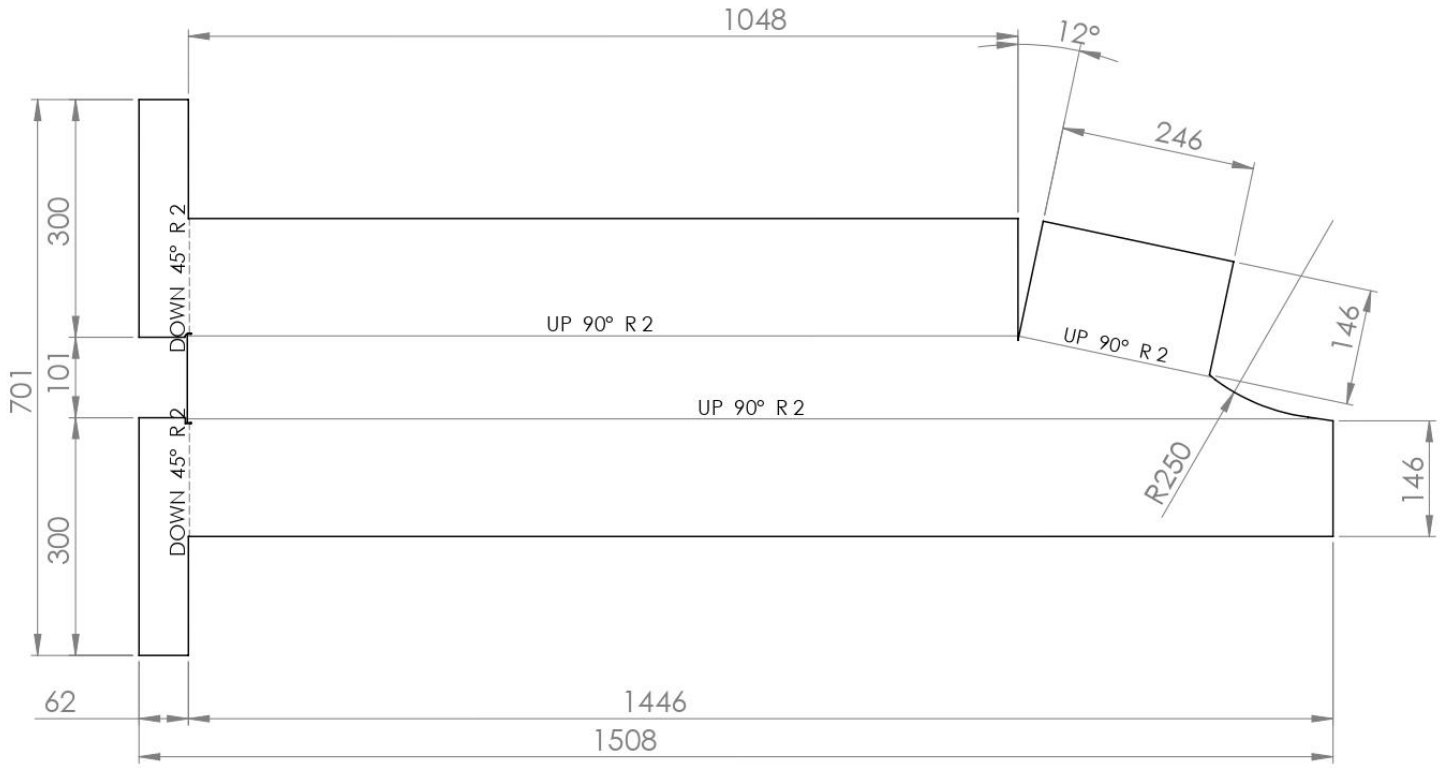

Flat Pattern

V-026	Canal	Mild Steel	2 x 1043 x 1050	1	
PART No	PART NAME	MATERIAL	SPECIFICATION	QUANTITY	REMARKS
	SCALE:1:10	DRAWN: ADAM MFANGAVO		SHEET 2 OF 2	
	DIMENSION: mm	CHECKED:		DEBUR AND BREAK SHARP EDGES	
	DATE: JUNE 2023	APPROVED:			

NM-AIST P.O Box 447 ARUSHA	GRAVITATIONAL WATER VORTEX POWER PLANT	DRG No. V-026	FORMAT A4

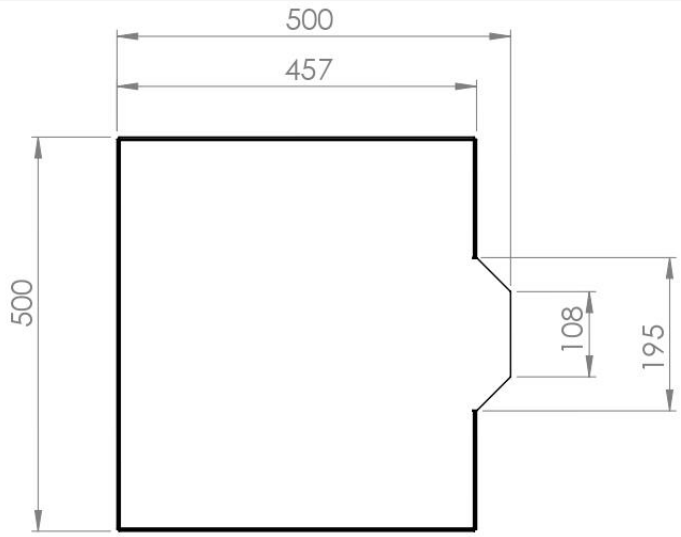

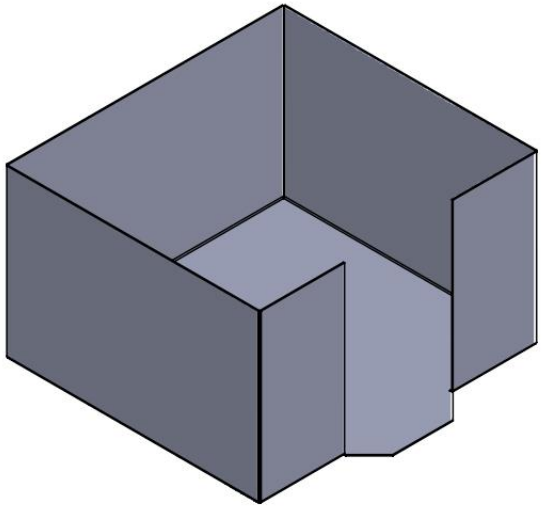

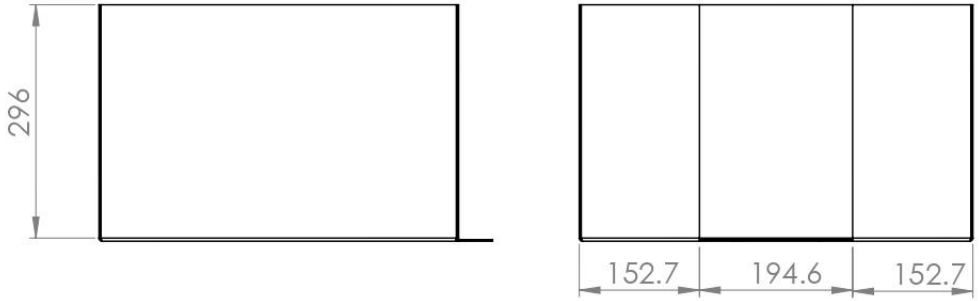

V-027	Water Receiver	Mild Steel	2 x 1043 x 1050	1	
PART No	PART NAME	MATERIAL	SPECIFICATION	QUANTITY	REMARKS
	SCALE:1:8	DRAWN: ADAM MFANGAVO		SHEET 1 OF 2	
	DIMENSION: mm	CHECKED:		DEBUR AND BREAK SHARP EDGES	
	DATE: JUNE 2023	APPROVED:			

NM-AIST
P.O Box 447
ARUSHA

GRAVITATIONAL WATER VORTEX POWER PLANT

DRG No.	FORMAT
V-027	A4

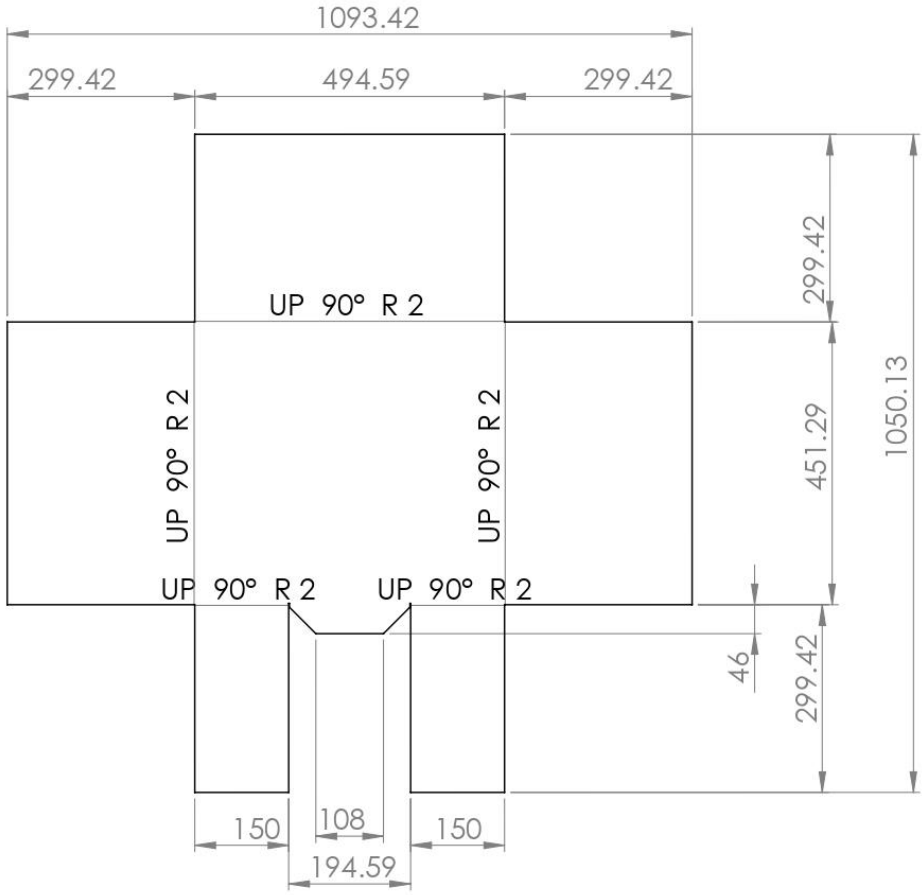

Flat Pattern

V-027	Water Receiver	Mild Steel	2 x 1043 x 1050	1	
PART No	PART NAME	MATERIAL	SPECIFICATION	QUANTITY	REMARKS
	SCALE:1:10	DRAWN: ADAM MFANGAVO		SHEET 2 OF 2	
	DIMENSION: mm	CHECKED:		DEBUR AND BREAK SHARP EDGES	
	DATE: JUNE 2023	APPROVED:			

NM-AIST P.O Box 447 ARUSHA	GRAVITATIONAL WATER VORTEX POWER PLANT	DRG No. V-027	FORMAT A4

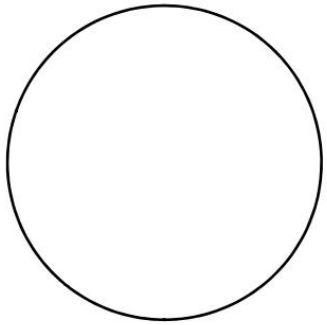

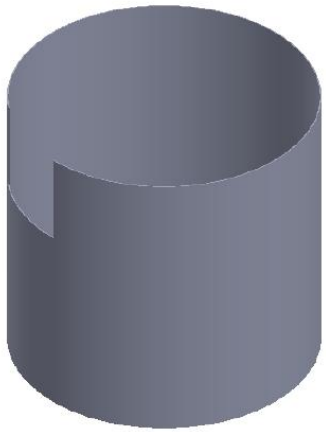

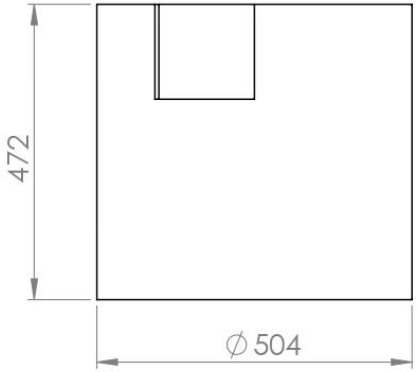

Flat Pattern

V-028	Basin Side Sheet	Mild Steel	2 x 1043 x 1050	1	
PART No	PART NAME	MATERIAL	SPECIFICATION	QUANTITY	REMARKS
	SCALE:1:10	DRAWN: ADAM MFANGAVO		SHEET 1 OF 1	
	DIMENSION: mm	CHECKED:		DEBUR AND BREAK SHARP EDGES	
	DATE: JUNE 2023	APPROVED:			

NM-AIST P.O Box 447 ARUSHA	GRAVITATIONAL WATER VORTEX POWER PLANT	DRG No. V-028	FORMAT A4

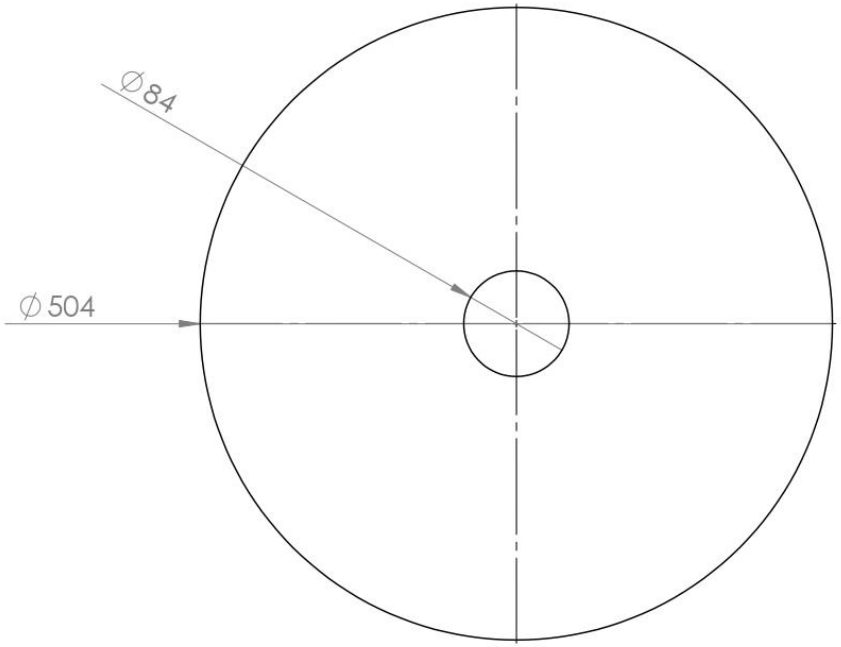

V-029	Basin Bottom Sheet	Mild Steel	2 x 1043 x 1050	1	
PART No	PART NAME	MATERIAL	SPECIFICATION	QUANTITY	REMARKS
	SCALE:1:5	DRAWN: ADAM MFANGAVO		SHEET 1 OF 1	
	DIMENSION: mm	CHECKED:		DEBUR AND BREAK SHARP EDGES	
	DATE: JUNE 2023	APPROVED:			

NM-AIST
P.O Box 447
ARUSHA

GRAVITATIONAL WATER VORTEX POWER PLANT

DRG No. V-029

FORMAT A4

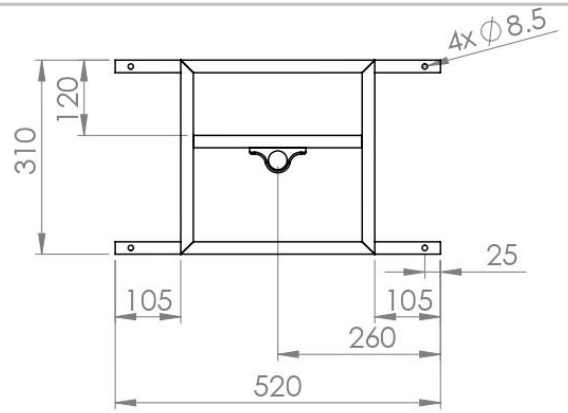

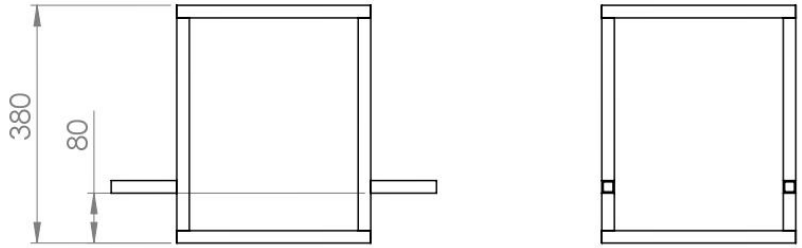

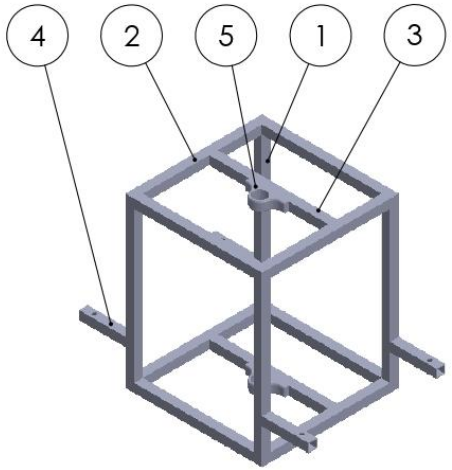

ITEM NO.	PART NUMBER	DESCRIPTION	QTY.
1	V-033	20x20x2x340	4
2	V-034	20x20x2x310 (45deg Chopped Both Ends)	8
3	V-035	20x20x2x270	2
4	V-036	20x20x2x10 (8.5Dia Drill 25mm From one End)	4
5	V-037	Bearing Housing	2

V-032	Blade Support	Mild Steel	2 x 1043 x 1050	1	
PART No	PART NAME	MATERIAL	SPECIFICATION	QUANTITY	REMARKS
	SCALE:1:10	DRAWN: ADAM MFANGAVO		SHEET 1 OF 1	
	DIMENSION: mm	CHECKED:		DEBUR AND BREAK SHARP EDGES	
	DATE: JUNE 2023	APPROVED:			

NM-AIST P.O Box 447 ARUSHA	GRAVITATIONAL WATER VORTEX POWER PLANT	DRG No. V-032	FORMAT A4

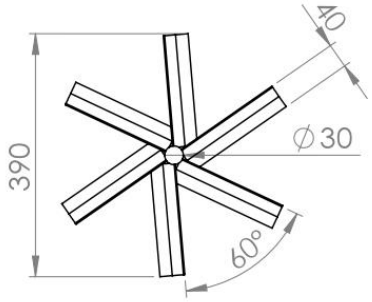

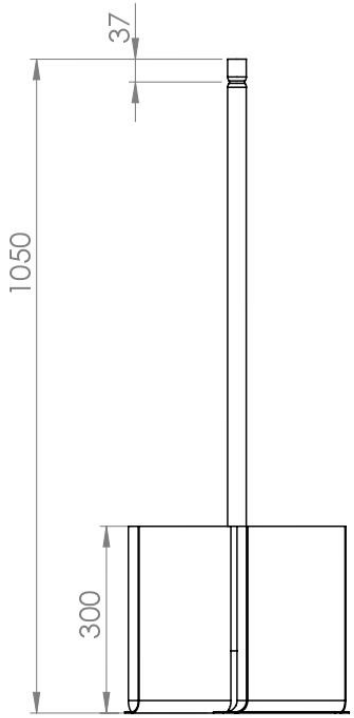

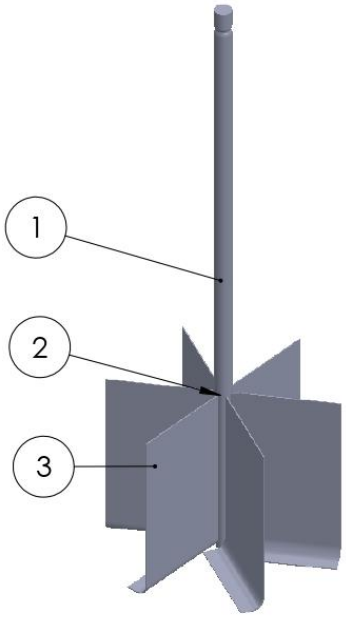

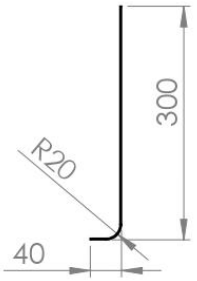

Runner Blade Cross-section

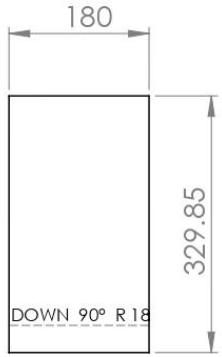

Runner Blade Flat Pattern

ITEM NO.	PART NUMBER	DESCRIPTION	QTY.
1	V-039	Runner Shaft(Round Bar 30 x 1050)	1
2	V-040	Runner Blades Mount	1
3	V-041	Runner Blade(Steel Sheet 2 x 180 x 329.85)	6

V-038	Runner SubAssy	Mild Steel	2 x 1043 x 1050	1	
PART No	PART NAME	MATERIAL	SPECIFICATION	QUANTITY	REMARKS
	SCALE:1:10	DRAWN: ADAM MFANGAVO		SHEET 1 OF 1	
	DIMENSION: mm	CHECKED:		DEBUR AND BREAK SHARP EDGES	
	DATE: JUNE 2023	APPROVED:			

NM-AIST P.O Box 447 ARUSHA	GRAVITATIONAL WATER VORTEX POWER PLANT	DRG No. V-038	FORMAT A4

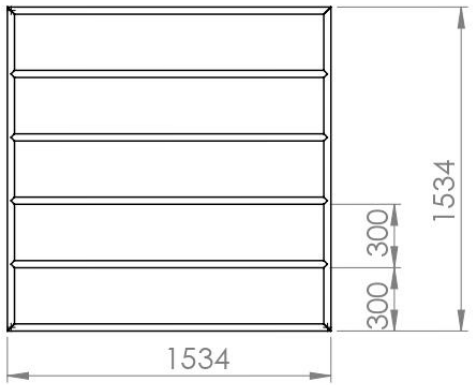

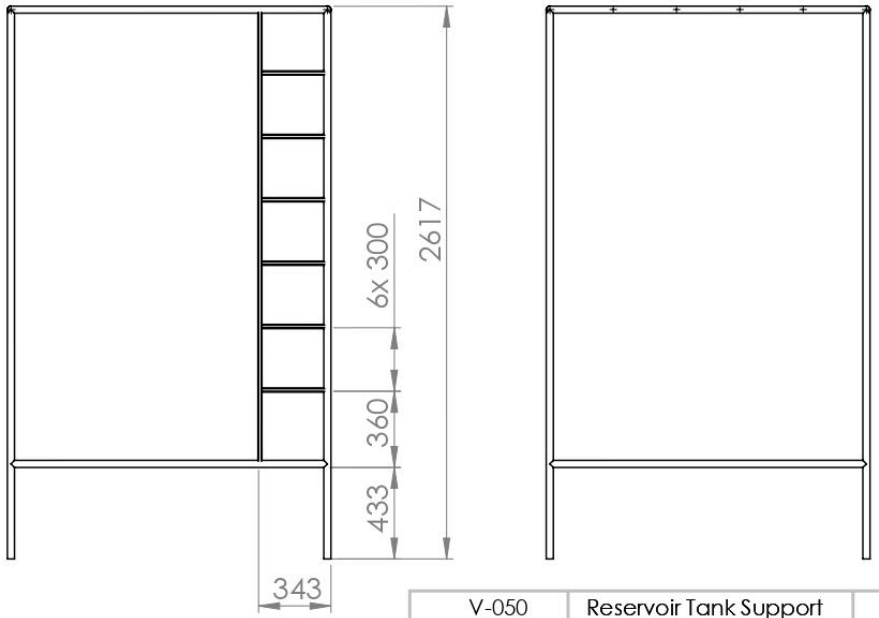

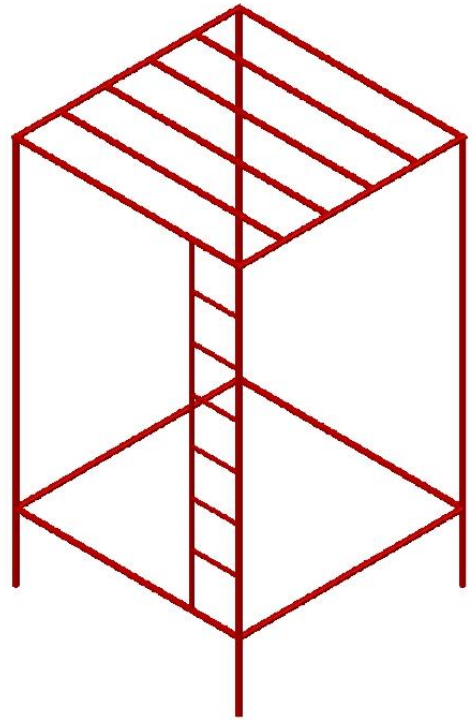

V-050	Reservoir Tank Support	Mild Steel	2 x 1043 x 1050	1	
PART No	PART NAME	MATERIAL	SPECIFICATION	QUANTITY	REMARKS
	SCALE:1:30	DRAWN: ADAM MFANGAVO		SHEET 1 OF 2	
	DIMENSION: mm	CHECKED:		DEBUR AND BREAK SHARP EDGES	
	DATE: JUNE 2023	APPROVED:			

NM-AIST
P.O Box 447
ARUSHA

GRAVITATIONAL WATER VORTEX POWER PLANT

DRG No. V-050

FORMAT A4

RESEARCH OUTPUTS

I. Publications

Faraji, A., Jande, Y. A. C., & Kivevele, T. (2022). Performance analysis of a runner for gravitational water vortex power plant. *Energy Science & Engineering*, *10*(4), 1055-1066.

Accepted article in the Tanzania Journal of Science published by the University of Dar es Salaam, College of Natural and Applied Sciences : Exergy analysis and performance testing of a gravitational water vortex turbine runner for small hydropower plants: An Experimental Approach".

II. Poster presentation

Received: 9 September 2021 | Revised: 19 January 2022 | Accepted: 24 January 2022

DOI: 10.1002/ese3.1085

MODELLING AND ANALYSIS

Performance analysis of a runner for gravitational water vortex power plant

Adam Faraji[1,2] | Yusufu Abeid Chande Jande[1,3] | Thomas Kivevele[1,3]

[1]Materials and Energy Science and Engineering Department, The Nelson Mandela African Institution of Science and Technology, Arusha, Tanzania

[2]Department of Mechanical Engineering, Arusha Technical College, Arusha, Tanzania

[3]Water Infrastructure and Sustainable Energy Futures centre, The Nelson Mandela African Institution of Science and Technology, Arusha, Tanzania

Correspondence
Adam Faraji, Materials and Energy Science and Engineering Department, The Nelson Mandela African Institution of Science and Technology, Nelson Mandela Rd, P.O. BOX 447, Arusha, Tanzania.
Email: farajia@nm-aist.ac.tz

Abstract

Micro-hydropower can be used to meet the needs of both isolated and rural communities for electricity. Due to its inexpensive initial investment, simple design, easy maintenance and low-head utilisation, the gravitational water vortex power plant (GWVPP) has recently piqued interest. The findings of numerical work employing a numerical simulation and analytical approach for the GWVPP are presented in this study. To understand the influence of each on the efficiency of GWVPP, four parameters (speed, hub-blade angle, number of blades and runner profile) were explored. Design-Expert software was used to investigate the interplay of each parameter/factor in order to maximise the contribution of each. Design-Optimal Expert's (custom) design tool was used to construct twenty-four experimental runs. To calculate the system efficiency, these runs were simulated in commercial computational fluid dynamics (CFD) software called Ansys CFX.

The numerical results were in good agreement with the experimental results, which yielded R^2 values of 0.9507 and 0.9603 for flat and curved profiles, respectively. Furthermore, the findings show that the chosen parameters have an impact on the GWVPP's efficiency via interaction as seen in response surface methodology (RSM). Furthermore, numerical analysis increased the curved blade profile runner's total efficiency by 3.65%. In comparison with the unoptimised scenarios, the efficiency of the flat runner profile increased by 1.69%.

KEYWORDS

blade profile, CFD, gravitation water vortex, micro-hydropower, runner

1 | INTRODUCTION

The enormous dependency on conventional energy resources such as fossil fuel has triggered world concern about environmental awareness, hence has promoted renewable energy resources. Hydropower has proven to be mainly exploited as one of the renewable energy resources due to its wide availability and greater capacity than other renewable sources.[1] However, for the best utilisation of these systems, maintaining the power and frequency stability of the power system plays an important role. Through a hydro-turbine nonlinearity approach, a stability analysis has been performed where results are helpful for practical applications.[2,3] Also, employing mathematical modelling

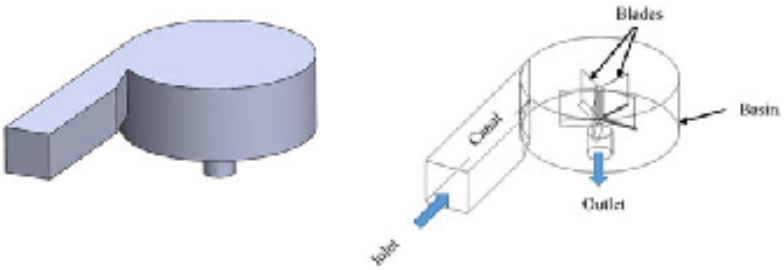

FIGURE 1 Three Dimension (3-D) base case

analysis, stability and damping is studied for large hydropower units.[4,5]

Furthermore, hydropower can be categorised into many types where one of them is micro-hydropower plants. According to Timilsina et al.,[6] micro-hydropower plants are small scale systems that can produce up to 100 kW. This scheme has recently become a growing interest globally because it plays an essential role in power generation in isolated and rural areas.

The gravitational water vortex power plant (GWVPP) is the micro-hydropower scheme applicable mainly in small rivers and streams with low flowrate and low heads. The main three compositions of the GWVPP include a canal, a runner and a basin. GWVPP has been reported to have several advantages such as safe to the environment, ease to manufacture, ease in installation, low costs of operations and maintenance, do not need a reservoir, is safe for aquatic life, increases surface water area, maximises the water velocity of flow on the surface area.[7-9]

Recently, there has been a growing interest in GWVPP. However, there is little work regarding this technology. Researchers have been paying attention to the effect of runner profiles (shapes) on the final performance of the GWVPP. Dhakal et al.[10] numerically studied three runner profiles to determine the most suitable shape. The curved runner profile was reported to have a higher efficiency of 82% than twisted and straight blades, which exhibited 63% and 46% efficiency, respectively. Kueh et al.[11] also experimentally studied the two profiles of the runner. Although the curved profile runner showed better efficiency of 22.24% over the flat profile, which exhibited 21.63%, this study's optimal efficiency was not reached because of the experimental limitations.[11] Khan et al.[8] studied basin to blade ratio configurations by utilising different runner profiles, where the findings revealed that cross-flow blades showing the best efficiency.

The experimental study made by Kueh et al.[11] faced various challenges that could not be solved due to testing limitations. For instance, optimal operating speed was not reached due to practical constraints, failing to determine maximum efficiency. Also, the optimisation of the runner model through various design parameters was not taken into account.

Computational fluid dynamics (CFD) has become a helpful tool for predicting flow patterns and other vital parameters at different conditions. This tool can be utilised during the design process to optimise the design before the actual manufacturing.

The concerns have encouraged the authors to research the use of numerical analysis to overcome experimental limitations at similar conditions to the base case. The same approach will be used to investigate and optimise the GWVPP runner's behaviour by varying speed, hub-blade angle and number of blades. The study aimed to perform numerical analysis and comparative analysis against experimental results for validation purposes. The criteria for evaluation of GWVPP are its final efficiency at different flow conditions under two-phase conditions.

2 | MATERIALS AND METHODS

During this study, numerical methods are used to analyse the efficiency of the GWVPP for flat and curved runner profiles. The base model used in the numerical analysis was chosen from the experimental setup by Kueh et al.[11] The base model was numerically optimised to improve its efficiency. Two phases (air and water at 25°C) were run in Ansys CFX 17.0 at the steady-state with the shear stress transport (SST) turbulence model.

2.1 | Model development

Solidworks software v.2016 was used to create the models. The meshing was done using Ansys ICEM once the established models from Solidworks were transferred. Furthermore, the Ansys ICEM meshed model was imported into the Ansys standalone CFX software, which was used to analyse and optimise the system using the set parameters. The numerical analysis proceeded in the order listed below. To begin, a numerical technique was used to check the agreement of experimental results (for both flat and curved profiles). The optimisation technique was then used, in which selected parameters were changed.

2.2 | Numerical analysis

Solidworks 2016 was used to create three-dimensional (3D) models of the components (canal, runner blades and basin) using the given base design. Four blades with a rotational speed of 4.08 to 2.5 rad/s were confined within a 1000 mm outer runner diameter. The GWVPP model is shown in Figure 1. The guide, which directs the water flow towards the basin, is part of the canal's entrance segment. The runner's rotational velocity is created by the water entering the basin tangentially, and the water is then released axially through the exit.

The computational domains are divided into two parts: a stationary domain that includes the inlet, canal, runner-basin interface, opening, wall and outlet. The rotating domain is the second domain, and it consists of a runner and a runner-basin interface.

Using Ansys ICEM CFD, unstructured tetrahedral mesh computational grids were created on both the stationary and rotational domains. In the Ansys CFX, the stationary and rotating meshes were independently meshed, and then all meshes were connected to a single computational domain. There were a total of 4,380,000 nodes in the network. Figures 2 and 3 illustrate the numerical mesh of the stationary domain (canal and basin) and the rotating domain (runner). The quality of the generated meshes was checked and confirmed using the Ansys ICEM tool.

A total of 4,380,000 nodes were used in this research. This figure was arrived at after a series of tests with meshes ranging from 500,000 to 5,000,000 nodes. The node variation ensures that the final results are not harmed by the amount of nodes.[12] Figure 4 depicts the results of the mesh dependency test. As a result of looking at Figure 4, mesh dependence sensitivity analysis was required. A universal grid interface method was used to create mesh connections between domains and interfaces. The turbulence was predicted using the SST turbulence model. During the numerical study, a two-phase flow with air and water was also used and separated by a discrete interface. Between the basin and runner interface, the frozen rotor was used as a numerical treatment. The set model results yield a steady-state solution for multiple frames of reference.

The root mean squared (RMS) convergence criteria were utilised, with an average residual target of 1×10^{-4} for mass, momentum and turbulence equations. To achieve adequate convergence, a physical time-step of 0.01 s was used with a maximum iteration of 1000. Figure 5 also shows the mass flow rate of the input portion and the static pressure at the stationary domain output. Tables 1 and 2 provide the design parameters and numerical boundary conditions, respectively.

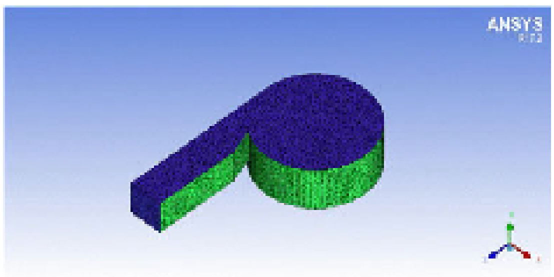

FIGURE 2 Numerical mesh in a stationary domain

2.3 | Procedure

2.3.1 | Base model validation

The numerical analysis used the base runner, which was built based on Kueh's experimental work.[11] The parameters of the numerical analysis were retrieved and listed, and their efficiencies were estimated using the parameters of the base model. In each case, the flow pattern and velocity vectors were observed. Ansys CFX was used to assess the base model's agreement with numerical analysis results in the first approach to numerical analysis. There were a total of twenty-four (24) cases run, with the results being recorded.

2.3.2 | Experimental design (selection of optimal parameters)

The effect variables on the efficiency of the GWVPP were investigated using response surface methodology (RSM). RSM is a statistical, scientific and mathematical technique for optimising independent variables while developing models.[13] This feature is available in the Design-Expert software. The RSM approach is a good choice for fitting quadratic surfaces and optimising process inputs with a small number of experiments, as well as analysing parameter interactions. It is a general-purpose strategy that combines design of experiments, regression analysis and optimisation methods to optimise the answers (output variables) that are influenced by numerous independent variables (input variables). Factors used by in RSM include runner speed (A), hub-blade angle (B), blade number (C) and blade profile (D) (D). Table 3 shows how RSM is designed, as well as coded and uncoded levels. This experiment was created using an optimal (custom) design and a quadratic model. A total of twenty-four runs were performed at random, with five interior points, eleven vertex points, six plane points and two edge points.

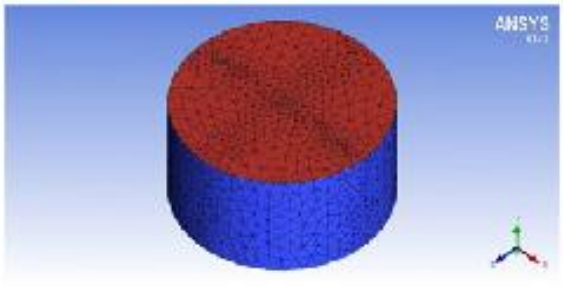

FIGURE 3 Numerical mesh in a rotating domain

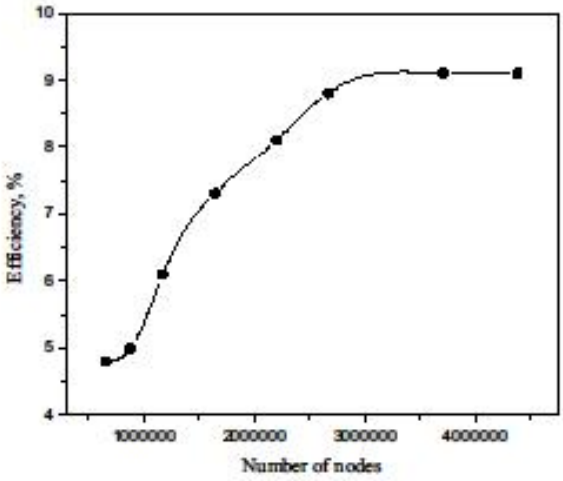

FIGURE 4 Mesh sensitivity analysis

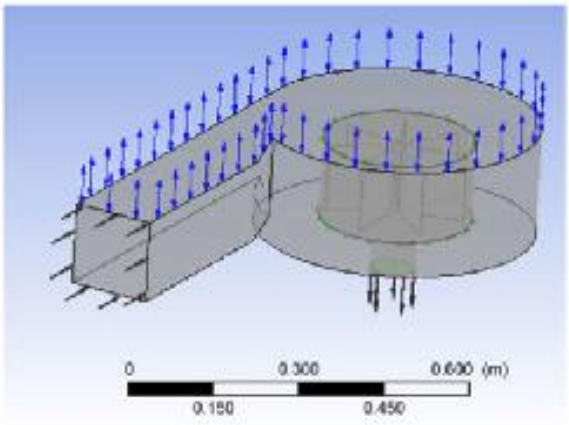

FIGURE 5 Base case setup

2.3.3 | Theoretical performance optimisation of the system

The numerical analysis was utilised to perform analyses that the brake system (in the experimental investigation) was unable to give due to a substantial friction torque needed throughout the experiment. The number of blades tested ranged from 3 to 12, the hub-blade angle varied from 15° to 22° at 1° intervals, and the runner rotational speed varied from 2.62 to 4.08 rad/s. This method aimed to determine the impact of these variables on the GWVPP's overall efficiency. Design-Expert software v.13 was used to produce the best parameter selection and combination. As a result, the base model's efficiency and the optimised model's final efficiency were linked. Additionally, the water flow pattern was observed using simulation techniques such as streamlines.

TABLE 1 Design parameters[11]

Head (H)	0.5 m
Number of blades	3 to 12
Hub-blade angle	15° to 22°
Rotational speed	Varying (2.5 to 4.08 rad/s)
Flow rate (Q)	0.00225 m^3/s
Static pressure	0 Pa

TABLE 2 Numerical boundary conditions

Inlet	Mass flow rate
Outlet	Static pressure (0)
Turbulence model	Shear Stress Transport (SST)
Type of simulation	Steady-state
Phase type	Phase (Air and Water at 25°C)

2.4 | Theory

The Ansys CFX solver can solve the steady-state and transient equations. Mass and momentum equations can be stated as displayed in equations (1) and (2)12:

$$\frac{\partial \rho}{\partial t} + \nabla \cdot (\rho U) = 0 \tag{1}$$

where ρ denotes density while U displays the vector of velocity U_{xyz}.

$$\frac{\partial (\rho U)}{\partial t} + \nabla (\rho U \otimes U) = -\nabla p + \nabla . \tau + S_M \tag{2}$$

where τ denotes stress tensor and $\otimes$ displays dyadic symbol; S_M denotes momentum of the external source term while stress tensor τ is related to the strain rate.[12]

$$\tau = \mu(\nabla U) + \left(\nabla U^T - \frac{2}{3}\delta \nabla . U\right) \tag{3}$$

TABLE 3 Independent variables (RSM optimal custom)

Independent variable	Symbol	Factor	Coded low	Coded high
Runner speed (rad/s)	A	Numerical	2.62	4.08
Hub-blade angle	B	Numerical	15°	22°
Number of blades	C	Numerical	3	12
Blade profile	D	Categorical	Flat	Curved

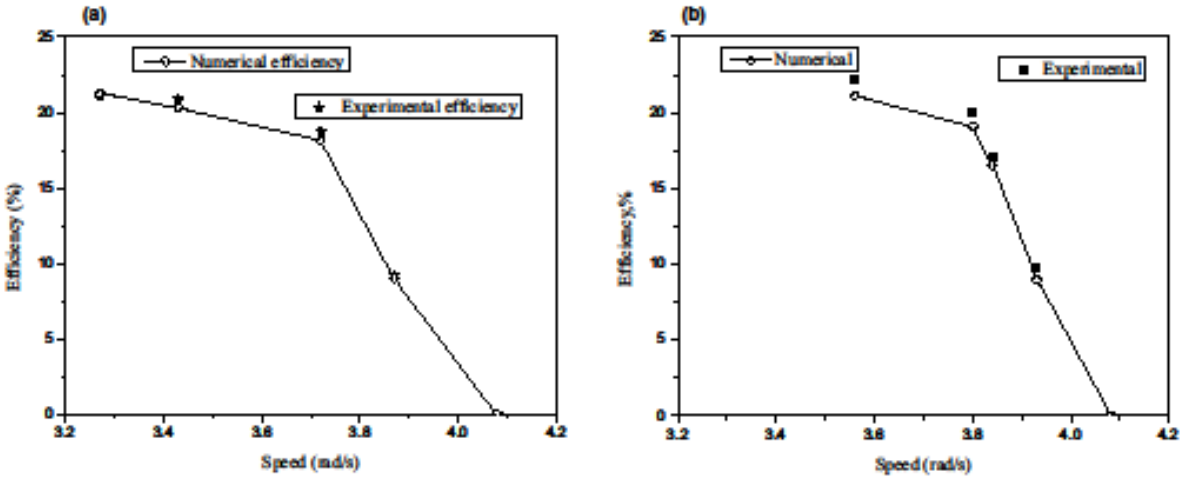

FIGURE 6 Experimental versus numerical (A) flat blade profile (B) curved blade profile

where T denoted static temperature and μ displays molecular viscosity. Mass and momentum conservation equations stated in equation (1) and (2) calculates the velocity fields.

The criteria used to measure the performance of the turbine is its final efficiency. Efficiency is considered as the percentage of the input power to the output power.

2.4.1 | Theoretical Power of the GWVPP

The maximum power output of hydropower can be obtained is as follows[6]:

$$P = \rho g Q H \tag{4}$$

where H is the gross head at the site and Q is the flow rate.

Similar to conventional hydropower, the performance of GWVPP is obtained by using its output efficiency. Because the GWVPP runner is classified as a combination between an impulse and a reaction turbine, the equation is written as Mulligan et al[14]:

$$P_{out} = T\omega = Q\rho\left(v_1 - v_b\right) r\omega \tag{5}$$

where P_{out} is the shaft power of the runner; T is the torque at the shaft while ω is the angular velocity, Q is the flow rate, ρ is water density, v_1 is the interface velocity between runner and basin, v_b is the blade velocity and r is the basin radius.

Interface velocity, runner blade velocity and torque produced were deduced by the available function calculator in the CFD-Post processing. A runner was assigned as a rotating domain. The rotation axis of the runner is selected to be in the y-direction. Angular velocity 'ω' was calculated by using the equation:

$$\omega = \frac{2.N.\pi}{60} \tag{6}$$

Thus, the efficiency of the GWVPP can be calculated by:

$$\eta = \frac{\left(v_1 - v_b\right) r\omega}{gH} \tag{7}$$

where v_1 is the interface velocity, and v_b is the blade velocity.

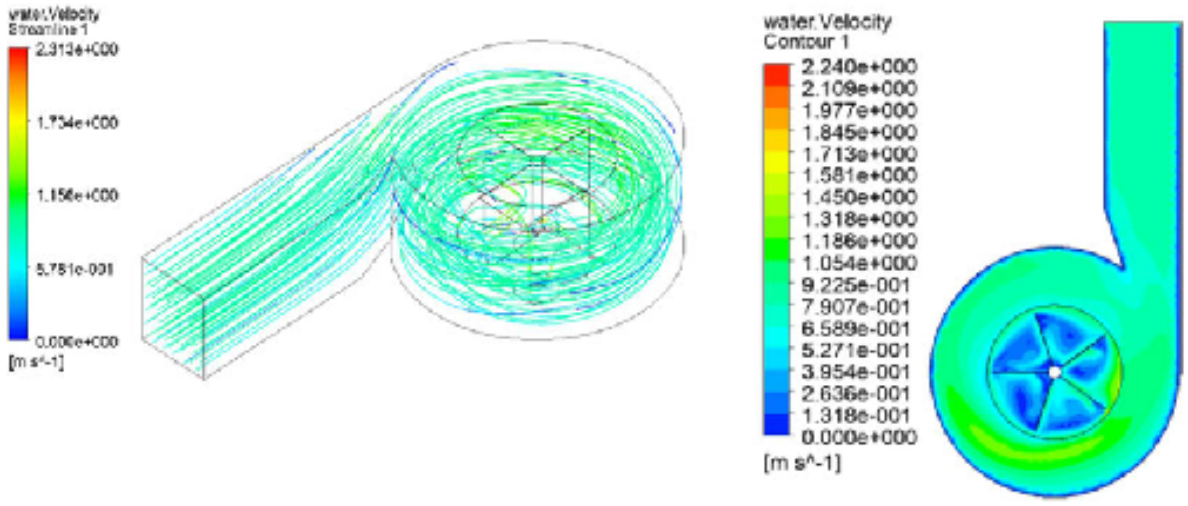

FIGURE 7 Model (A) Streamlines (B) velocity contour

TABLE 4 Simulated factors and their responses

Run	Factor 1 A: speed, rad/s	Factor 2 B: Angle, Degree	Factor 3 C: blades	Response 1 Efficiency (flat), %	Response 2 Efficiency (curved), %
1	3.27664	18	8	16.02	18.07
2	3.6128	18	7	14.08	17.2
3	3.6128	18	7	14.08	17.2
4	2.62	16	6	23.32	25.89
5	4.08	18	12	9.47	11.2
6	3.9048	22	7	10.09	12.88
7	3.32749	15	11	11.28	13.09
8	2.62	17	12	12.05	16.87
9	4.007	18	6	12.48	14.6
10	3.32749	15	11	11.28	13.09
11	4.08	15	12	8.5	9.8
12	3.1821	20	3	15.52	17.3
13	3.6055	22	12	11.82	13.35
14	3.6055	22	12	11.82	13.35
15	3.0799	15	8	17.42	18.2
16	2.8901	15	3	17.55	20.63
17	4.08	22	3	8.08	11.54
18	2.62	22	6	19.32	21.03
19	2.62	20	7	19.89	21.5
20	3.6128	18	7	17.02	18.74
21	4.08	15	3	9.11	12.06
22	3.1821	20	3	15.25	16.9
23	2.839	19	3	18.42	21.24
24	2.62	22	12	13.87	15.55

TABLE 5 Response transformation and model fitting

Response (Efficiency)	Response range	Ratio[a]	Fitting	Transformation
Curved	9.8–25.89	2.64	Quadratic	None
Flat	8.08–23.32	2.89	Quadratic	None

[a]Ratio of maximum to the minimum response.

TABLE 6 ANOVA for the quadratic model

	Flat profile					Curved profile				
Source	Sum of Squares	df	Mean Square	*F*-value	*p*-value	Sum of square	df	Mean square	*F*-value	*p*-value
Model	316.54	9	35.17	30.02	<0.0001	348.20	9	38.69	37.62	<0.0001
A-speed	161.28	1	161.28	137.65	<0.0001	178.28	1	178.28	173.37	<0.0001
B-Angle	0.0103	1	0.0103	0.0088	0.9265	1.82	1	1.82	1.77	0.2047
C-blades	27.94	1	27.94	23.85	0.0002	34.59	1	34.59	33.63	<0.0001
AB	0.0658	1	0.0658	0.0562	0.8161	5.38	1	5.38	5.23	0.0382
AC	25.84	1	25.84	22.05	0.0003	13.87	1	13.87	13.49	0.0025
BC	9.29	1	9.29	7.93	0.0137	11.83	1	11.83	11.51	0.0044
A^2	0.0305	1	0.0305	0.0260	0.8741	3.55	1	3.55	3.45	0.0843
B^2	2.84	1	2.84	2.42	0.1421	8.98	1	8.98	8.74	0.0104
C^2	37.18	1	37.18	31.73	<0.0001	31.73	1	31.73	30.86	<0.0001
Residual	16.40	14	1.17			14.40	14	1.03		
Lack of Fit	10.60	9	1.18	1.02	0.5228	12.74	9	1.42	4.26	0.0625
Pure Error	5.80	5	1.16			1.66	5	0.3322		
Cor Total	332.94	23				362.59	23			

3 | RESULTS AND DISCUSSIONS

3.1 | Validation results

Numerical analysis performed based on the data from the experimental test has shown good agreement with the experimental results. The combined numerical and experimental results for flat and curved tests are displayed in Figure 6. The purpose of these tests was to study the agreement of the numerical approach against the experimental method. For both flat and curved blade profiles, the numerical and experimental results are in good agreement. This result suggests that the numerical approach can further investigate the vortex system for the optimisation process. Figure 7 depicts the streamlines and velocity contours in the internal flow field of GWVPP. From both presentations, some distortion can be observed to due to availability of blades. Some turbulences can also be observed as the result of interaction between runner and the basin.

3.2 | Optimisation of parameters by RSM

The actual design parameters as proposed by Design-Expert software and their corresponding responses as Ansys CFX software are displayed in Table 4. The output presented by Design-Expert software offers an unaliased quadratic model for the efficiency of the GWVPP.

Equations (8) and (9) shows the final models of quadratic equations for GWVPP efficiency.

$$\text{Efficiency (flat profile)} = 24.3584 - 7.60184A + 2.11494B - 1.40191C - 0.0393932AB + 0.588195AC + 0.0671479BC - 0.171252A^2 - 0.0674256B^2 - 0.142724C^2 \quad (8)$$

$$\text{Efficiency (curved profile)} = 56.4381 - 27.5295A + 2.57002B - 1.23527C + 0.356225AB + 0.430987AC + 0.0757838BC + 1.84777A^2 - 0.120001B^2 - 0.131851C^2 \quad (9)$$

3.3 | Statistical analysis

3.3.1 | Model fitting

The effects of independent variables, including runner speed (A), hub-blade angle (B), the number of blades (C) and blade profile (D), on the efficiency of the GWVPP are given in Table 5. The results depict that curved blade profile efficiency rose by 3.65% while flat blade improved by 1.69%. In addition, coefficients of the quadratic equation were computed from experimental data to predict the values of the response variable. Observation from Table 6

displays the lack of fit F-value of 1.02 for flat profile, implying the lack of fit is insignificant relative to the pure error. On the other hand, for curved profile, lack of fit, F-value is observed to be 4.26, implying lack of fit is also insignificant.

3.3.2 | Analysis of variance

Analysis of variance (ANOVA) was carried out to ensure proper fit of the derived model. A test for the significance of the regression model and lack of fit coefficient was determined. A confidence level value (F-value) and probability value (p-value) were employed as a basis for ranking the significant factors. The effectiveness of these factors was ranked in the order of rotational speed > number of blades > hub-blade angle as it can observed in Table 6. ANOVA results in Table 6 indicates outputs of equations (8) and (9). It can be observed from Table 6 that the model of F-value of GWVPP efficiency for a flat profile and curved profile are 30.02 and 37.62, respectively, while their corresponding model of p-value is less than 0.0001 for both profiles. These F-value and p-value suggest that the models were significant and statistically accurate, and there is only a 0.01% chance that an F-value could occur due to noise. Therefore, the terms A, B, C, AB, AC, BC, A^2, B^2, C^2 are significant model terms.

Table 7 summarises the statistical parameters. This study shows that the R^2 for flat and curved profiles being 0.9507 and 0.9603, respectively, demonstrating that the quadratic model could adequately describe the influence of speed (A), hub-blade angle (B) and blades number (C). Thus, R^2 is closer to one; it indicates a better model fitting to actual data.[13] The predicted R^2 for both responses of flat and curved profiles correlated with adjusted R^2, suggesting the data from Ansys CFX are correct, and their deviations are insignificant. Moreover, these findings indicate that the predicted models for flat and curved profiles can be applied to navigate the design space.

Additionally, the Predicted R^2 of 0.8165 and 0.8555 for flat and curved profiles reasonably agree with the Adjusted R^2 of 0.9191 and 0.9348, respectively; that is the difference is less than 0.2.

The graph of actual versus simulated data was plotted to establish the validity of the model. The residuals show the difference between the experimented data and the predicted value. Figure 8a,b presents the correlation between predicted and simulated data; all data were found around the line of best fit, suggesting that the simulated

TABLE 7 Statistical parameters

Parameter	Flat profile	Curved profile
Standard deviation	1.08	1.01
Mean	13.99	16.30
C.V. %	7.74	6.22
R^2	0.9507	0.9603
Adjusted R^2	0.9191	0.9348
Predicted R^2	0.8165	0.8555
Ade. precision	19.0980	23.0059

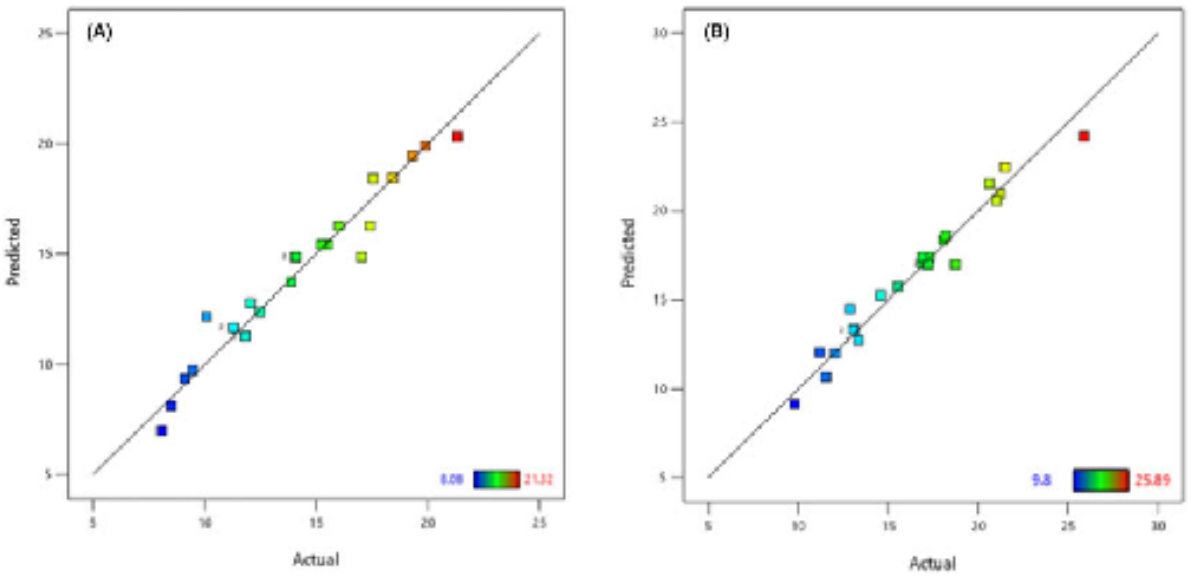

FIGURE 8 Predicted value versus simulated value for the yield of (A) flat profile (B) curved profile

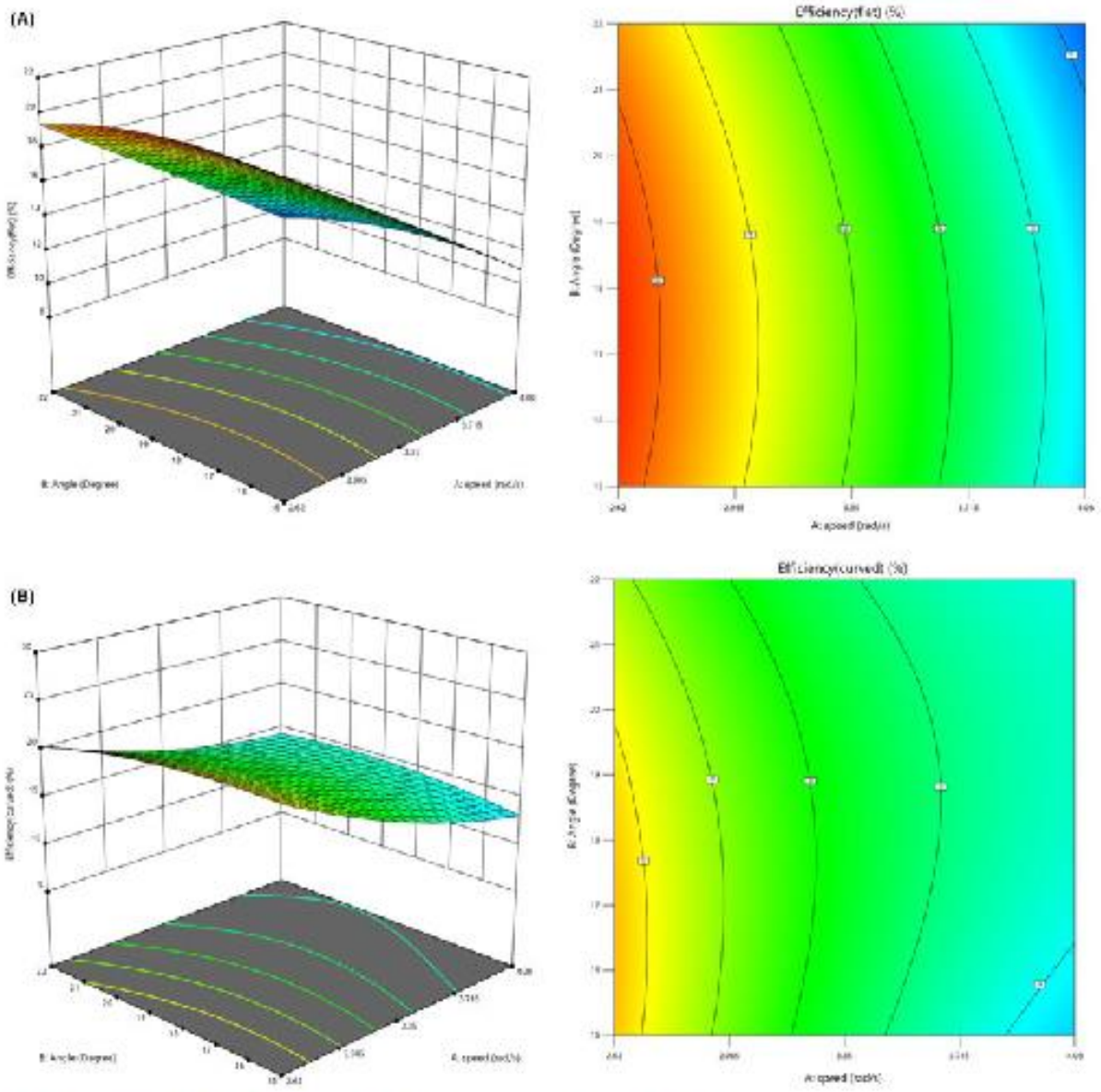

FIGURE 9 3D plot and contour for (A) flat profile and (B) curved profile (factors A and B)

data agreed with predicted values without any abnormalities in the models.

3.4 | Discussion: Derived models interpretation

The Response graphs obtained from the Design-Expert software has provided the best visualisation of interactions for the factors under study. Three dimensional (3D) and contour plots were developed to understand the interactions of each parameter and establish their contribution towards the final efficiency of the GWVPP.[15] The surface plots (3D and contour) for the flat and curved runner profiles are displayed in Figures 9–11. Figure 9 shows the interactions of two factors, namely, factor A (speed) and factor B (hub-blade angle) to check their influence against factor D (blade profiles i.e. flat and curved). The effect of these two factors on the final efficiency of the GWVPP for the flat and curved profiles is observed. The plots reveal that both parameters, speed and hub-blade angle contribute to the efficiency of the GWVPP at a particular range for all profiles under study. For example,

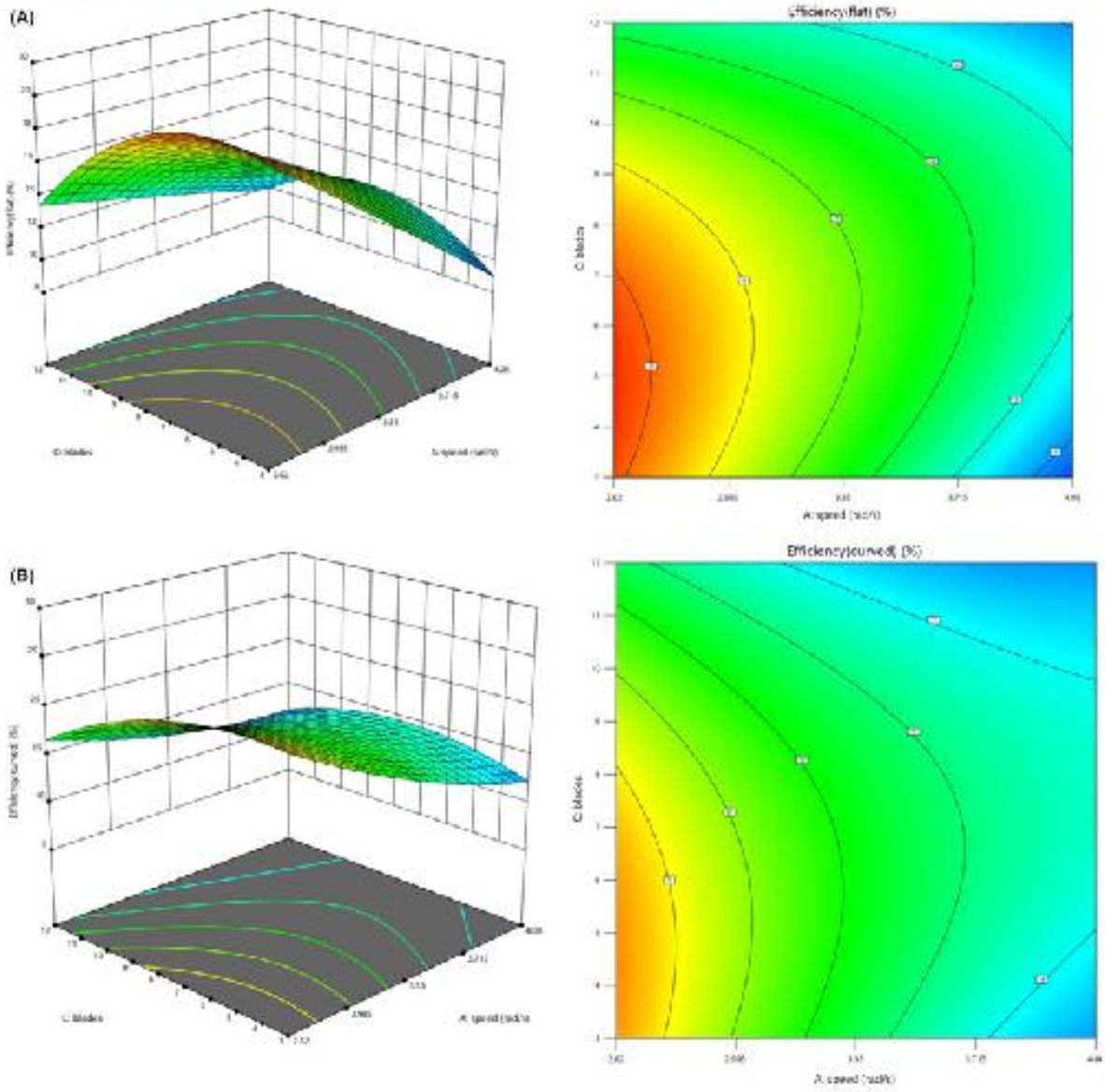

FIGURE 10 3D plot and contour for (A) flat profile and (B) curved profile (factors A and C)

although a shallow bell-shaped structure can be seen in the flat profile in Figure 9A, the strong bell-shaped is observed in curved profiles in Figure 9B. This result suggests that these factors are crucial in the performance of the GWVPP and are in agreement with the works of literature.[6-9]

Also, the effect of interactions of factor A (speed) and factor C (number of blades) to factor D (blade profiles i.e. flat and curved), as displayed in Figure 10, was studied. A clear bell-shaped structure is seen for the flat profile in Figure 10A, while for the curved profile in Figure 10B, the twisting of the plots is observed. Again, these results suggest that these factors are essential in the performance of GWVPP, although the twist seen in the curved profile may mean two factors are not optimally blended.[8]

Moreover, the combination of factor B (hub-blade angle) and factor C (number of blades) to factor D (blade profiles i.e. flat and curved) is considered to observe their effect on the efficiency of the GWVPP.

For both flat, Figure 11A and curved, Figure 11B profiles depict a bell-shaped structure plot. This behaviour suggests that these two factors have a significant contribution to the efficiency of the GWVPP. As per several works of literature,[6-8,10,16] runner speed typically

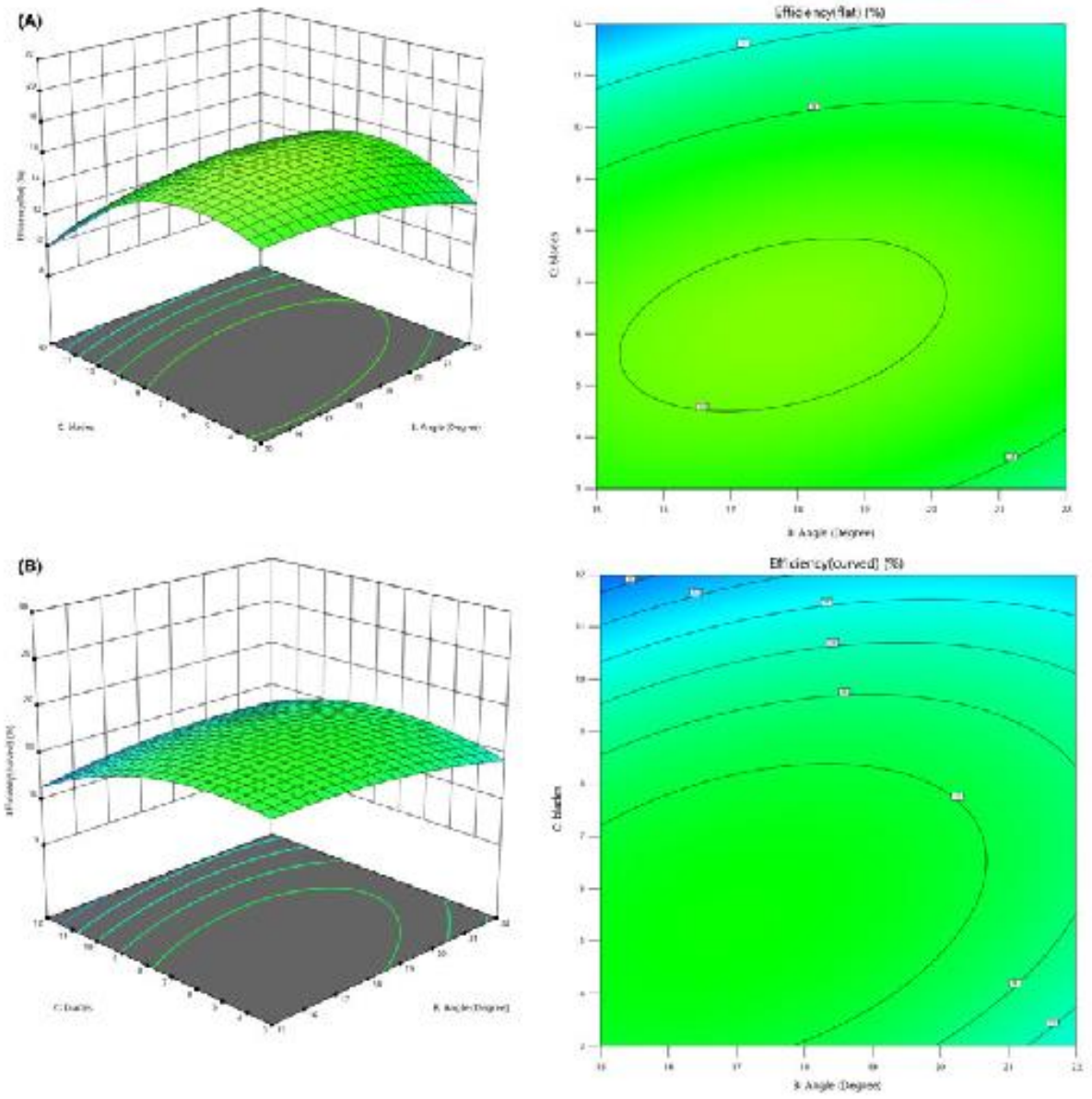

FIGURE 11 3D plot and contour for (A) flat profile and (B) curved profile (factors B and C)

follows the bell-shaped structure implying that the efficiency of the GWVPP increases as speed rises. Still, after reaching a certain speed (optimal), the efficiency starts to fall.

4 | CONCLUSION

The paper examined the application of CFD for the validation of experimental tests. Essential components regarding GWVPP were modelled in 3D by using the Solidworks software. The modelled features include; water canal, the water basin (both considered stationary domains) and the runner (considered rotating domain). On the other hand, Design-Expert through RSM was utilised to optimise the interactions of factors. RSM gave the combination of each parameter to get the optimum blend. The study has further used CFD software to study and predict the effect of four parameters on the efficiency of the GWVPP. These parameters include runner speed (A), hub-blade angle (B), the number of blades (C) and blade profile (D) designed along with coded and

uncoded levels. Through the blending of these four parameters, the system efficiency is improved. The reason being the applied approach minimised one-factor-at-a-time (OFAT) selection limitations. The study shows that a numerical approach together with proper blending of parameters can be used to perform an analysis of the GWVPP. Also, Design-Expert software can be exploited to determine the combinations of parameters. Results of the investigation have shown good agreement with the experimental work. Additionally, the results show that the chosen parameters affect the GWVPP through interaction observed in RSM.

Furthermore, numerical analysis improved the runner's overall efficiency of curved blade profile by 3.65%. In contrast, the efficiency of the flat runner profile rose by 1.69% compared to the unoptimised cases. The observed results depict that it is possible to validate experimental results using Ansys CFX as one of the CFD tools.

ACKNOWLEDGEMENTS

The authors acknowledge the following: (i) the Water Infrastructure and Sustainable Energy (WISE Futures) centre under the Nelson Mandela African Institution of Science and Technology (NM AIST) for their financial support and (ii) the PIV lab of Korea Maritime and Ocean University (KMOU) for valuable support during Ansys CFX analysis.

ORCID

Adam Faraji https://orcid.org/0000-0001-8627-7729
Thomas Kivevele https://orcid.org/0000-0003-4539-6021

REFERENCES

1. Okot DK. Review of small hydropower technology. *Renew Sustain Energy Rev*. 2013;26:515-520.
2. Liu D, Li C, Malik O. Nonlinear modeling and multi-scale damping characteristics of hydro-turbine regulation systems under complex variable hydraulic and electrical network structures. *Appl Energy*. 2021;293:116949.
3. Liu D, Wang X, Peng Y, et al. Stability analysis of hydropower units under full operating conditions considering turbine nonlinearity. *Renew Energy*. 2020;154:723-742.
4. Liu D, Li C, Malik OP. Operational characteristics and parameter sensitivity analysis of hydropower unit damping under ultra-low frequency oscillations. *Int J Electr Power Energy Syst*. 2022;136:107689.
5. Liu D, Li C, Tan X, Xueding L, Malik O. Damping characteristics analysis of hydropower units under full operating conditions and control parameters: accurate quantitative evaluation based on refined models. *Appl Energy*. 2021;292:116881.
6. Timilsina AB, Mulligan S, Bajracharya TR. Water vortex hydropower technology: a state-of-the-art review of developmental trends. *Clean Technol Environ Policy*. 2018;20:1737-1760.
7. Dhakal S, Nakarmi S, Pun P, Thapa AB, Bajracharya TR. Development and testing of runner and conical basin for gravitational water vortex power plant. *J Inst Eng*. 2014;10:140-148.
8. Khan NH, Cheema TA, Chattha JA, Park CW. Effective Basin–Blade configurations of a gravitational water vortex turbine for microhydropower generation. *J Energy Eng*. 2018;144:04018042.
9. Rahman MM, Tan JH, Fadzlita MT, Muzammil ARWK. A review on the development of gravitational water vortex power plant as alternative renewable energy resources. In: *International Conference on Materials Technology and Energy*. IOP Publishing; 2017;217:012007.
10. Dhakal R, Bajracharya TR, Shakya SR, et al. Computational and experimental investigation of runner for gravitational water vortex power plant. In: *2017 IEEE 6th International Conference on Renewable Energy Research and Applications (ICRERA)*. IEEE Publisher; 2017:365-373.
11. Kueh TC, Beh SL, Ooi YS, Rilling DG. Experimental study to the influences of rotational speed and blade shape on water vortex turbine performance. In: *Fifteenth Asian congress of fluid mechanics (15ACFM)*. IOP Publishing; 2017;822:012066.
12. CFX Ansys. Ansys Cfx-solver theory guide. *ANSYS CFX Release*. 2009;15317:724-746.
13. Montgomery DC, Myers RH, Anderson-Cook CM. *Response Surface Methodology – Process and Product Optimization Using Designed Experiments*. WILEY; 2016.
14. Mulligan S, Casserly J. *The Hydraulic Design and Optimisation of a Free Water Vortex for the Purpose of Power Extraction*. Institute of Technology Sligo; 2010.
15. Wanchat S, Suntivarakorn R, Wanchat S, Tonmit K, Kayanyiem P. A parametric study of a gravitation vortex power plant. *Adv Mater Res*. 2013;805-806:811-817.
16. Power C, McNabola A, Coughlan P. A parametric experimental investigation of the operating conditions of gravitational vortex hydropower (Gvhp). *J Clean Energy Technol*. 2016;4:112-119.

How to cite this article: Faraji A, Jande YAC, Kivevele T. Performance analysis of a runner for gravitational water vortex power plant. *Energy Sci Eng*. 2022;10:1055–1066. doi:10.1002/ese3.1085

TANZANIA JOURNAL OF SCIENCE

ISSN 0856-1761 (Print) & ISSN 2507-7961 (Online)

An international journal published by the University of Dar es Salaam, College of Natural and Applied Sciences

Websites: https://tjs.udsm.ac.tz/index.php/tjs
https://www.ajol.info/index.php/tjs

Telephone/Fax: +255 22 2410129
E-mail: **tjs@udsm.ac.tz**

Our Ref. CoNAS/TJS/2024

Editorial Office
P. O. Box 35065, Dar es Salaam
TANZANIA

19th July 2024

Dear Adam Faraji -Corresponding author,

Re: Acceptance of Your Paper No. TJSP 1535.

I acknowledge receipt of the corrected version of your paper titled "Exergy analysis and performance testing of a gravitational water vortex turbine runner for small hydropower plants: An Experimental Approach".

I am pleased to inform you that your paper is now accepted for publication in the *Tanzania Journal of Science* and will appear in *Volume 50 Issue No. 3 of 2024*. The manuscript will soon be transferred to the Technical Editor for typesetting. You will be contacted once the galley proof is ready for proofreading.

Thank you very much for choosing to publish in our esteemed journal and for your fine contribution.

We look forward to your continued contributions to the journal.

Yours sincerely,

Ebede

Prof. Evelyne I. Mbede
Chief Editor,
Tanzania Journal of Science

Currently Indexed by: ***African Journals OnLine (AJOL); CAB International or CABI*** *(Centre for Agriculture and Bioscience International, UK),* ***CAB Abstracts, CAB Global Health, CAB Direct; Google Scholar; Journals for Free; Crossref; EBSCO Publishing***

Exergy analysis and performance testing of a gravitational water vortex turbine runner for small hydropower plants: An Experimental Approach

Abstract

Gravitational water vortex power plants (GWVPPs) have recently gained popularity due to their low initial investment, simple design, ease of maintenance, and low head utilization. However, the technology suffers from poor performance issues caused by the non-optimized parameters of its crucial components, such as the runner. In this study, the performance of a runner (16° blade-hub angle, six blades, and a curved blade profile) for a GWVPP was experimentally examined. The study also employed an exergy analysis. The experimental results revealed that the efficiency of the GWVPP system was in the range of 9.84% to 25.35%, the torque was in the range of 0.08 to 0.23 Nm, and the output power was in the range of 2.96 to 7.33 W. Furthermore, an exergy analysis of the system showed an exergy efficiency of 43.58%. Additionally, the error analysis of the GWVPP revealed ranges of 0.1 - 0.5 W for power, 0.01 - 0.03 Nm for torque, and 1.3–3.1% for efficiency, suggesting that the experimental setup and instrumentation of this study were reasonably accurate. On the basis of the analyzed results, the newly developed vortex runner and GWVPP system is therefore recommended for energy generation in low-head and flow rate small hydropower plant systems.

Keywords – Micro-hydropower; gravitational water vortex; runner; exergy efficiency; test rig.

Introduction

The overreliance on traditional energy sources, like fossil fuels, has led to environmental concerns, prompting the development of renewable energy options like hydro-turbine power generation, which is cost-effective and practical (Okot, 2013). Hydropower (HP) projects are classified based on size, either small (SHP) or large (LHP), but this classification varies by country due to a lack of consensus (Paish, 2002). Pico, micro, mini, and small systems are subcategories of SHP, with pico generating less than 10 kW, micro generating over 10 kW but less than 100 kW, mini generating over 100 kW but less than 1 MW (Kaunda et al., 2012, Timilsina et al., 2018). SHP systems, either reservoirs or run-of-river types, generate power by diverting water from a river's main channel through a weir, reducing investment costs. The system's working principle involves converting falling water energy into rotating shaft power through a turbine, which can be impulse or reaction-based (Paish, 2002).

In recent years, Micro-hydropower systems are gaining popularity as a renewable energy technology to provide electricity to remote areas with high costs and low incomes. (Williamson et al., 2014). The selection of a turbine for a hydroelectric power plant (HPP) site is influenced by factors such as available head and flow rate, generator operating speed, and power requirements for low flow conditions (Okot, 2013). Micro-HP turbines like Archimedes screw turbine, gravitational water vortex power plant (GWVPP), and waterwheel turbine are suitable for low head and low flow rate conditions.

GWVPP is a micro-HP scheme suitable for low flow rates and heads in rivers and streams, offering a new addition to the 0.7 to 2 m head range (Zotlöterer, 2017). The GWVPP system, consisting of a runner, basin, and canal, offers environmental safety, ease of manufacture, low maintenance costs, no water storage, increased surface water area, and aquatic life safety (Dhakal et al., 2014, Rahman et al., 2017, Khan et al., 2018).

Recent interest in GWVPPs has led to studies assessing their performance, focusing on energy efficiency. The impact of runners' shapes on overall efficiency has been studied. Dhakal's study found that curved running was 82% more efficient than twisted and straight blades, outperforming the other two profiles (Dhakal et al., 2017b). Kueh's experimental study on runner profiles revealed that despite a 22.24% improvement in efficiency, the ideal efficiency was not achieved due to limitations in friction torque and load-cell components (Kueh et al., 2017). Chen's study on basin-to-blade ratio setups revealed that cross-flow blades outperformed other runner profiles with an efficiency of 68.84% (Khan et al., 2018). Two different runner profiles were optimized numerically, with the findings indicating that curved profiles exhibited better efficiency (ranging from 9.80% to 25.89%) compared to flat profiles (with efficiency ranging from 8.8% to 23.32%) (Faraji et al., 2022).

Previous research on GWVPPs was primarily relied on traditional energy efficiency, but exergy efficiency offers a more comprehensive view of energy quality. Exergy efficiency measures the valuable work a system can produce, considering irreversible processes and inefficiencies. This study applied an exergy-based method to evaluate the effectiveness of a GWVPP, aiming to experimentally study the GWVPP system by using the optimized parameters of the numerical study of Faraji et al. (2022) and perform an exergy analysis of the GWVPP system. The study involved the complete design, manufacturing, and experimental testing of a GWVPP test rig. The test rig underwent evaluation at different rotational speeds, assessing power, torque, and efficiency and applying the first law of thermodynamics to determine system exergy efficiency.

Materials and Methods

Experimental set-up

The experimental test rig includes a 1000 L water storage tank, a two hp centrifugal pump, a 1000 L overhead reservoir, a GWVPP basin, a canal, and a runner assembly. The basin and canal are placed above the water storage tank, and the GWVPP runner optimizes the design with specific parameters. These parameters were selected based on a previous study by Faraji et al. (2022). The GWVPP runner's performance was evaluated using digital tachometers and Prony brake dynamometers at various operating speeds. The experimental test rig (Figure 1) was located at the Nelson Mandela African Institution of Science and Technology (NM-AIST) in Tanzania. Replicas or controls were used for reliability and statistical significance.

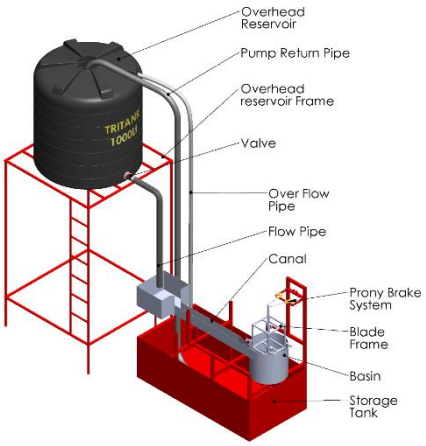

Figure 39: Experimental setup of the three-dimensional gravitational water vortex power plant (GWVPP).

The experimental setup consisted of a blade frame/support, overhead reservoir frame, pump, pipe, storage tank, and overhead reservoir. The blades were secured with mild steel sheets and angle iron, while the overhead reservoir was made from class B black steel pipe. A 2 hp centrifugal pump supplied water to the overhead reservoir, and a 50 mm diameter flexible pipe supplied water to the basin inlet. A storage tank was installed to prevent wastage, and an overhead reservoir was used to create an artificial flow to the canal, storing water that

eventually flowed to the canal entrance. The water is pumped to the reservoir, guided by gravity, and a ball gate valve regulates the flow rate.

Selection of materials

The experimental test rig, primarily made of steel, was constructed for its mobility, portability, and cost-effectiveness, as detailed in Table 1, showcasing the local materials used.

Table 1. The experimental test rig: materials, specifications, and quantity.

Part	Materials	Specifications	Quantity
Basin	Mild steel sheet	1570 × 500 × 2 mm	1 pc*
Canal	Mild steel sheet	2100 × 400 × 2 mm	1 pc
Runner	Mild steel sheet	300 × 180 × 2 mm	6 pcs
	Black pipe	Φ50 × 300 mm	1 pc
Storage tank	Mild steel sheet	2000 × 600 × 2 mm	2 pcs
	Mild steel sheet	1000 × 600 × 2 mm	2 pcs
	Mild steel sheet	2000 × 1000 × 2 mm	1 pc
	Angle iron	40 × 40 × 3 mm	2 pcs
Runner support	Square hollow	20 × 20 × 1.5 mm	2 pcs
	section	40 × 40 × 3 mm	1 pc
	Angle Iron	Φ40 × 1200 mm	1 pc
	Mild steel shaft	CFK P206	2 pcs
	Bearing		
Prony brake	Square hollow	20 × 20 × 1.5 mm	1 pc
	section	Φ8 × 800 mm	1 pc
	Wire rope	M12 v 150 mm	1 pc
	Bolt and nut	12 × 12 × 300 mm	1 pc
	Iron block		
Overhead reservoir	Black pipe (class B)	Φ100 × 2500 mm	6 pcs
Frame	Square hollow	40 × 40 × 2 mm	4 pcs
	section		

* pc – piece

Basin and canal fabrication

The basin and canal structures were made from mild steel iron sheets, with the inlet width adjusted according to the optimized design, as shown in production drawings and Figure 2.

(a) (b)

Figure 40: Basin and canal: (a) orthographic view, (b) isometric view. All dimensions are in millimeters.

Runner fabrication

Experimental work used a six-blade curved-blade profile type runner made from 1 mm mild steel sheets to reduce costs and ensure easy shape acquisition, as shown in Figure 3.

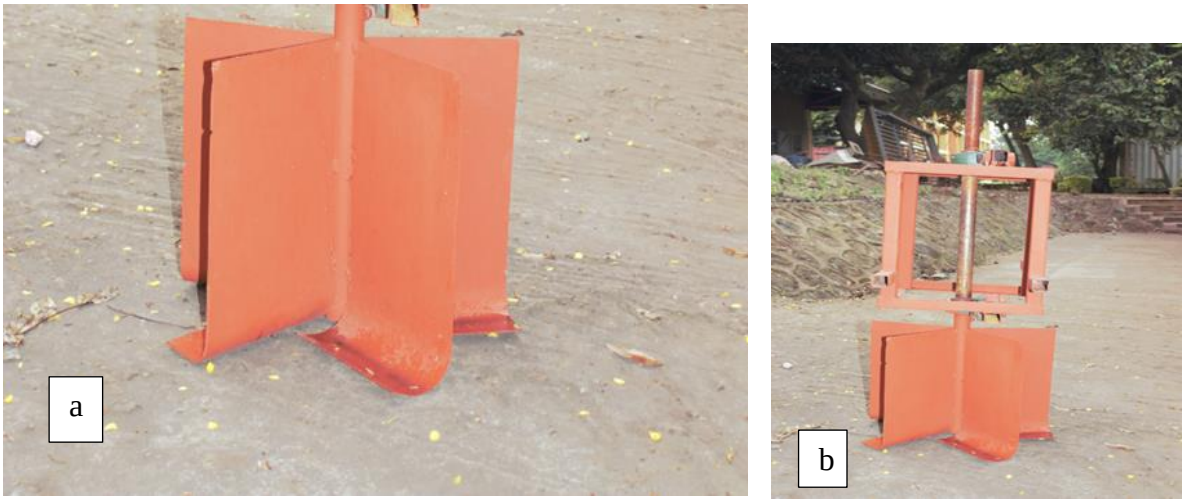

Figure 41: Fabricated blades used in the experimental setup: (a) blades and (b) blades with shaft support.

Data collection procedure

The experiments used the bucket or volumetric method to measure the flow rate by closing the basin aperture and opening the overhead reservoir valve, a method similar to previous studies (Gheorghe-Marius and Tudor, 2013, Marian et al., 2013, Nishi and Inagaki, 2017). Equation (1) was used to determine the flow rate, Q, for the existing system.

$$Q = \frac{Volume\ of\ the\ basin}{Time\ spent\ to\ fill\ the\ basin} \quad (27)$$

The upper frame of a vortex air core runner was supported using a class B black steel tube to support the shaft and bearings. Data was collected by determining the system's torque and

rotation speed using Mulligan and Hull (2010) and Dhakal et al. (2017a) methods. A Prony braking mechanism was used to measure brake force and torque. A braking system was installed to measure output power and friction torques. The runner's rotational speed was measured using a digital tachometer. Data collection began with the runner at rest and continued with the turbine's rotational speed. The output power, torque, and efficiency were determined using equations (2), (3), and (4), respectively which are according to (Mulligan and Hull, 2010) and (Dhakal et al., 2017a).

$$P_{output} = \frac{2\pi grN}{60}\left(M_{weight} - M_{counterweight}\right), \quad (28)$$

where, r is the radius of the pulley, M_{weight} is the mass of the first weigh scale, and $M_{counterweight}$ is the mass of the second weigh scale.

$$T = gr\Delta m, \quad (29)$$

where, g, is the acceleration due to gravity, r is the pulley radius, and Δm is the change in mass between the first and second weigh scales.

$$H = \frac{T\omega}{\rho QgH}, \quad (30)$$

where, ω is the rotational speed in rpm and H is the head.

Exergy analysis of the system

The first law of thermodynamics was applied to analyze the exergy of a system, considering the control volume as an open system, and using Equation (5) (Abuelnuor et al., 2020).

$$0 = \sum\left(1 - \frac{T_o}{T_j}\right)\dot{Q} - W + \sum_i m_i e_{fi} - \sum_e m_e e_{fe} - E_d, \quad (31)$$

where T_j = temperature at the boundary (K), T_o = temperature at the environment (K), W = energy transfer via control volume (W), ṁ = mass flow rate (kg/s), Q = heat transfer rate (W).

Furthermore, $e_f = h - h_o - T_o(s - s_o) + 0.5\ (V^2) + gz$; where h_o = enthalpy (kJ / kg), h = enthalpy of the working fluid (kJ / kg), V = velocity of the working fluid (m/s), g = acceleration gravity (m^2/s), s = entropy of the working fluid (kJ/kg K), s_o = environment entropy (kJ / kg K), E_d = destruction of exergy due to irreversibility (W) and z = elevation (m).

The control volume operated under ambient conditions, which were assumed to be 25 ° C (temperature), 1 atm (atmospheric pressure), and 1000 kg/m^3 (density of water). These assumptions reduced Equation (5) to Equation (6), which was used to calculate E_d (exergy destruction due to irreversibility).

$$E_d = \dot{m}\left[\left(\frac{c_1^2 - c_2^2}{2}\right) + g(z_1 - z_2)\right] - W, \quad (32)$$

where c_1 and c_2 are the water velocities in m/s at the inlet and outlet, respectively. The water velocities were determined by the division of flow by the respective inlet and outlet areas and z_1 and z_2 were the elevations in m at the input and outlet, respectively. Elevations were determined using a tape measure, as shown in Figure 4.

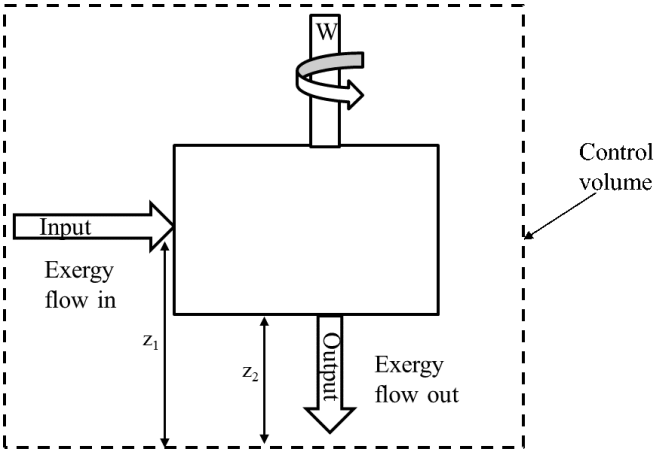

Figure 42: Schematic of exergy flow under the controlled volume of GWVPP system.

The steady-flow energy equation (SFEE) was utilized to calculate the work done by the system, considering the conservation of energy Equation 7 (Dixon and Hall, 2013) was used to determine the work done (W) by the system.

The energy balance was as follows:

Energy input = Energy output

$$\dot{m}\left(h_1 + \frac{c_1^2}{2} + z_1 g\right) + Q = \dot{m}\left(h_2 + \frac{c_2^2}{2} + z_2 g\right) + W \qquad (33)$$

where h_1 and h_2 are the specific enthalpies at the inlet and outlet, respectively, $\frac{1}{2}c^2$ is the kinetic energy per unit mass, gz is the potential energy per unit of mass, and W is work (W).

A hydraulic turbine operates with no heat transfer, work W = +W work produced, and no change in internal energy, $u_1 = u_2$

Thus, $h_1 - h_2 = u_1 + p_1 v_1 - (u_2 + p_2 v_2)$

$$h_1 - h_2 = p_1 v_1 - p_2 v_2)$$

Equation (7) becomes:

$$W = \dot{m}\left(\frac{c_1^2 - c_2^2}{2} + g(z_1 - z_2) + p_1(v_1 - v_2)\right), \quad (34)$$

The study calculates the specific volume of a fluid by comparing the atmospheric pressure (p_1) and specific volumes v_1 and v_2 at the inlet and outlet.

The exergy efficiency of the system was determined by Equation (9):

Thus, the exergy efficiency $= \frac{Exergy\ output}{Exergy\ input}$ which is according to Vakilabadi et al. (2019), Abuelnuor et al. (2020) and Moshi (2021).

$$\varphi = \frac{W}{W + E_d} \quad (35)$$

Error analysis

An error analysis was conducted to identify and quantify errors in experimental measurements, identifying potential sources such as speed recording tachometers and weigh scales, to capture random uncertainty (Bachynski et al., 2019). To calculate the random uncertainty, S_R, of the experimental data, the following equation was used:

$$S_R = \frac{S_x}{\sqrt{N-1}} \quad (36)$$

where S_x is the standard deviation of both speed and mass.

The study assessed the impact of errors on power, torque, and efficiency parameters in tachometer and weigh scale measurements using propagating errors, utilizing equations for power, torque, and efficiency (Figliola and Beasley, 2020).

$$\delta P = P\sqrt{\left(\frac{\delta\omega}{\omega}\right)^2 + \left(\frac{\delta\Delta m}{\Delta m}\right)^2} \quad (37)$$

$$\delta T = \delta \Delta m \tag{38}$$

$$\delta\eta = \eta\sqrt{\left(\frac{\delta T}{T}\right)^2 + \left(\frac{\delta\omega}{\omega}\right)^2} \tag{39}$$

Results and Discussions

Performance analysis of the GWVPP runner

The performance analysis of the GWVPP runner revealed an output power range of 2.96-7.33 W, torque of 0.08-0.23 Nm, and efficiency of 9.84%-25.35%. The higher efficiency was attributed by the optimized working parameters. The experimental efficiency was slightly lower than the numerical analysis of which was reported a maximum efficiency of 25.89% (Faraji et al., 2022). Figures 5 - 7 displays the performance curves showing maximum power (7.63 W) and torque (0.231 Nm) at a speed of 2.64 rad/s, with the highest efficiency (25.35%), indicating stable vortex flow without distortion (Dhakal et al., 2017b, Khan et al., 2018). The experiment exhibited excellent performance due to stable vortex flow and uniform water flow, resulting in maximum power, torque, and efficiency. Reduced rotational speed affected performance due to distorted vortex and basin water level changes. The optimal speed was 2.64 rad/s, ensuring maximum performance. The study found that the runner's rotational speed significantly influenced output power, torque, and efficiency. A zero-output power, torque, and efficiency value corresponded to the maximum rotational speed without braking force. When load was applied, rotational speed decreased, suggesting increased braking force and undistorted vortex flow as supported by Khan *et al.* (Khan et al., 2018) in Figure 9(a), Dhakal *et al.* (Dhakal et al., 2017b) in Figure 15, and Kueh *et al.* (Kueh et al., 2017) in Figure 7.

The performance parameters decreased due to a distorted vortex caused by disturbance in vortex flow and changes in basin water level, resulting from a further reduction in rotational speed (Khan et al., 2018, Kueh et al., 2017). The performance parameters and rotational speed in turbines have an inverse relationship until a maximum value is reached, this is according to studies by Khan *et al.* (Khan et al., 2018) in Figure 9(a), Ullah *et al.* (Ullah et al., 2019) in

Figures 7−12, and Saleem *et al* .(Saleem et al., 2020) in Figure 16. The highest efficiency is achieved when the runner's rotation speed is half the vortex speed, as the vortex flow generates lift and rotation. Slow or fast rotation can reduce turbine efficiency (Mulligan and Casserly, 2010, Rahman et al., 2016). The vortex flow created a pressure gradient along the turbine blades, which caused them to generate lift and rotate (Li et al., 2023). The study analysis provides valuable insights into the design and operation of micro-HP systems, enabling engineers to optimize efficiency and performance by adjusting input parameters.

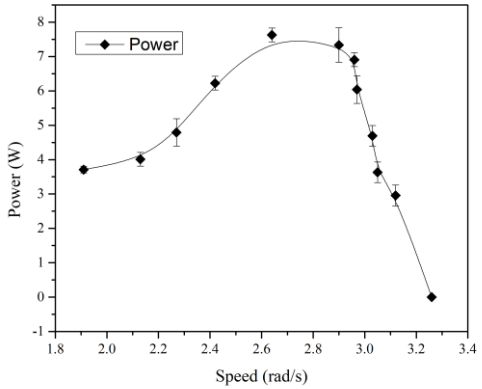

Figure 43: Effect of rotation speed on runner power.

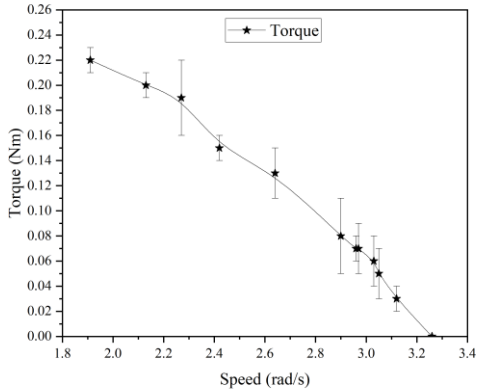

Figure 44: Effect of rotation speed on runner torque.

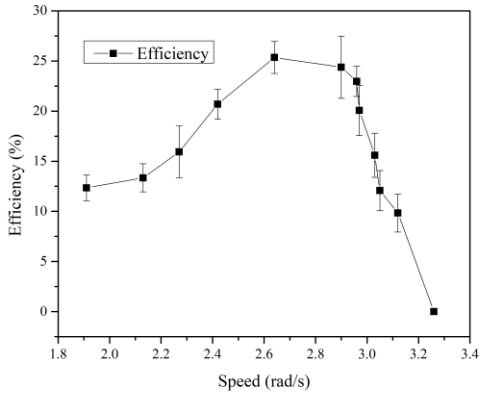

Figure 45: Effect of rotation speed on runner efficiency.

Exergy analysis

The study found a high exergy efficiency of 43.58% for the GWVPP runner, slightly higher than previous studies, such as Hossain et al. (2020) ranging from 35.0% to 39.2% and Maruf et al. (2021) ranging from 35.07% to 36.59%. This efficiency is attributed to optimized working parameters, such as speed, blade-hub angle, number of blades, and blade profile. Exergy efficiency measures the proportion of input energy converted into useful work (Rosen and Dincer, 2001).

Error analysis

The study found that the power, torque, and efficiency measurements were reliable and precise, with error ranges ranging from 0.1 to 0.5 W, 0.01 to 0.03 Nm and 1.3 – 3.1%, respectively (Figures 5 - 7). The torque measurement process was more reliable and less prone to errors, possibly due to the propagation of errors in these parameters. Efficiency errors were generally low, with most falling within the 1.3% to 3.1% range. The efficiency error depended on both power and torque errors, with lower errors at lower rotational speeds and higher errors at higher speeds. Overall, the experimental setup and instrumentation were reasonably accurate.

3. Conclusion

The study evaluated the efficiency and capabilities of a gravitational water vortex power plant (GWVPP) turbine runner using exergy analysis and performance testing methods. The results shows that the turbine runner efficiencies ranging from 9.84% to 25.35%, torque values ranging from 0.08 Nm to 0.23 Nm, and output power ranging from 2.96 to 7.33 W. From these results, it is clearly shown that GWVPP technology offers a low-cost alternative to traditional hydroelectric power plants, with minimal maintenance requirements and efficient utilization of low head resources. Moreover, beyond its immediate applications, this research contributes to the broader discourse on sustainable energy solutions. By demonstrating the feasibility and

efficacy of GWVPP technology. Lastly, but not least, the studies from this research advocates for the exploration and adoption of innovative approaches to harnessing innovative water energy sources. So, in this case, future energy research should focus on optimizing GWVPP energy capacity, its scalability as well as environmental impact assessments.

Data Availability

Data supporting the findings of this study are available in the article.

Conflict of Interest

The authors declare that they have no conflict of interest.

Acknowledgment

We acknowledge the financial support of the Water Infrastructure and Sustainable Energy (WISE Futures) Centre of Excellence of the Nelson Mandela African Institution of Science and Technology.

References

Abuelnuor AA, Ahmed K, Saqr KM, Nogoud YA and Babiker ME 2020 Exergy analysis of large and impounded hydropower plants: Case study El Roseires Dam (280 MW). *Environmental Progress & Sustainable Energy,* 39**,** e13362.

Bachynski E, Thys M and Delhaye V 2019 Dynamic response of a monopile wind turbine in waves: Experimental uncertainty analysis for validation of numerical tools. *Applied Ocean Research,* 89**,** 96-114.

Dhakal R, Bajracharya T, Shakya S, Kumal B, Kathmandu N, Khanal K, Kavre N, Williamson S, Gautam S and Ghale D. Computational and experimental investigation of runner for gravitational water vortex power plant. Proceedings of a meeting held, 2017a. 8.

Dhakal R, Bajracharya T, Shakya S, Kumal B, Khanal K, Williamson S, Gautam S and Ghale D. Computational and experimental investigation of runner for gravitational water vortex power

plant. 2017 IEEE 6th International Conference on Renewable Energy Research and Applications (ICRERA), 2017b San, Diego, USA. IEEE Publisher, 365-373.

Dhakal S, Nakarmi S, Pun P, Thapa AB and Bajracharya TR 2014 Development and testing of runner and conical basin for gravitational water vortex power plant. *Journal of the Institute of Engineering,* 10**,** 140-148.

Dixon SL and Hall C 2013. *Fluid mechanics and thermodynamics of turbomachinery*, Butterworth-Heinemann.

Faraji A, Jande YAC and Kivevele T 2022 Performance analysis of a runner for gravitational water vortex power plant. *Energy Science & Engineering,* 10**,** 1055-1066.

Figliola RS and Beasley DE 2020. *Theory and design for mechanical measurements*, John Wiley & Sons.

Gheorghe-Marius M and Tudor S 2013 Energy capture in the gravitational vortex water flow *Journal of Marine Technology & Environment,* 1.

Hossain S, Chowdhury H, Chowdhury T, Ahamed JU, Saidur R, Sait SM and Rosen MA 2020 Energy, exergy and sustainability analyses of Bangladesh's power generation sector. *Energy Reports,* 6**,** 868-878.

Kaunda CS, Kimambo CZ and Nielsen TK 2012 Potential of small-scale hydropower for electricity generation in Sub-Saharan Africa. *ISRN Renewable Energy,* 2012**,** 1-15.

Khan NH, Cheema TA, Chattha JA and Park CW 2018 Effective basin–blade configurations of a gravitational water vortex turbine for microhydropower generation. *Journal of Energy Engineering,* 144**,** 04018042.

Kueh T, Beh S, Ooi Y and Rilling D. Experimental study to the influences of rotational speed and blade shape on water vortex turbine performance. Fifteenth Asian congress of fluid mechanics (15ACFM), 2017 Sarawak, Malaysia. IOP Publishing 822 (2017) 012066, doi:10.1088/1742-6596/822/1/012066, .

Li W, Huang Y, Ji L, Ma L, Agarwal RK and Awais M 2023 Prediction model for energy conversion characteristics during transient processes in a mixed-flow pump. *Energy,* 271**,** 127082.

Marian MG, Sajin T and Azzouz A. Study of micro hydropower plant operating in gravitational vortex flow mode. Applied Mechanics and Materials, 2013. Trans Tech Publ, 601-605.

Maruf MH, Rabbani M, Ashique RH, Islam MT, Nipun MK, Haq MAU, Al Mansur A and Shihavuddin A 2021 Exergy based evaluation of power plants for sustainability and economic performance identification. *Case Studies in Thermal Engineering,* 28**,** 101393.

Moshi R 2021 The Exergy Analysis for the Air Gasification in a Hybrid Fixed Bed Gasifier.

Mulligan S and Casserly J 2010 The hydraulic design and optimisation of a free water vortex for the purpose of power extraction. *Sligo: Institute of Technology Sligo.*

Mulligan S and Hull P 2010 Design and optimisation of a water vortex hydropower plant. *Sligeach: Department of Civil Engineering and Construction, IT Silgo*.

Nishi Y and Inagaki T 2017 Performance and flow field of a gravitation vortex type water turbine. *International Journal of Rotating Machinery,* 2017.

Okot DK 2013 Review of small hydropower technology. *Renewable and Sustainable Energy Reviews,* 26**,** 515-520.

Paish O 2002 Small hydro power: technology and current status. *Renewable and sustainable energy reviews,* 6**,** 537-556.

Rahman M, Hong TJ, Tang R, Sung LL and Tamiri FBM 2016 Experimental study the effects of water pressure and turbine blade lengths & numbers on the model free vortex power generation system. *International Journal of Current Trends in Engineering & Research (IJCTER),* 2**,** 13-17.

Rahman M, Tan J, Fadzlita M and Muzammil A. A Review on the development of Gravitational Water Vortex Power Plant as alternative renewable energy resources. International Conference on Materials Technology and Energy, 2017. IOP Publishing, 217 (2017) 012007.

Rosen MA and Dincer I 2001 Exergy as the confluence of energy, environment and sustainable development. *Exergy, an International journal,* 1**,** 3-13.

Saleem AS, Cheema TA, Ullah R, Ahmad SM, Chattha JA, Akbar B and Park CW 2020 Parametric study of single-stage gravitational water vortex turbine with cylindrical basin. *Energy,* 200**,** 117464.

Timilsina AB, Mulligan S and Bajracharya TR 2018 Water vortex hydropower technology: a state-of-the-art review of developmental trends. *Clean Technologies and Environmental Policy,* 20**,** 1737-1760.

Ullah R, Cheema TA, Saleem AS, Ahmad SM, Chattha JA and Park CW 2019 Performance analysis of multi-stage gravitational water vortex turbine. *Energy Conversion and Management,* 198**,** 111788.

Vakilabadi MA, Bidi M, Najafi A and Ahmadi MH 2019 Exergy analysis of a hybrid solar-fossil fuel power plant. *Energy Science & Engineering,* 7**,** 146-161.

Williamson S, Stark B and Booker J 2014 Low head pico hydro turbine selection using a multi-criteria analysis. *Renewable Energy,* 61**,** 43-50.

Zotlöterer. 2017. *Gravitation water vortex power plants* [Online]. Available: http://www.zotloeterer.com/welcome/gravitation-water-vortex-power-plants/. Accessed on 2 May 2022 [Accessed].

Poster presentation

Computational Investigation of Water Vortex Turbine for Low Head Waters for Free-flowing Streams Suitable for Micro-hydropower

Adam Faraji Mfangavo – Ph.D candidate

School of Materials, Energy, Water and Environmental Science

The Nelson Mandela African Institution of Science and Technology, P.O BOX 447,

Arusha Tanzania

farajia@nm-aist.ac.tz

Key words: Gravitational water vortex, water turbines, CFD

Abstract

Gravitational water vortex power plant is a green technology that generates electricity from alternative energy source. In the vortex power plant, water is introduced into a circular basin tangentially that creates a free vortex and energy is extracted from the free vortex by using a turbine. However, there are still insufficient literatures available for the technology to proceed beyond prototyping stage. The maximum efficiency obtained by the researchers are approximately 30% while the commercial companies claimed about 50% of efficiency with 500W to 20kW of power generated. Hence, the aim of this paper is to determine the gap in the vortex power plant technology development through past works and a set of research recommendations will be developed as efforts to accelerate the development of GWVPP.

Introduction

Gravitational water vortex system is one of the mini/micro hydropower systems, and can be considered as a useful application of Free Surface vortex (FSV) principle (Yaakob & Ahmed, 2015). Water vortex turbine produces power by creating artificial water vortex formed due to the tangential passage of water through a rectangular canal to a basin (cylindrical/spiral) having a bottom exit hole. It doesn't require direct control mechanism and doesn't require a penstock. Hence, the cost of fabrication and construction is low and can be realized using the locally available machines and equipment(Wanchat & Suntivarakorn, 2012).

This research work will employ Computational Fluid Dynamics, CFD to optimize gravitational vortex energy system capable to generate electricity from low heads. The CFD model will be validated by experimental rig.

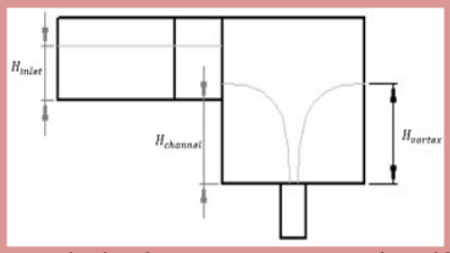

Gravitational Water Vortex Power Plant side view

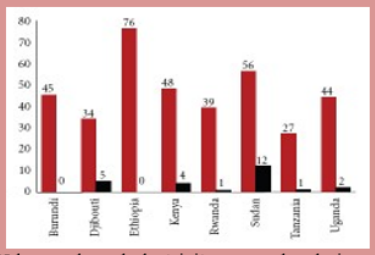

Urban and rural electricity access levels in EA (Rosnes and Vennemo 2008)

Objective of the study

1. To develop models of turbine runner by using established parameters
2. To run simulation by different runner diameters to get the optimal runner diameter
3. To run simulation for different runner length to get the optimal runner length
4. To establish the optimal geometrical parameters in terms of runner diameter and runner length

Methodology

Computational Fluid Dynamics (CFD)

Conclusion

For sustainable development of our countries, application of resources surrounding us is INVITABLE. We have good number of water bodies lets optimize this valuable resources for our society.

Acknowledgement

The author would like to express his gratitude to the school of BuSH and NM AIST at large for this valuable course program.